universiteit hasselt
KNOWLEDGE IN ACTION

2013 | Faculteit Wetenschappen

DOCTORAATSPROEFSCHRIFT

MORPHOLOGY AND RECOMBINATION IN P3HT:PCBM ORGANIC SOLAR CELLS

Proefschrift voorgelegd tot het behalen van de graad van
doctor in de wetenschappen, fysica, te verdedigen door:

Donato Spoltore

Promotor: prof. dr. Jean V. Manca
Copromoter: prof. dr. Milos Nesladek

D/2013/2451/40

Chairman	Prof. dr. Ken Haenen, Universiteit Hasselt
Promoter	Prof. dr. Jean Manca, Universiteit Hasselt
Co-Promoter	Prof. dr. Milos Nesladek, Universiteit Hasselt
Members of the jury	Prof. dr. Wouter Maes, Universiteit Hasselt
	Dr. Emilie Bourgeois, Universiteit Hasselt
	Dr. Wibren Oosterbaan, Universiteit Hasselt
	Dr. ir. Koen Vandewal, Universiteit Hasselt – Stanford University (USA)
	Prof. dr. Emilio Palomares, ICIQ - Institut Català d'Investigació Química
	Dr. Samira Khelifi, Universiteit Gent

Alla mia famiglia
Alle persone che mi amano
E che amo

Quando c'è bisogno non solo di intelligenza agile e di spirito versatile ma di volontà ferma, di persistenza e di resistenza io mi sono detto a voce alta: tu sei abruzzese!

Benedetto Croce (1866-1952)

Table of contents

Acknowledgements

First of all I would like to thank my promoter, Professor Jean Manca, for giving me the possibility to do my PhD, for his kindness full of humanity, his work suggestions and for talking to me in Italian making me feel closer to home. Grazie Jean.

Besides my promoter I would like to thank Fortunato for having made that call almost 5 years ago suggesting that I should apply for a position at UHasselt. We have known each other for 13 years now and whether we were late for a lesson for only 2 persons at the University of L'Aquila or walking along some deadly dangerous paths on Abruzzo's mountains or eating great pizza he made or walking California's deserts or enjoying the snowy tropical beaches in Norway, I think I can call him a true friend.

I would also like to thank the Professors with whom I had the chance to discuss and exchange ideas in Hasselt: Professor Dirk Vanderzande for helping me with chemistry concepts, Professor Wouter Maes for helping me and for having read my last paper like 30 times, Professor Ward de Ceuninck for his help with my setup, Professor Hans-Gerd for the nice discussions in Paris, I really regret they were only for such a short period and Professor Milos Nesladek.

Thanks to Wibren who helped me a lot in the first part of my PhD and with my first paper, also thanks to Tanya and Artjom for making my family happy on those summer days.

Thank you Samira for all your help and for believing in me when nobody was, I really appreciated it. Thanks also to Professor Marc Burgelman for helping me and for his humor.

I want to thank a lot also Professor Emilio Palomares for inviting me in Tarragona even if he didn't know me well and to John Clifford and Aurelio for the warm welcome to Spain.

Special thanks goes to all the lab technicians for keeping our lab running effectively. In particular I would like to thank Jan for his help with my setup, without him it wouldn't work even now. Johnny "Harry Potter" Baccus for turning impossible requests magically into reality. Lieven for his help in critical moments. I don't know if people fully realize how precious the help of all of you is, thank you.

Thanks also to Relinde, Marina, Ellen, Lea and Lysette for saving us all from bureaucracy every day.

I'm also very grateful to all the colleagues Wiebke, Nikolina, Farnoosh, Lidia, Gopal, Jurgen, Wim, Wouter, Lien, Koen Gilissen, Jeroen Stryckers, Pieter Robaeys, Huguette, Pieter Verstappen, Suleyman, Joke, Linny, Yaso, Paulius, Sathya for the nice years passed together in UHasselt. In particular I would like to thank the persons I collaborated closer: Tim who brought a huge amount of enthusiasm making me feel also happier, for helping me with the thesis, in Germany and in Paris. Emilie who read my thesis and came twice at the synchrotron measuring days and nights. Bert for the nice and stimulating discussions. Sabine for helping me and Jeroen Drijkoningen for discussions, for measuring with us in Paris and for telling me the first time about Game of Thrones.

I cannot forget those people who passed through UHasselt and now are somewhere else around the world: my French friends Sylvain and Vincent, Hans Moons, Mikhail, Ludwig Goris but especially Abay and Koen

Vandewal that helped me a lot at the beginning of my PhD. Their departure was a really sad moment. Nonetheless Koen managed to always help me with suggestions, inspirations, ideas and correcting deeply my last paper. Thank you a lot my friend.

Un ringraziamento speciale va alla mia ragazza Consuelo che ha portato un'intera tavolozza schizoide di colori alla mia nera visione dell'esistenza. Grazie di sopportarmi, incoraggiarmi, spronarmi. Scieu. (Un saluto anche a Anna!)

Grazie anche alla mia famiglia, Papà, Mamma, Zia Maria, Angela, Luigi, Zia Lina per avermi cresciuto, educato, nutrito, consolato, incoraggiato e molto altro. Anche se certe volte mi fate un pò dispiacere siete le persone più importanti per me.

Vorrei poi ringraziare le molte altre persone con le quali ho condiviso questi anni in Belgio, in particolare la comunità italiana di Hasselt: Emanuele e le sue passeggiate del fine settimana, le sue cene e le sue attività di gruppo. Dopo la sua partenza il Belgio è stato un posto più triste. Filippo "Brega" Morini per portare con se sempre l'atmosfera italiana. Mirco per la sua fiducia incrollabile nella madrepatria e per aver movimentato le nostre giornate. Giulia e Lorenzo per gli scambi cultural-gastronomici milanapolepugliabruzzoveronesi, è un peccato avervi conosciuto solo alla fine, mi mancherete. I cannot forget, of course, all the other persons: Reza, Ambily, Pia, Ariel, Carlos, Jimmy, Eva, Isabella, Cristina, Martin, Urko, Amparo, Miguel, Suvlay. A special thanks is for Caro, a sweet friend with a lot of affinities, her words "the important thing is we are together" saved our days several times. Don't worry Caro I'm not going to forget you.

Ringrazio anche gli amici di sempre: Riccardo, Evenzio, Carlo, Alex, Gipis, Domenico, Andrea, Mauro, Mucca, Natascina, Vinicio, Filippo, Fede, Anna, Silvia, Lucia, Cignale. Anche se ci vediamo una volta ogni due anni ogni volta è come se ci fossimo lasciati due minuti fa. I miei ricordi più belli sono con voi nella città che non c'è più.

Ringrazio anche gli amici dell'Università dell'Aquila, Alfredo, Ines, Alessio, Emanuela, Elisa, Debora (anche per l'aiuto a SOLEIL), Roberto, Andrea Marini.

Thanks also to all the persons I forgot, forgive me the list is long.

Grazie a tutti!
Thanks everybody!
Dank jullie wel!

Publications

The papers in bold are included in this thesis:

- **D. Spoltore, T. Vangerven, P. Verstappen, F. Piersimoni, S. Bertho, K. Vandewal, W. Maes, A. De Sio, L. Lutsen, D. Vanderzande, and J.V. Manca, *"Effect of molecular weight on morphology and photovoltaic properties in P3HT:PCBM solar cells"* Submitted to Advanced Energy Materials**

- P. Robaeys, E. Bourgeois, J. D'Haen, W. Dierckx, W. Dexters, D. Spoltore, F. Bonaccorso, A.C. Ferrari, K. Haenen, J.V. Manca, and M. Nesladek, *"Mechanisms of P3HT:PCBM bulk heterojunction solar cells performances enhancement upon graphene addition"* In preparation

- **S. Khelifi, E. Voroshazi, D. Spoltore, F. Piersimoni, S. Bertho, T. Aernouts, J. Manca, J. Lauwaert, H. Vrielinck, and M. Burgelman, *"Effect of light induced degradation on electrical transport and charge extraction in polythiophene:fullerene solar cells"* Submitted to Solar Energy Materials and Solar Cells**

- F. Piersimoni, G. Degutis, S. Bertho, K. Vandewal, D. Spoltore, T. Vangerven, J. Drijkoningen, M. K. Van Bael, A. Hardy, J. D'Haen, W. Maes, D. Vanderzande, M. Nesladek and J. Manca, *"Influence of fullerene photodimerization on the PCBM crystallization in polymer:fullerene bulk heterojunctions under thermal stress"* Journal of Polymer Science Part B: Polymer Physics (2013)

- S. Bertho, B. Campo, F. Piersimoni, D. Spoltore, J. D'Haen, L. Lutsen, W. Maes, D. Vanderzande, and J. Manca, *"Improved thermal stability of bulk heterojunctions based on side-chain functionalized poly(3-alkylthiophene) copolymers and PCBM"* Solar Energy Materials and Solar Cells 110, 69 (2013)

- F. Ouhib, M. Tomassetti, J. Manca, F. Piersimoni, D. Spoltore, S. Bertho, H. Moons, R. Lazzaroni, S. Desbief, C. Jerome, and C. Detrembleur, *"Thermally Stable Bulk Heterojunction Solar Cells Based on Cross-Linkable Acrylate-Functionalized Polythiophene Diblock Copolymers"* Macromolecules 46, 785 (2013)

- **D. Spoltore, W.D. Oosterbaan, S. Khelifi, J.N. Clifford, A. Viterisi, E. Palomares, M. Burgelman, L. Lutsen, D. Vanderzande, and J.V. Manca, *"Effect of Polymer Crystallinity in P3HT:PCBM Solar Cells on Band Gap Trap States and Apparent Recombination Order"* Advanced Energy Materials 3, 466 (2013)**

- **B. Conings, L. Baeten, H.-G. Boyen, D. Spoltore, J. D'Haen, M.K. Van Bael, and J.V. Manca, *"Generalized approach to the description of recombination kinetics in bulk heterojunction***

***solar cells-extending from fully organic to hybrid solar cells"* Applied Physics Letters 100, 203905 (2012)**

- G.K.V.V. Thalluri, D. Spoltore, F. Piersimoni, J.N. Clifford, E. Palomares, and J.V. Manca, *"Study of interface properties in CuPc based hybrid inorganic–organic solar cells"* Dalton Transactions 41, 11419 (2012)

- J. Vandenbergh, B. Conings, S. Bertho, J. Kesters, D. Spoltore, S. Esiner, J. Zhao, G. Van Assche, M.M. Wienk, W. Maes, L. Lutsen, B. Van Mele, R.A.J. Janssen, J. Manca, and D.J.M. Vanderzande, *"Thermal Stability of Poly[2-methoxy-5-(20-phenylethoxy)-1,4-phenylenevinylene] (MPE-PPV):Fullerene Bulk Heterojunction Solar Cells"* Macromolecules 44, 8470 (2011)

- B. Conings, L. Baeten, H. Boyen, D. Spoltore, J. D'Haen, L. Grieten, P. Wagner, M. Van Bael, and J. Manca, *"Influence of Interface Morphology onto the Photovoltaic Properties of Nanopatterned ZnO/Poly(3-hexylthiophene) Hybrid Solar Cells. An Impedance Spectroscopy Study"* The Journal of Physical Chemistry C 115, 16695 (2011)

- S. Bertho, W.D. Oosterbaan, V. Vrindts, J.-C. Bolsée, F. Piersimoni, D. Spoltore, J. D'Haen, L. Lutsen, D. Vanderzande, and J.V. Manca, *"Poly(3-alkylthiophene) nanofibers for photovoltaic energy conversion"* Advanced Materials Research (Durnten-Zurich, Switz.) 324, 32 (2011)

- S. Khelifi, K. Decock, J. Lauwaert, H. Vrielinck, D. Spoltore, F. Piersimoni, J. Manca, A. Belghachi, and M. Burgelman, *"Investigation of defects by admittance spectroscopy measurements in poly(3-hexylthiophene):(6,6)-phenyl C61-butyric acid methyl ester organic solar cells degraded under air exposure"* Journal of Applied Physics 110, 094509 (2011)

Conference contributions

Oral presentations

- *'Effect of crystallinity in P3HT:PCBM solar cells on bandgap trap states and apparent recombination order'* at HOPV 2012 in Upsala, Sweden, 6-9 May 2012; D. Spoltore, W. D. Oosterbaan, S. Khelifi, J. Clifford, A. Viterisi, E. Palomares, M. Burgelman, L. Lutsen, D. Vanderzande, J. Manca

- *'Investigation of charge transport and recombination using extraction current transient on organic solar cells'* at Scientific Meeting of Polyspec (SBO project of IWT, Flanders) in Hasselt, Belgium, 21 October 2010; D. Spoltore

- *'Investigation of charge transport and recombination using extraction current transient on solar cells made with alternative acceptors'* at 'SolarNtype' Network Meeting in Alicante, Spain, 22-24 September 2010; D. Spoltore

- *'Investigation of charge transport and recombination in Poly(3-alkylthiophene)/Fullerene bulk heterojunctions from extraction current transients'* at MRS Spring meeting 2010 in San Francisco, USA, 5-9 April 2010; D. Spoltore, A. Gadisa, W. D. Oosterbaan, M. Parchine, G. Krishna, V. Vrindts, L. Lutsen, D. Vanderzande, J. Manca

- *'Description of charge transport and recombination in MDMO-PPV:PCNEPV using the method of CELIV' at 'SolarNtype'* Network Meeting in Warsaw, Poland, 14-15 October 2009; D. Spoltore

Contributions to oral presentations

- *'Nanomorphology & next generation organic based solar cells'* at Next-Generation Organic Photovoltaics in Groningen, Netherlands, 2-5 June 2013, invited talk; F. Piersimoni, D. Spoltore, J. Kesters, W. Dierckx, J. Drijkoningen, T. Vangerven, L. D'Olieslaeger, S. Bertho, B. Conings, A. Ethirajan, J. Liesenborghs, J. D'Haen, L. Lutsen, H.G. Boyen, W. De Ceuninck, W. Maes, D. Vanderzande, J.V. Manca

- *'CTC's in organic based solar cells'* at International Minotor Workshop 2012 in Mons, Belgium, 29-31 May 2012, invited talk; F. Piersimoni, D. Spoltore, P. Robaeys, J.C. Bolsée, S. Bertho, H. Moons, W. Oosterbaan, H.G. Boyen, M. Nesladek, D. Vanderzande, J. Manca

- *'Lifetime of bulk heterojunction solar cells: the next challenge'* at HOPV 2012 in Uppsala, Sweden, 6-9 May 2012, invited talk; S. Bertho, B. Conings, F. Piersimoni, D. Spoltore, J. D'Haen, L. Lutsen, B. Van Mele, G. Van Assche, D. Vanderzande, J.V. Manca

- *'Towards bulk heterojunction solar cells with stable morphology'* at SPIE 2011 in San Diego, USA, 21-25 August 2011, invited talk; S. Bertho, B. Conings, F. Piersimoni, D. Spoltore, J. D'Haen, L. Lutsen, H.G. Boyen, B. Van Mele, G. Van Assche, D. Vanderzande and J. Manca

- *'Nano-morphology and its stability versus photovoltaic properties in bulk heterojunction solar cells'* at EMRS 2011 in Nice, France, 9-13 May 2011, invited talk; S. Bertho, K. Vandewal, F. Piersimoni, D. Spoltore, B. Conings, J. D'Haen, L. Lutsen, H.G. Boyen, D. Vanderzande and J. Manca

- *'Nanofibres for photovoltaic energy conversion'* at CIMA 2011 in Beirout, Lebanon, 15-17 March 2011, invited talk; S. Bertho, W. Oosterbaan, J.C. Bolsée, F. Piersimoni, D. Spoltore, J. D'Haen, L. Lutsen, D. Vanderzande and J.V. Manca

Posters

- *'Molecular weight versus morphology and electro-optical properties in polymer:fullerene solar cells'* at Next-Generation Organic Photovoltaics in Groningen, Netherlands, 2-5 June 2013; D. Spoltore, T. Vangerven, P. Verstappen, F. Piersimoni, S. Bertho, W. Maes, L. Lutsen, M. Nesladek, D. Vanderzande, and J.V. Manca

- *'Investigation of defects in P3HT:PCBM organic solar cells aged under constant illumination'* at International scientific conference Photovoltaics at the nanoscale in Hasselt, Belgium, 24-28 October 2011; S. Khelifi, D. Spoltore, F. Piersimoni, E. Voroshazi, K. Decock, J. Lauwaert, T. Aernouts, H. Vrielinck, J.V. Manca and M. Burgelman

- *'Investigation of the electro-optical properties of polymer:polymer solar cells'* at SolarNtype Network Meeting in Alicante, Spain, 22-24 September 2010; F. Piersimoni, D. Spoltore, P. Adriaensens, L. Lutsen and J.V. Manca

Abbreviations and symbols

AM1.5	Air Mass 1.5
BHJ	Bulk Heterojunction
CB	Chlorobenzene
CELIV	Charge Extraction by Linearly Increasing Voltage
CT	Charge Transfer
d	Sample Thickness
DOS	Density of States
e	Elementary Charge
EQE	External Quantum Efficiency
eV	Electronvolt
E_{CT}	Charge Transfer Energy
FET	Field Effect Transistor
FF	Fill Factor
FTPS	Fourier Transform Photocurrent Spectroscopy
HOMO	Highest Occupied Molecular Orbital
ITO	Indium Tin Oxide
I-V	Current-Voltage
J_{SC}	Short Circuit Current
LUMO	Lowest Unoccupied Molecular Orbital
MW	Molecular Weight
n	Charge Carrier Density
ns	Nanosecond
ODCB	1,2-dichlorobenzene
OPV	Organic Photovoltaic
OSC	Organic Solar Cell
P3HT	poly(3-hexylthiophene-2,5-diyl)
PCBM	1-(3-methoxycarbonyl)propyl-1-phenyl-[6,6]-methanofullerene
PCE	Power Conversion Efficiency
PDI	Polydispersity
PEDOT-PSS	poly(3,4-ethylenedioxythiophene)-poly(styrenesulfonate)
RR	Regioregularity
SAED	Selected Area Electron Diffraction
SCLC	Space Charge Limited Current
TEM	Transmission Electron Microscopy
TPC	Transient Photocurrent
TPV	Transient Photovoltage
UV-Vis	Ultraviolet-Visible (Spectroscopy)
V_{OC}	Open Circuit Voltage
α	Absorption Coefficient
η	Power Conversion Efficiency
λ	Wavelength
μ_h	Hole Mobility
μ_e	Electron Mobility
τ	Charge Carrier Lifetime
$\tau_{\Delta n}$	Small Perturbation Carrier Lifetime

1. Organic Solar Cells

In this chapter a general introduction on the working principles of organic solar cells is provided, followed by a description of the principal material investigated.

1.1. General introduction

Organic solar cells have received increasing interest in recent years due to their potential for low cost production as well as their lightweight and mechanical flexibility, esthetical possibilities and interesting thermal behavior and response under diffuse and indoor light. The efficiencies of this particular class of solar cells underwent an impressive improvement in the last years (Figure 1) reaching lately 11%.[1]

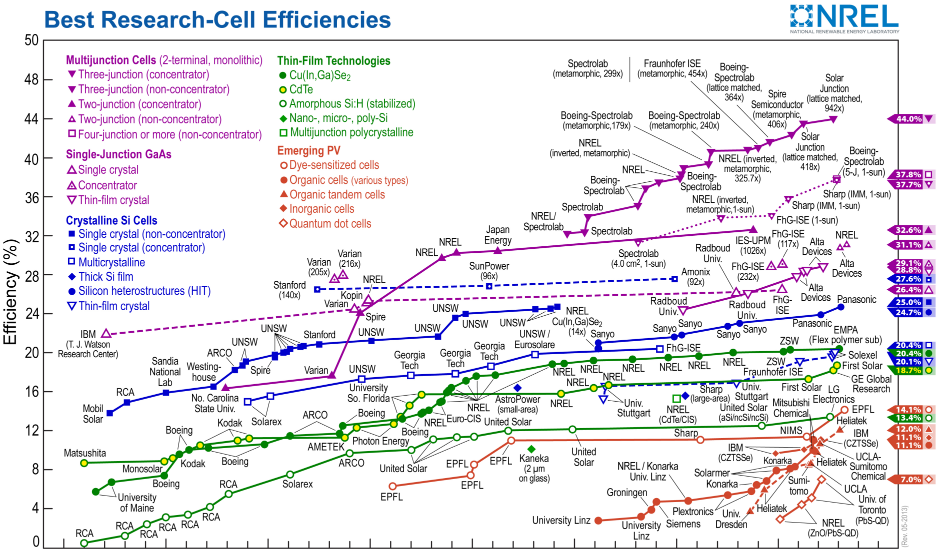

Figure 1 Efficiency improvement in time of the different solar cell technologies. In orange full dots the organic solar cells efficiencies are depicted.[2]

The first step in the rush for efficient organic solar cells was the discovery of dark conductivity in organic materials in 1954.[3] In 1970, the Nobel Prize winners Shirakawa, Heeger and MacDiarmid discovered the conductivity of π-conjugated polymers. The semiconducting and light absorbing properties of conjugated polymers made them a very interesting choice for photovoltaics.

The absorption coefficient of organic semiconductors is typically very high compared with the one of inorganic semiconductors. Therefore, a much smaller amount of material is needed to absorb all the photons with energy higher than the energy gap of the polymer. Typically, a layer around 100 nm thick (~1000 times thinner than silicon solar cells) is sufficient to absorb all the light.

The first organic solar cell was prepared by sandwiching a single material between two metal electrodes of different work functions. The efficiency of this design is low (<1%),[4] due to the low dielectric constant of organic materials. In fact, the absorbed photon gives rise to a strongly Coulombly bound electron-hole pair (an exciton), with a binding energy of 0.5-1 eV,[5] which has to be separated in order to obtain a current. The exciton has a lifetime below 1 ns. The corresponding diffusion length is, therefore, only a few nanometers, much less than the absorption length and therefore not enough for a high exciton to charge conversion ratio.

A big step forward was made in 1985 when Tang [6] showed a bilayer organic solar cell with a planar heterojunction (Figure 2 (a)) delivering ~1% efficiency. In this configuration the donor material absorbs light, the created excitons reach the interface with the acceptor material, which is normally a strongly electronegative material, where the electron-hole couple gets dissociated thanks to the energy offset at the interface provided by the acceptor. In fact, the electron can go to a state of much lower energy within the acceptor. However, only excitons created within their diffusion length from the interface can contribute to the photovoltaic effect. Therefore, again due to the short diffusion length of excitons in conjugated polymers, the current is limited also for the bilayer design.

A novel concept to circumvent the low exciton diffusion length was found in 1992.[7] The bulk heterojunction (BHJ) solar cell (Figure 2 (b)) features a distributed junction all over the active layer: both components interpenetrate one another, so that the interface between them is not planar any more, but spatially distributed. Active layers consisting of donor:acceptor material blends can be deposited by using a solution of a soluble fullerene derivative (typically 1-(3-methoxycarbonyl)propyl-1-phenyl-[6,6]-methanofullerene, PCBM) as acceptor and a conjugated polymer as donor. In this way, a higher portion of excitons created in the layer, which is sufficiently thick to absorb all the incident sunlight, can reach an interface within their diffusion length. It is evident that the morphology of the active layer becomes a crucial issue in BHJs: too large phases limit the photocurrent due to the low exciton diffusion length, whereas a too fine intermixing hinders the charge extraction.

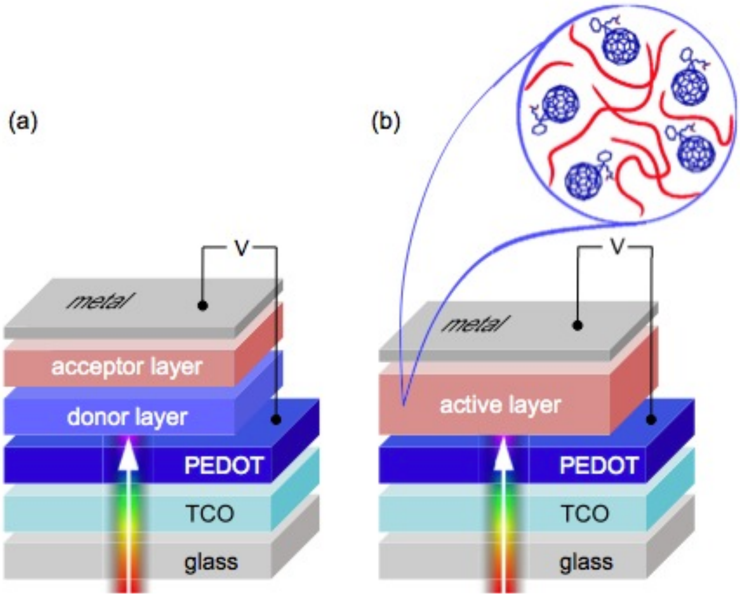

Figure 2 Scheme of the two solar cell designs: (a) the bilayer solar cell and (b) the bulk heterojunction design.[8]

Simple optimization methods have been proposed in the last years. The choice of solvents with a higher boiling point led, in 2001,[9] to enhanced efficiencies of PPV:PCBM solar cells from around 1% to 2.5%, due to the slower drying time and thus better self-organization. Two years later,[10] it was shown that the photovoltaic performance of blends of the semi-crystalline donor material poly(3-hexylthiophene-2,5-diyl) (P3HT) with PCBM could be improved by applying a thermal treatment after film deposition resulting in an improved morphology. The efficiency could be raised from 0.4 to 3.5%. Optimization by novel routes (e.g. using additives to optimize the phase separation) is an ongoing process and in the last years further steps in improving the power conversion efficiency (PCE) have been made.[11-13]

1.2. Current–voltage characteristics and solar cell parameters

The most important parameter describing the performance of a solar cell is the power conversion efficiency η. It is determined recording the current density J versus voltage V, under solar illumination. The parameters describing η are: the open circuit voltage (V_{OC}), the voltage for which the current is zero; the short circuit current (J_{SC}), the current for which the voltage is zero; the fill factor (FF), which is defined as the maximum output power of the solar cell divided by the product of open circuit voltage and short circuit current (surface of the green square divided by the surface of the red square in Figure 3); and the incident radiant power P_i from the light source.

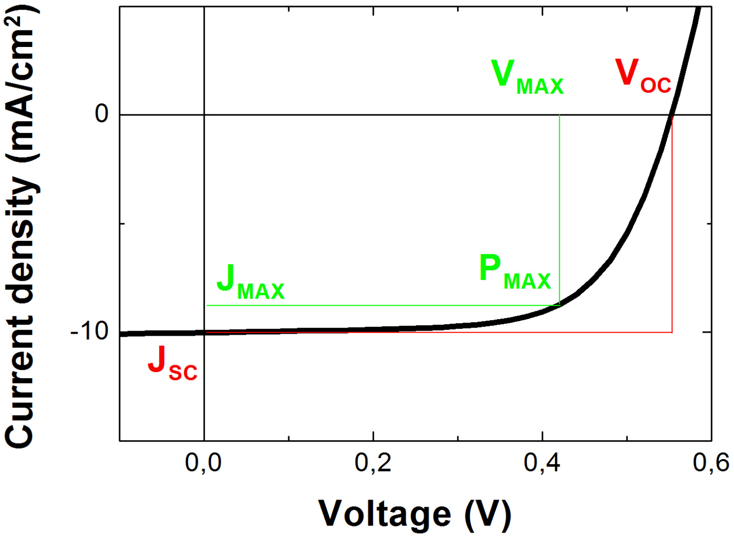

Figure 3 Current voltage characteristics of a solar cell

$$FF = \frac{P_{max}}{V_{OC} \cdot J_{SC}} = \frac{V_{max} \cdot J_{max}}{V_{OC} \cdot J_{SC}} \qquad (1)$$

The efficiency is the ratio of the maximum output power of the solar cell and the incident radiant power:

$$\eta = \frac{P_{max}}{P_i} = \frac{FF \cdot V_{OC} \cdot J_{SC}}{P_i} \qquad (2)$$

In order to compare the performances of different photovoltaic devices under the same solar conditions, an international standard input illumination spectrum is used, with an incident radiant power of 1000 W/m^2 (AM 1.5).

1.3. Working principles of BHJ solar cells

In the following paragraphs a short description of the working principles of BHJ organic solar cells is given, step by step, from generation to extraction.

1.3.1. Charge carriers generation

As a general principle, both the donor and the acceptor can absorb the incoming light, but we will consider, for simplicity, that the light is absorbed in the donor phase (Figure 4).

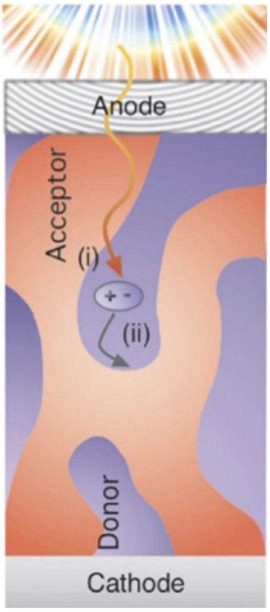

Figure 4 Light absorption in a BHJ solar cell: light is absorbed in the donor phase, an exciton is created which can then diffuse to the interface with the acceptor[8]

The absorption of photons with energy above the optical bandgap (difference between the Highest Occupied Molecular Orbital (HOMO) and the Lowest Unoccupied Molecular Orbital (LUMO)) of the donor lead to the generation of singlet excitons. The excitons can then diffuse to the acceptor. As mentioned before, excitons have a certain lifetime, after which they recombine radiatively. If they can find the donor/acceptor interface within their lifetime, there is a charge transfer of the electron to the acceptor. The efficiency of the exciton creation and diffusion depends strongly on sample thickness and morphology. Accommodating just the requirements of exciton dissociation, the phase separation should be as small as possible. However, because in a solar cell the following steps, which are electron-hole pair dissociation and charge transport to the electrodes, need phase separations as coarse as possible, the best dimension is a trade-off between these opposite requirements.

After the electron transfer to the acceptor phase, a process extremely fast in the order of tenths of femtoseconds,[14] the two charges are not free yet. They form a charge transfer complex (CTC), with the electron on the fullerene acceptor and the hole on the polymer still weakly bound (Figure 5).

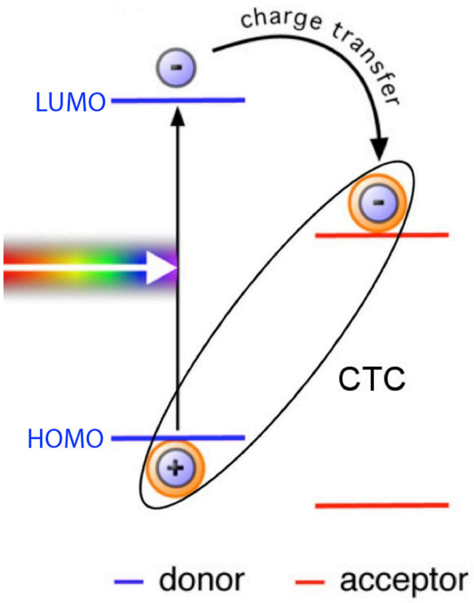

Figure 5 Electron transfer and Charge Transfer Complex in bulk heterojunction solar cells[8]

The CTC can either split, giving two free polarons, or recombine to the ground state.

The recombination of the CTC to the ground state is known as geminate recombination. It is a monomolecular process because it is proportional to the polaron pair concentration, not to the product of electron and hole densities.

1.3.2. Charge carriers transport

After being successfully separated at the donor-accepter interface, electrons and holes are transported mostly in the corresponding phases to the respective electrodes (Figure 6), which means that the holes travel in the donor material (the polymer) and the electrons in the acceptor material (the fullerene). The charge carriers transport in organic semiconductors is mainly characterized by the disordered nature of the materials. The charge carriers are localized to molecular sites due to energetic and spatial disorder in the bulk.

Figure 6 Charge carriers transport in the corresponding phase to the respective electrodes[8]

In a conjugated polymer, the molecular site is defined by the conjugation length of a polymer segment, that is, the overlap of neighboring sp^2 orbitals forming a delocalized π-bond. Breaks in the conjugation cause energetic barriers for the charge carriers to be present, while along a delocalized state a charge carrier can move freely.

The distribution of the electronic states in an organic disordered semiconductor is often described with a Gaussian density of states (DOS),[15] which also accounts for the random distribution of the molecular sites. Due to the low screening effects in organic materials, caused by the low dielectric constant, a charge carrier residing on a molecule distorts the molecular lattice and is hence known as a negative or positive polaron. To be transported, a localized polaron has to move from one state to another by means of a hopping process.[16] The hopping transport is schematized in Figure 7. After the photogeneration the occupied states follow the density of available states. With increasing time, the charge carriers relax in energy, going down to unoccupied states until an equilibrium is reached. In order to be transported, the charge carriers need to be thermally activated to the transport energy. If the thermal energy is not sufficient to reach the transport energy, the charge carriers may get trapped in deep states in the DOS. This phenomenon is described by the multiple trapping and release model.[17] Charge carriers residing below the transport energy are assumed to be immobile and first have to be activated to a site above the transport energy to be transported.

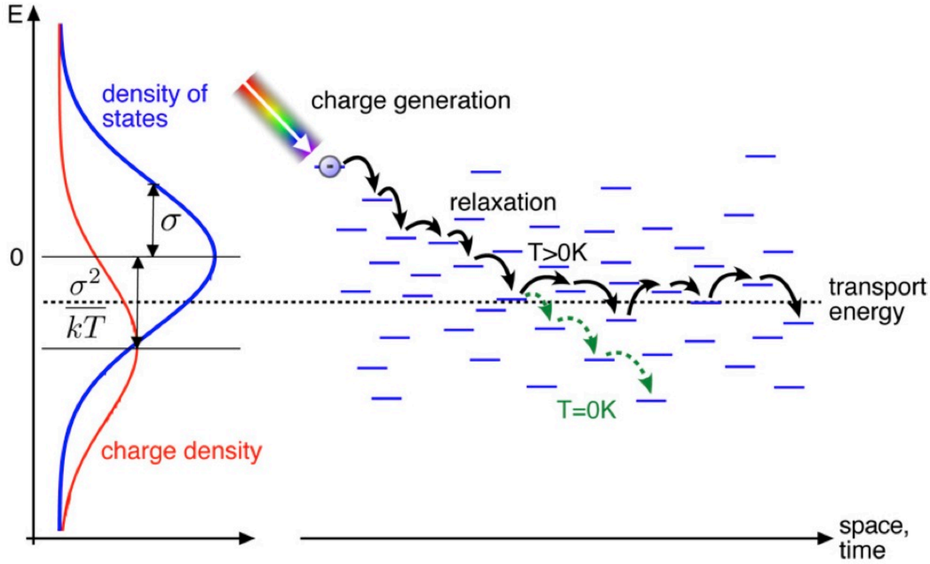

Figure 7 Carriers transport in organic materials. The density of states distribution is assumed to be Gaussian, the charges generated by the light relax to deep states toward equilibrium. To be transported, a charge carrier needs to be thermally activated to the transport energy.[8]

A macroscopic parameter describing the charge transport properties is the charge carrier mobility μ. From experiments, a Poole-Frenkel behavior of μ can be found: $\mu \propto exp(\sqrt{E})$ where E is the electric field. An increase in mobility with temperature is also observed,[15] the functional shape of which depends on the shape of the DOS: for an exponential DOS $\mu \propto exp(-E_a/k_BT)$ with E_a the activation energy, whereas $\mu \propto exp-(\sigma/k_BT)^2$ for a Gaussian DOS with σ the energetic width of the DOS.

1.3.3. Non-geminate recombination

During the transport of the photogenerated charge carriers to their respective electrodes, free polarons can meet each other and recombine. This process, limiting solar cell performance, is called non-geminate recombination as the charge carriers involved are coming from different precursors. Non-geminate recombination has been widely discussed in literature in recent years.[17-25]

1.3.3.1. Langevin recombination

The Langevin model has been used to model the non-geminate recombination process taking place in organic semiconductors.[26,27] Langevin proposed a rate describing the recombination of two opposite charged ions in a large ion reservoir. In the absence of an electric field, the two ions can avoid recombination only if their kinetic energy is larger than the Coulomb attraction. In other words, the two oppositely charged carriers will recombine if the distance between them is smaller than the Coulomb radius:

$$r_c = \frac{e^2}{4\pi\varepsilon_r\varepsilon_0 kT} \qquad (3)$$

In case of organic materials with $\varepsilon_r \cong 3.4$ (e.g. P3HT:PCBM blend [28]) this distance can be as large as 17 nm. The recombination rate is described by:

$$R = k_L(np - n_i^2) \cong k_L \cdot n^2 \qquad (4)$$

This is a second order recombination process depending on the concentrations of free electrons and free holes in the device. The recombination rate is linked to these concentrations through a recombination coefficient, k_L. Assuming equal electron and hole concentrations $n = p$, and neglecting the intrinsic charge concentration n_i, the recombination coefficient k_L can be written, in the framework of the Langevin model, as:

$$k_L = \frac{q}{\varepsilon}(\mu_h + \mu_e) \qquad (5)$$

where ε is the dielectric constant of the material and μ_h and μ_e are the hole and electron mobility, respectively. It is a very simple model considering recombination as a diffusive process in which the charges recombine when their distance is smaller than the coulomb radius (direct recombination).

1.3.3.2. Trap-assisted recombination

Lately, several papers reported a recombination order higher than two in P3HT:PCBM solar cells.[29-31] This phenomenon was explained in the framework of a trap-assisted recombination model,[17,20] where it is assumed that the recombination process is a second order bimolecular type, with a recombination coefficient k depending on the concentration of charges n:

$$k(n) = k_0 \cdot n^{\lambda-1} \qquad (6)$$

In this case we can write the recombination rate as:

$$R = k(n) \cdot n^2 \propto k_0 \cdot n^{\lambda+1} \qquad (7)$$

where $\lambda + 1$ is an empirical reaction order (the apparent recombination order) with respect to n, and k_0 is the constant part of the recombination coefficient.

The dependence of the recombination coefficient on the charge carrier concentration can be explained in the framework of the multiple trapping model.[17] The mobility depends on the charge carrier density because of the presence of a tail of trapped states inside the gap.[23,32] The charge transport in this kind of materials is due to hopping between localized states of the density of states. The total charge carrier concentration can be thought of as being composed in part of free charges and in part of trapped charges in the tail of the density of states. By assigning a constant mobility μ_0 to the free carriers and zero mobility to the trapped carriers, the average carrier mobility can be written, for electrons, as:[23,33]

$$\mu(n) = \mu_{0,e} \frac{n_{free}}{n_{free} + n_{trap}} = \mu_{0,e} \frac{n_{free}}{n_{tot}} \qquad (8)$$

Substituting Equation (8) in Equation (5) and using Equation (7), the recombination rate can be rewritten as:

$$\begin{aligned} R &\cong \frac{q}{\varepsilon}\left(\mu_h(p) + \mu_e(n)\right) \cdot n_{tot} \cdot p_{tot} \\ &= \frac{q}{\varepsilon}\left(\mu_{0,h} \cdot p_{free} \cdot n_{tot} + \mu_{0,e} \cdot n_{free} \cdot p_{tot}\right) \end{aligned} \qquad (9)$$

If $n_{trap} \gg n_{free}$, as might be the case under standard organic solar cells working conditions, we can approximate the previous equation as:[23]

$$R \cong \frac{q}{\varepsilon}\left(\mu_{0,h} \cdot p_{free} \cdot n_{trap} + \mu_{0,e} \cdot n_{free} \cdot p_{trap}\right) \qquad (10)$$

So recombination can be thought of as being dominated by free carriers recombining with trapped carriers. If we make the simplified assumption of a symmetric device (with equal hole and electron densities) and assume charge distributions like:[25,33]

$$n_{free} \propto e^{\frac{qV}{2k_BT}} \qquad (11)$$

$$n_{trap} \propto e^{\frac{qV}{2E_T}} = n_{free}^{\frac{k_BT}{E_T}} \qquad (12)$$

where $\mathrm{E_T}$ is the Urbach energy (the characteristic energy) of the exponential trap distribution, we can draw an expression of the apparent recombination order for the particular case of a symmetric device with an exponential distribution of trap states:[25]

$$R \propto n_{free} \cdot p_{trap} = n_{trap}^{\frac{E_T}{k_BT}+1} \propto n^{\lambda+1} \qquad (13)$$

The variation of the apparent recombination order between differently prepared devices most probably results from variations in the crystallinity of the photoactive layer causing different trap concentrations in these layers.[24,34-38]

This apparent recombination order should not be interpreted as a physical mechanism of recombination, but it gives a useful indication of the amount of traps in the device.[25,39]

1.4. Degradation of BHJ solar cells

Besides the power conversion efficiency the stability of organic solar cells (OSCs) is a critical factor which needs to be considered to successfully commercialize this technology. During the last years the interest in this field has grown significantly.[40,41] Traditionally, organic materials exhibit a modest stability. Their chemical resistance to oxygen in combination with UV/Vis light or high temperatures is limited.[42-48] Fullerene derivatives that are traditionally used as electron acceptor materials may delay the degradation of the electron donating polymer,[49,50] but BHJs based on polymer:fullerene blends have shown thermal instability of the active layer morphology. OSCs based on P3HT:PCBM have been widely investigated in terms of device stability and degradation. Among the failure mechanisms, photodegradation of the active layer forms the most complex stability problem. This process is sensitive to the presence of oxygen and water, as these stress factors can cause both photo-oxidation of the polymer as well as degradation at the interfaces of the device. In a study of photo and thermo-oxidation of P3HT, Manceau [51] showed that modifications of the chemical structure of P3HT occur during degradation, which results in the formation of numerous oxidized species affecting the properties of the materials. Another study by Hintz,[52] where samples were degraded under controlled atmospheric conditions (dry synthetic air and relative humidity < 2%), showed that illumination with wavelengths close to the absorption maximum of the polymer leads to a break in the π-conjugated system. Trap formation can be a major source of instability and deteriorate charge carrier mobility and exciton diffusion length.[53] Polymers exhibit a reversible *p*-type doping whose density increases upon exposure to air or moisture [54] due to charge reaction with oxygen in dark and under light exposure.[55-59] It has been shown [48] that P3HT:PCBM devices degraded under ambient air exposure exhibit a *p*-type doping of the blend, which was related to reaction of the active layer with oxygen. The doping concentration increased in the degraded sample, leading to a lowering of the charge carrier mobility and of the device performance.

Degradation of OSCs does not only depend on the organic materials but also on the device architecture. Currently, device lifetime is not only limited by photo-oxidation of the polymer or the fullerene but also by failures at the photoactive layer/electrodes interfaces. Indeed, Reese [60] reported that P3HT:PCBM active layers under prolonged illumination of 1000 h at 1 sun intensity and under inert conditions, without additional layers, exhibited no photo oxidation, in contrast to complete devices where the photodegradation is caused by charge collection layers and interfaces.[61]

1.5. Model material system: P3HT:PCBM solar cells

Polymer semiconductors can often have a semi-crystalline nature due to a relatively rigid π-conjugated backbone. They generally crystallize into one-dimensional (1-D) nanostructures, such as nanowires, via π-π interactions. The packing orientation, crystal morphologies, and relation between crystal growth direction and π-stacking directions are different among polymer materials. This suggests that molecular weight, side chain length, rigidity of chain backbone and crystal growth conditions (such as choice of solvent) all have an effect on the crystallization kinetics.

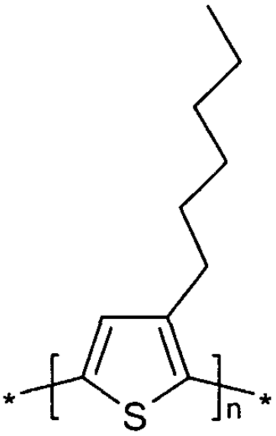

Figure 8 Poly(3-hexylthiophene-2,5-diyl) (P3HT)

P3HT crystallizes into nanofibers from dilute solutions in a poor solvent (i.e. *p*-xylene), in which the polymer dissolves only at elevated temperatures. The P3HT nanofibers exhibit an average width of 15-20 nm, a length of some μm, and a thickness of 4 nm, which corresponds to two or three P3HT chain layers (Figure 9).[62]

The charge carrier mobility in FET measurements from a single P3HT nanofiber has been reported to be as high as 0.07 cm^2/Vs,[63,64] which is comparable to that of thin P3HT films (~10^{-3} cm^2/Vs).

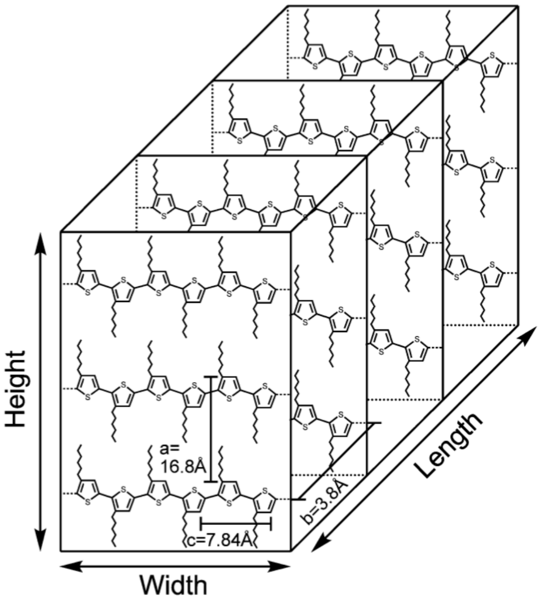

Figure 9 A typical P3HT fiber: the height is around 4 nm, the width around 15 nm and the length some μm [62]

P3HT chain folding in a nanofiber structure is expected because of the considerably greater contour length of P3HT (65 nm for MW=29 Kg/mol) than the fiber width (15 nm), despite the relatively rigid backbone of P3HT assumed to hamper chain folding. The lamellar thickness (i.e., fold length) varies with crystallization temperature, while the nanofiber width can be increased by raising crystallization temperature.

Results of more recent work [65] demonstrated that the dimensions of P3HT nanofibers can be controlled by varying the molecular weight and the concentration of the solutions. When the molecular weight of P3HT is less than a critical value (M_n ~10kDa), the width of P3HT nanofibers corresponds to the length of the extended polymer chain. For higher molecular weight, the width of the nanofibers remains constant about 15 nm, regardless of the increase in M_n (Figure 10).

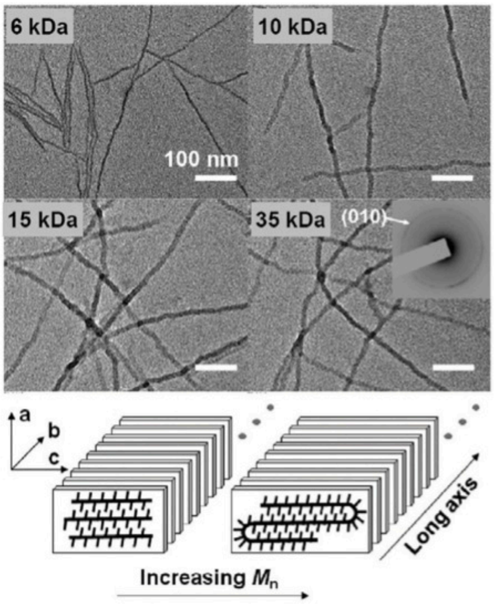

Figure 10 TEM images of P3HT nanofibers and schematic illustration of the extended and folded P3HT backbone packing prepared from low Mn (left) and high Mn (right)[65]

This result suggested that the conformation of P3HT chains in nanofibers begins to change from fully extended to folded at a critical M_n. Fiber formation, in dilute solution in a poor solvent (*p*-xylene), was found to be accompanied by molecular weight fractionation.[62] The M_n values of (redissolved) polymer from fibers had increased to 102–148% of their overall values, while those for non-aggregated polymer in solution had reduced to 33–58%. Due to this fractionation, also the polydispersity of the polymer fraction incorporated in the fibers reduced significantly for many of the polymers. The MW fractionation upon fiber formation indicates that high MW polymer chains tend to precipitate first. Increasingly lower MW material is then incorporated in the fibers until a certain lower MW boundary has been reached. It can be expected that besides a high MW also a high regioregularity (RR) of the individual polymer chain increases its tendency to precipitate.

Also alkyl side chain length affects poly(3-alkythiophene) (P3AT) properties. Conductivity decreases and solubility increases with increasing side-chain length. It was found that an increase in alkyl chain length reduces the overall energy barrier for fiber formation, inducing a strong increase in the vibrational structure.[62,66]

Also in a thin film, solvent vapor treatment produces nanofibers. Solvent annealed P3HT thin films exhibited a nanofiber structure (widths of ~ 20-22 nm and heights of 4-5 nm) and nanofiber length was controlled by solvent vapor pressure (0~56.5 kPa).[66,67] Polymer semiconductor thin films prepared by solution cast processes are composed of both polycrystalline and amorphous domains. Since charge transport in polymer semiconductor thin films is limited by amorphous regions, considerable efforts have been devoted to enhancing crystalline domains.

It has been reported that polymer crystallization is strongly dependent on molecular weight during the film forming process. In a paper from Chang [68] it is suggested that for the low MW, (MW<22 kD) with chain lengths shorter than the contour length, there is a higher statistical probability that one molecule is folded into a cross section perpendicular to the axis of the fiber, leading to defective crystals (Figure 11 (a)). In the intermediate MW group (29 kD–52 kD) the polymer chains are long enough that they can fold into lamellae without chain ends inside the crystals. In this regime the crystal quality of the fibers is expected to be highest with the lowest number of defect sites (Figure 11 (b)). Once the chain lengths significantly exceeds the contour length (MW>76 kD), the polymer chain needs to either reenter the same fiber at some distance along the axis of the fiber or fold into another fiber (Figure 11 (c)).

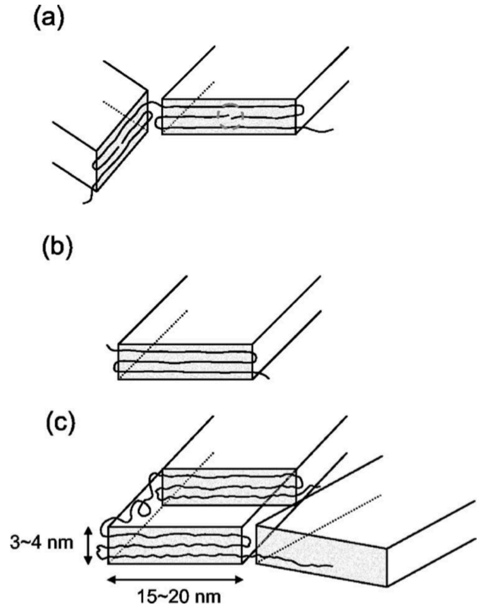

Figure 11 Fibers of P3HT for MW<22 kD (a), MW≈29 kD–52 kD (b) and MW>76 kD (c) [68]

In this way, the number of molecules linking different fibers is enhanced. On the other hand, the more pronounced polymer entanglement during growth, the possible presence of branches and the percentage of chain segments located on the disordered surface of fibers might lead to an overall higher degree of conformational disorder, producing chains containing kinks, bends, and twists. Consequently, the highest MW fibers are expected to have a lower crystal quality.

P3HT chain orientation in crystallites is affected by RR of the hexyl side chains. Two different orientations of the microcrystalline P3HT domains with respect to the substrate have been identified:[69]

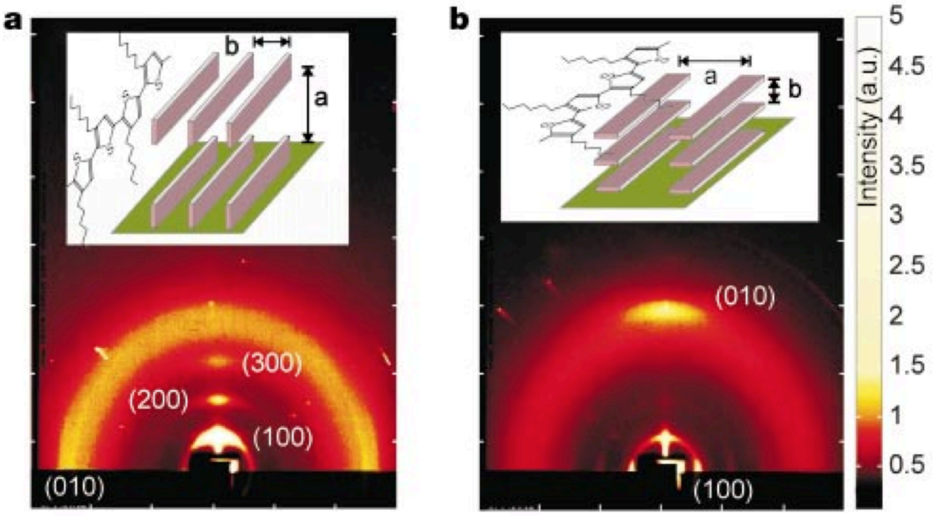

Figure 12 Two different orientations of ordered P3HT domains with respect to the substrate. The wide-angle X-ray scattering images are a colour representation of the two-dimensional distribution of scattered intensity from spin-coated, 70–100 nm thick P3HT films with regioregularity of 96% (a) and 81% (b). The vertical (horizontal) axes correspond to scattering normal (parallel) to the plane of the film. The insets show schematically the different orientations of the microcrystalline grains with respect to the substrate.[69]

They are evident from the different intensity distributions of the (100) reflections due to the lamella layer structure and the (010) reflections due to π–π interchain stacking. In samples with high regioregularity (>91%) the preferential orientation of ordered domains is with the (100)-axis normal to the film and the (010)-axis in the plane of the film (Figure 12 (a), edge on). In contrast, in samples with low regioregularity (81%), the crystallites are preferentially oriented with the (100)-axis in the plane and the (010)-axis normal to the film (Figure 12 (b), face on). The cause is not fully understood. In films prepared by slow casting from a dilute solution the (100)-axis is normal to the film for all polymers.

The highest Field Effect Transistor (FET) mobilities (0.05-0.1 cm^2/Vs) are observed for samples with the higher RR (96%) and the largest size of crystallites with in plane orientation of the (010) axis. For spin-coated samples with RR 81%, the FET mobility is only $2*10^{-4}$ cm^2/Vs. The FET mobility for casted films is more than one order of magnitude larger compared to spincoated films and only slightly lower than for high RR polymers. The large mobility anisotropy caused by different preferential orientations of the ordered, microcrystalline domains is a clear evidence that the transport is no longer dominated by the remaining amorphous regions of the polymer film but starts to reflect the transport properties of charge carriers in ordered polymer domains. The residual disorder in the films manifests itself in a thermally activated mobility at low temperatures. This is interpreted in terms of a distribution of disorder-induced, deeply localized states below the high-mobility electronic states at which charge transport occurs.[66]

1.6. Aims of the thesis

Improving efficiency and stability of organic solar cells, keeping the technology costs at a low side end, is the strongest driving force of current OPV research. Better understanding of the fundamental physical properties of organic solar cells is necessary to go further towards the commercialization of such devices. This thesis is focused on the study of crucial factors governing the photovoltaic parameters. **In particular, this work focuses on the non-geminate recombination of charge carriers, which has been proven to be one of the main loss pathways in organic solar cells.** The V_{OC} as well as the fill factor are mainly shaped by non-geminate recombination and by the relative weight of direct and trap-assisted recombination in the system studied.[70-73] It is of particular interest, therefore, to understand the mechanism influencing the recombination in solar cells to try, finally, to control and reduce it. In this work, the P3HT:PCBM bulk heterojunction system is studied as it is a well known model system with specific crystallization properties.

An important part of this work was the introduction of new measurement techniques in our lab to measure mobility and recombination. In particular I built up a setup allowing to perform several kind of measurements like Time of flight (TOF), Charge Extraction by Linearly Increasing Voltage (CELIV), Transient Photovoltage (TPV) and Transient Photocurrent (TPC).

The following **research questions** are addressed in this work:

I. *Is there a connection between the non-geminate recombination, the morphology of the active layer of solar cells and the amount of band gap trap states?*

II. *Which is the effect of changing the molecular weight of the donor polymer? How the photovoltaic parameters evolve? How is the crystallinity affected and how this reflects on non-geminate recombination?*

III. *What happens when a solar cell device is degraded under continuous light conditions and how does the degradation relate to the band gap trap states and recombination?*

IV. Can the description of recombination kinetics in fully organic bulk heterojunction solar cells be extended to hybrid organic:inorganic solar cells?

2. Experimental

In this chapter an overview is given of the techniques used to study recombination and mobility, followed by a description of the solar cell device preparation.

2.1. Description of the setup

Introducing new measurements techniques in our lab and building the setup to perform these measurements has been an important part of this work. The setup I built gives the possibility to make several kinds of measurements, Time of Flight (TOF), Charge Extraction by Linearly Increasing Voltage (CELIV), photo-CELIV, Transient Photovoltage (TPV), Transient Photocurrent (TPC). It could also be adapted to measure Double Injection Transient (DOI), Charge Extraction by Pulsed Voltage (CEPV) and Charge Extraction (CE). The schematic of the setup is shown in Figure 13.

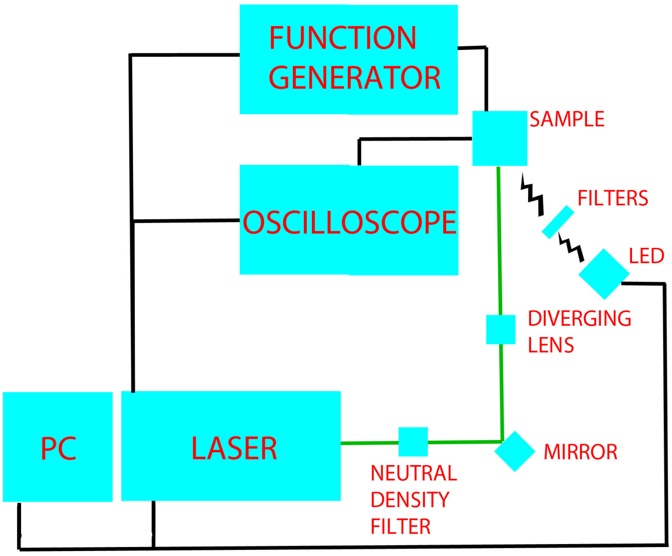

Figure 13 Schematic of the setup for CELIV, TPV and TPC

The function generator is a Tektronix AFG 3101, the digital oscilloscope is a Tektronix TDS 620B. They are both shown in Figure 14. Part of the experiments have been performed with a nanosecond tunable nitrogen pumped dye laser. Now, a pulsed Nd:Yag laser (Minilite I from Excel technology) is used with a second harmonic generator to obtain a wavelength of 532 nm. The light of the laser is attenuated with a neutral density filter and then a mirror reflects the beam into a diverging lens with a focal length of -9 mm to expand the beam (Figure 15). For TPV measurements a Light Emitting Diode (LED) producing white light (LZP-00CW00 from Led Engin) is used together with different neutral density filters to have different bias light intensity (Figure 16). The samples are kept in an aluminum sample holder filled with nitrogen and connected to the instruments with sma cables to reduce the environmental noise influence in measurements.

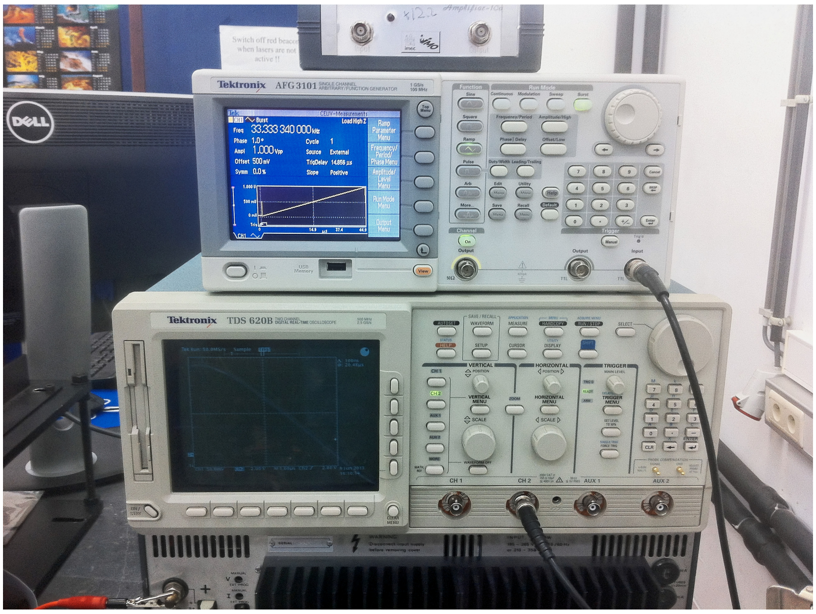

Figure 14 Function generator Tektronix AFG 3101 (above) and digital oscilloscope Tektronix TDS 620B (below).

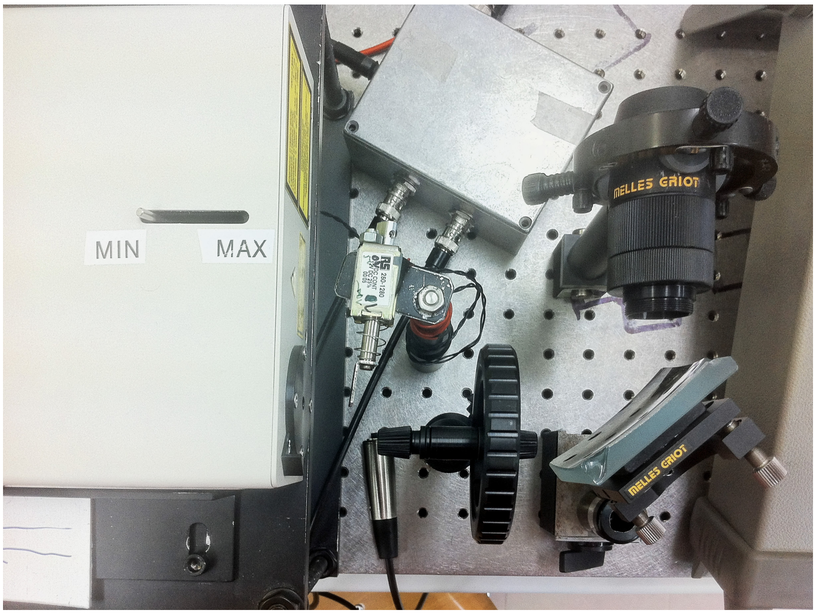

Figure 15 Laser Minilite I on the left, neutral density filter in the middle. The mirror on the right reflects the beam into the diverging lens on top right.

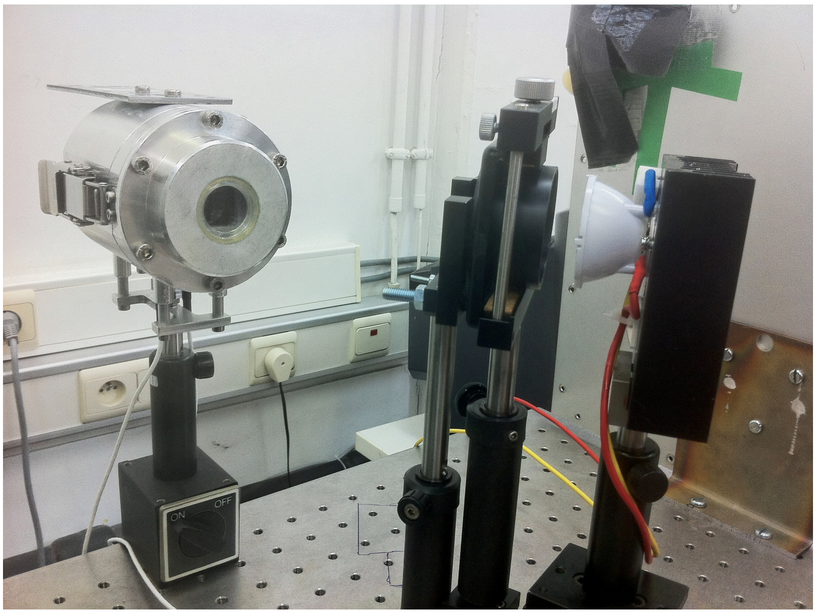

Figure 16 On the left the sample holder. On the right the LED with a focusing lens and the holder for the neutral density filters.

2.2. Measuring recombination and mobility

A description of the techniques used in this work to measure mobility and recombination is provided below.

2.2.1. Charge Extraction by Linearly Increasing Voltage (CELIV)

The CELIV technique was introduced by Juška in 2000.[74] At the beginning, it has been used to study the charge carrier mobility in microcrystalline silicon solar cells.[75] In fact, unlike other common techniques like Time of Flight (TOF), CELIV can be used in samples with high conductivity. Results obtained with CELIV were found to be in good agreement with TOF and other techniques.[76-79] It has also been shown that CELIV is suitable to measure mobility and charge carriers density relaxation in polymeric solar cells.[30,78,80-84]

For CELIV measurements we use the function generator and the digital oscilloscope. A synthetic scheme of the experiment is drawn in Figure 17. A linearly increasing voltage pulse is applied to the sample to extract the equilibrium charge carriers:

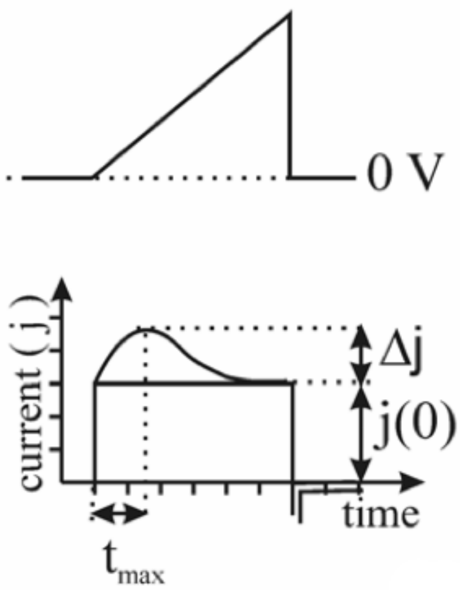

Figure 17 Schematic time diagram of a CELIV experiment[85]

The current response is monitored by the oscilloscope. At the beginning of the current transient a current step of amplitude j(0) is measured. A solar cell is an RC differentiating circuit. Therefore, at the beginning the current transient shows the derivative (a step) of the voltage input (a ramp). The following current increase Δj is related to the conductivity current caused by the transport of the equilibrium carriers in the film. The current continues to increase together with the voltage until the equilibrium carriers are extracted from the film and the current drops back to the capacitive step.

If the sample to measure is undoped, with low conductivity, a pumping light pulse is needed to photogenerate charges before extracting them with the voltage pulse (photo-CELIV). The light pulse is supplied by the laser. A synthetic scheme of the experiment is given in Figure 18**.**

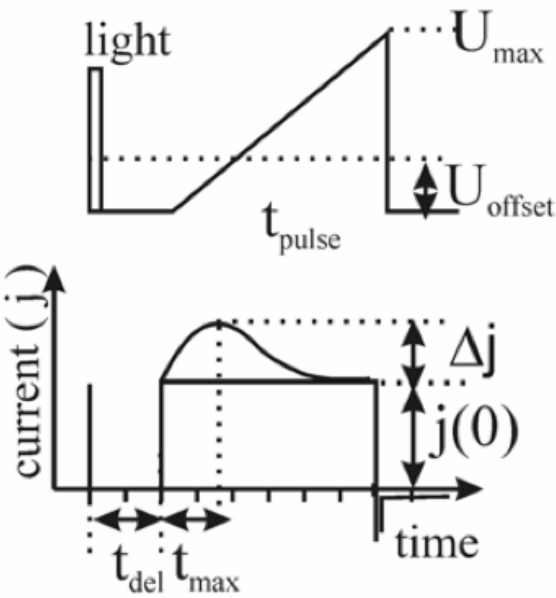

Figure 18 Schematic time diagram of a photo-CELIV experiment [85]

The voltage pulse starts after a delay time t_{del} from the laser pulse.

There are three different ways of extracting the mobility from the CELIV transient, depending on the material conductivity:

I. *Low conductivity ($\Delta j \ll j(0)$):*[74]

$$\mu = K\frac{t_{pulse}d^2}{U_{max}t_{max}^2} \qquad (14)$$

where K = 2/3 for volume and K = 2 for surface generation, t_{max} is the time when the current reaches its maximum, d is the thickness, t_{pulse} is the length of the voltage pulse and U_{max} is the maximum of the voltage pulse.

II. *High conductivity ($\Delta j \gg j(0)$):*

$$\mu = \frac{j(0)\; t_{pulse}d^2}{\Delta j\; U_{max}t_{max}^2} \qquad (15)$$

III. *Moderate conductivity ($\Delta j \approx j(0)$):*

$$\mu = \frac{t_{pulse}d^2}{U_{max}t_{max}^2\left(1 + 0.36\,{}^{\Delta j}\!/_{j(0)}\right)} \qquad (16)$$

where (1 + 0.36Δj/j(0)) is a numerically calculated correction factor.[80]

In the majority of the samples measured we were in the moderate conductivity case.

By varying the delay between the laser pulse and the voltage pulse, it is possible to measure simultaneously the time dependence of charge carrier mobility and the time dependence of charge carriers concentration, allowing therefore to study also recombination. By subtracting the dark current transient from the current transient recorded in light at different t_{del} followed by integration the difference in time, we get the charge carrier concentration n:

$$n = \frac{1}{ed}\int_0^{t_{pulse}} \left(j_{light}(t) - j_{dark}(t)\right) dt \qquad (17)$$

Analyzing the experimentally measured carrier concentration as a function of light delay time we obtain information about the non-geminate recombination in the measured time interval.

Despite the advantages of CELIV (possibility to measure samples with high conductivity, simultaneous measurement of mobility and recombination, possibility to measure the relaxation of mobility in time), there are also some limitations. At least one blocking contact is needed, otherwise the injected current from the electrodes would cover the characteristic current transient. Electric field dependencies are inaccurate as the voltage is constantly increasing during measurements. It is not possible to clearly relate the measured mobility to holes or electrons. It was proposed in the past that the CELIV mobility represents mainly the mobility of the fastest carrier,[85] while recently it has been proposed that CELIV is probing an ambipolar mobility and therefore the type of charges with the higher charge carrier density is the one that is probed (the hole in P3HT:PCBM solar cells).[86] In our experience, measurements done on P3AT:PCBM systems compare well with SCLC measurements on hole only diodes suggesting the CELIV mobility in this system probes mainly the hole mobility (Figure 19).

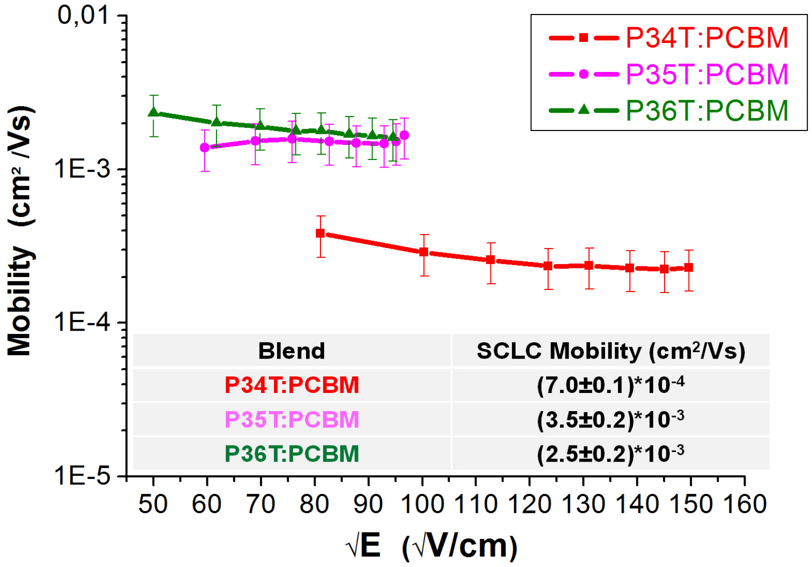

Blend	SCLC Mobility (cm^2/Vs)
P34T:PCBM	**(7.0±0.1)*10^{-4}**
P35T:PCBM	**(3.5±0.2)*10^{-3}**
P36T:PCBM	**(2.5±0.2)*10^{-3}**

Figure 19 CELIV and SCLC mobilities for three P3AT:PCBM systems

2.2.2. Transient Photovoltage (TPV) and Transient Photocurrent (TPC)

Transient Photovoltage (TPV) is an optoelectronic technique in which the device is held at open circuit under continuous illumination (light bias).[31,87,88] A weak laser light perturbation to the background illumination is then applied to the device and the resulting voltage transient is monitored (Figure 20). The main purpose of TPV measurements is to evaluate the charge carrier lifetime. The setup is the same as for CELIV with the only addition of the LED as light bias.

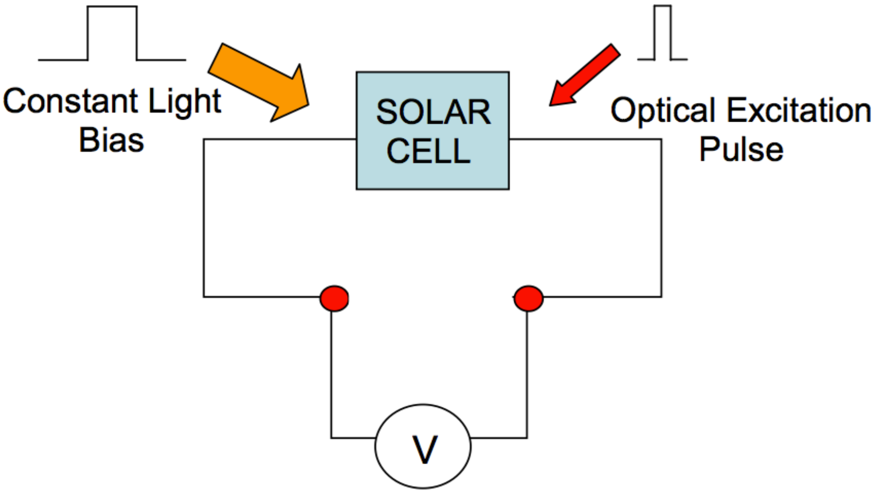

Figure 20 Schematic of a TPV setup [34]

During the measurement the devices are kept at open circuit while being illuminated with the LED light bias, the intensity of which is used to control the open circuit voltage V_{OC}. A small optical perturbation is applied using the laser with wavelength of 532 nm resulting in a voltage transient with an amplitude $\Delta V << V_{OC}$. In this way the measurements are carried out in the small perturbation regime with the transient showing the shape of a single exponential (pseudo first order behavior).[31,89] In this case the dependence of the small perturbation carrier lifetime on V_{OC} (varied by varying the bias light) is:[31]

$$\tau_{\Delta n} = \tau_{\Delta n_0} e^{-\beta V_{oc}} \qquad (18)$$

with $\tau_{\Delta n_0}$ the small perturbation lifetime for $V_{OC}=0$ and β a fitting parameter.

Transient Photocurrent (TPC) is used to obtain an estimate of the amount of additionally photogenerated charge carriers created due to the laser employed in TPV studies. The same small laser perturbation as for TPV delivers a current transient measured through the 50Ω entrance impedance of the oscilloscope, in dark (Figure 21). This TPC transient is then integrated over time to calculate the amount of photogenerated charges.

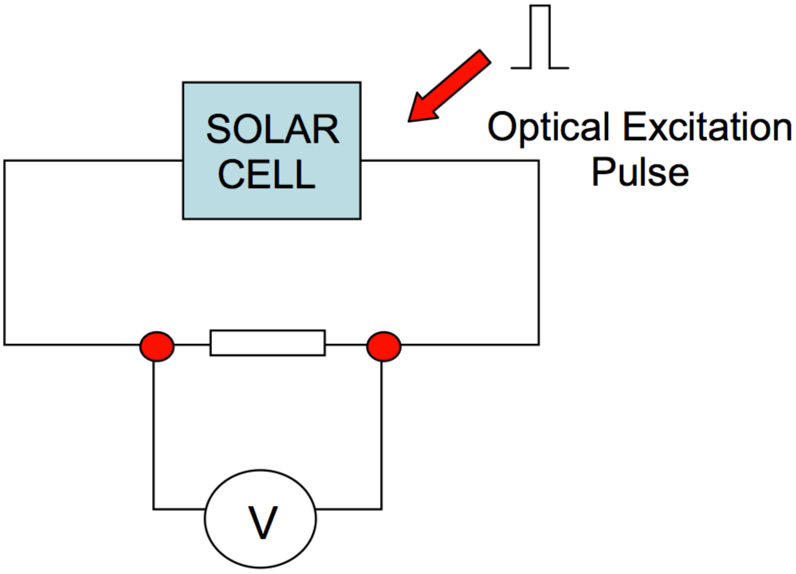

Figure 21 Schematic of a TPC setup [34]

Using the number of charges calculated in this way and using also the voltage transient amplitude coming from TPV allows to calculate the differential capacitance defined as C = ΔQ/ΔV, where ΔQ is the current integral. Using a differential charging technique it is possible to calculate the charge carrier concentration in the sample as:[31]

$$n = \frac{1}{Aqd}\int_0^{V_{oc}} CdV \tag{19}$$

where A is the device area, d is the device thickness. The dependence of charge carriers on V_{OC} is:

$$n = n_0 e^{\gamma V_{oc}} \tag{20}$$

where n_0 is the carrier concentration prefactor, and γ is a constant.

To find the relationship between small perturbation lifetime and charges density, which allows us to study the recombination, we start from the continuity equation for electrons in a solar cell:

$$\frac{dn}{dt} = -\frac{1}{q}\frac{dj_n}{dx} + G - R \tag{21}$$

where n is the electron concentration, q the elementary charge, j the electron current, G the generation rate and R the recombination rate. Measuring the recombination at open circuit using TPV, $1/q \cdot (dj_n/dx)$ is almost zero and cancels with the spatial derivative of the hole current. Therefore:

$$\frac{dn}{dt} = G - R \tag{22}$$

Linearizing Equation (22) and using Equation (7) the rate of decrease of the pulse-induced excess charge density can be expressed as:[90,91]

$$\frac{d\Delta n}{dt} \cong -\frac{dR}{dn} \cdot \Delta n = -k_0 \cdot (\lambda + 1) \cdot n^{\lambda} \cdot \Delta n \tag{23}$$

Therefore, the time evolution of Δn is exponential and the lifetime is given by $\tau_{\Delta n} = \left(\frac{dR}{dn}\right)^{-1}$ for each steady state. This implies, using Equation (23), Equation (22) and Equation (7):

$$\frac{dn}{dt} \cong \frac{d\Delta n}{dt} \cdot \frac{n}{\Delta n \cdot (\lambda + 1)} \tag{24}$$

which is a known result in the study of rate constants for higher order reactions.[31] By replacing Equation (18), Equation (19) and Equation (23) into Equation (24) we finally obtain:

$$\frac{dn}{dt} \approx -\frac{n^{\lambda+1}}{(\lambda + 1)\tau_{\Delta n_0} n_0^{\lambda}} \tag{25}$$

By integrating this expression, we get:[20]

$$t \cong \left(n^{-\lambda} - n_{t=0}^{-\lambda}\right) \cdot \frac{(\lambda + 1) \cdot \tau_{\Delta \mathrm{n}_0} \cdot n_0^{\lambda}}{\lambda} \propto n^{-\lambda} \tag{26}$$

representing the decay dynamic, where $n_{t=0}$ is the initial charge density. The recombination coefficient can be written as:[20]

$$k(n) \approx \frac{n^{\lambda-1}}{(\lambda + 1)\tau_{\Delta n_0} n_0^{\lambda}} \tag{27}$$

The value of -λ is readily accessible by taking the slope of the log-log plot of the small perturbation lifetime vs the charge density (Equation (26)). In the case of strictly Langevin recombination λ is expected to be 1. However, since in the presence of traps the recombination coefficient (Equation (27)) depends on the charge carrier concentration, slopes with λ > 1 are found.

2.3. P3HT fibers solar cell preparation

The morphology of the polymer, and therefore of the active layer, has a key role in the performance of organic solar cells. Since P3HT-based solar cell photovoltaic parameters depend on the fiber content of the solution, it is important to control this parameter. Our group developed a technique to obtain nanofibers in highly concentrated solutions, providing a controlled morphology directly upon deposition.[92]

For this procedure, P3HT is usually prepared via the Rieke method.[93] The regioregularity is typically >94% and the M_n is ~25 kg/mol (polydispersity index 1.8). P3HT fibers are prepared by slow cooling to room temperature of an heated, orange coloured solution of P3HT in *p*-xylene.[62] After the preparation of the P3HT fibers in the *p*-xylene solution, PCBM is added to the solution in a 1:1 weight ratio. The casting solution is stirred at room temperature to blend the two materials. Solar cells are prepared starting from indium tin oxide (ITO, 100 nm) coated glass plates, upon which ~30 nm of poly(3,4-ethylenedioxythiophene–polystyrenesulfonate) (PEDOT–PSS) is spin-coated. The active layer (P3HT:PCBM 1:1) is then spin-coated on top of the PEDOT–PSS layer. The solution from which the active layer is spin-coated, is heated gradually to a given temperature (between ~30 and ~60 °C) to vary the fiber content. At each temperature used for the experiment, the solution is left to stabilize for at least 30 minutes before the spin-coating of the active layer. Finally, a calcium layer (~25 nm) and an aluminum layer (~70 nm) are evaporated to form the top contact of the solar cell.[92]

At each solution temperature used to prepare a photovoltaic device, a small amount (1-2 drops) of the casting solution is isolated just after spin-coating and diluted in ~4 mL of *p*-xylene of the same temperature. UV–Vis measurements are performed on this highly diluted solution after cooling to room temperature. The obtained UV–Vis spectra are fitted as a sum of previously recorded spectra of PCBM, well-dissolved P3HT and fully fibrillar P3HT, all in *p*-xylene. The known relation between the latter two spectra has been used to determine the fiber content in the solution.[62,92] An example is given in Figure 22.

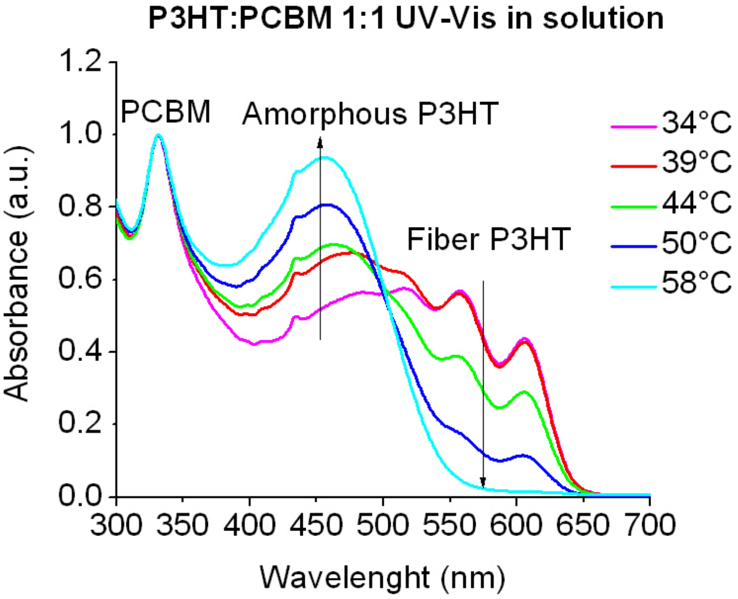

Figure 22 UV-vis spectra of P3HT fiber dispersions blended with PCBM at various temperatures

Because PCBM inhibits P3HT crystallization during spin coating,[94,95] and neither thermal annealing nor slow drying is applied, the fiber fraction in the solid-state spin-coated films can be approximated by the one determined by UV–Vis in dispersion.

2.4. Preparation of P3HT solar cells with different molecular weight

It has been proven that the molecular weight (MW) of the donor polymer in polymer:fullerene bulk heterojunction solar cells has an effect on the photovoltaic properties of devices based on poly(3-hexylthiopene) (P3HT).[68,96-110] However, the regioregularity (RR) as well as the polydispersity index (PDI) often strongly varies for the different MW P3HT samples. This does not allow to completely disentangle the effect of solely the MW on the photovoltaic properties. The RR in particular has proven to have a strong effect on the solar cell performance and needs to be controlled carefully.[38] The different polymer fractions are usually obtained through different synthesis processes or repetitive soxhlet extractions. We introduced recycling Gel Permeation Chromatography (r-GPC) [111] as a versatile technique to fractionate a single master batch of donor polymer in order to obtain a systematic variation of MW with an almost constant PDI and RR. In GPC the polymer is dissolved in a proper solvent and injected into a column containing porous beads. The pores capture the smaller polymer chains and hold them inside the column for a longer time compared to the bigger polymer chains. When the polymer chains exit the column, they pass through a detector. The detector data are compared whit a calibration sample with a known elution behavior according to the molecular weight. However it is also possible to fractionate a polymer batch with a higher resolution if the dissolved polymer is recycled (r-GPC) into the column since e.g. higher molecular weight fractions will exit the column more rapidly than the lower molecular weight fractions (Figure 23). The separated fractions are collected and measured against a calibrated sample afterwards. It’s important to note that the mechanical properties of the calibration standard (polystyrene) are not the same as P3HT which causes an overestimate of the determined molecular weight. r-GPC is however a very powerful technique to compare molecular weights at a relative scale.

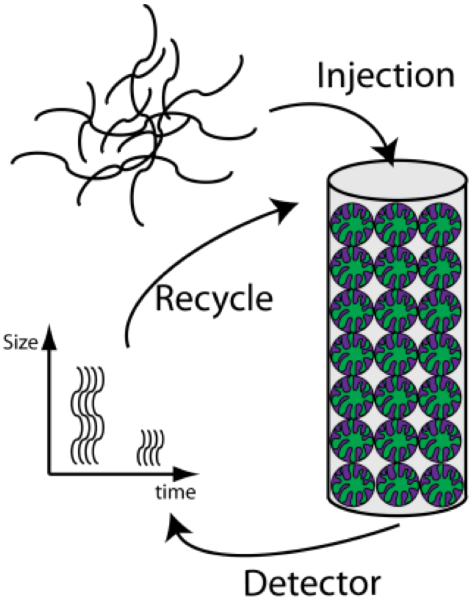

Figure 23 r-GPC working principle (courtesy Tim Vangerven).

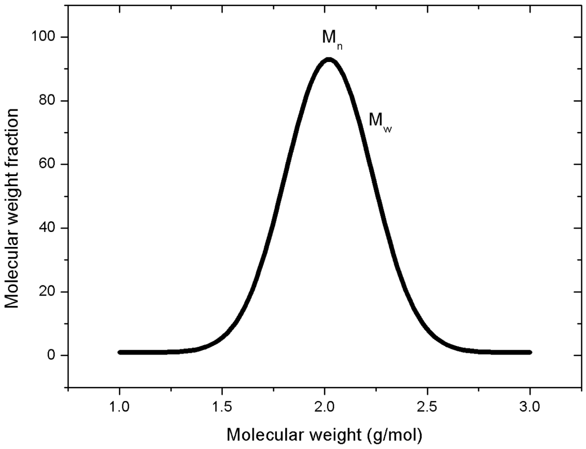

Figure 24 Number average molecular weight (M_n) and the weight average molecular weight (M_w)

The most important parameters which it is possible to determine with GPC are the number average molecular weight (M_n) and the weight average molecular weight (M_w). The M_n is the value for which there are an equal amount of molecules at the low and high molecular weight side. M_w illustrates the value at which there are equal masses of molecules at the high and low molecular weight side. The ratio between M_w and M_n is the polydispersity PDI. The formulas for M_w, M_n and PDI are:

$$M_w = \frac{\sum_i N_i {M_i}^2}{N_i M_i}\ ;\ M_n = \frac{\sum_i N_i M_i}{N_i}\ ;\ PDI = \frac{M_w}{M_n} \qquad (28)$$

Below the GPC graphs for the polymer fractions used in this work:

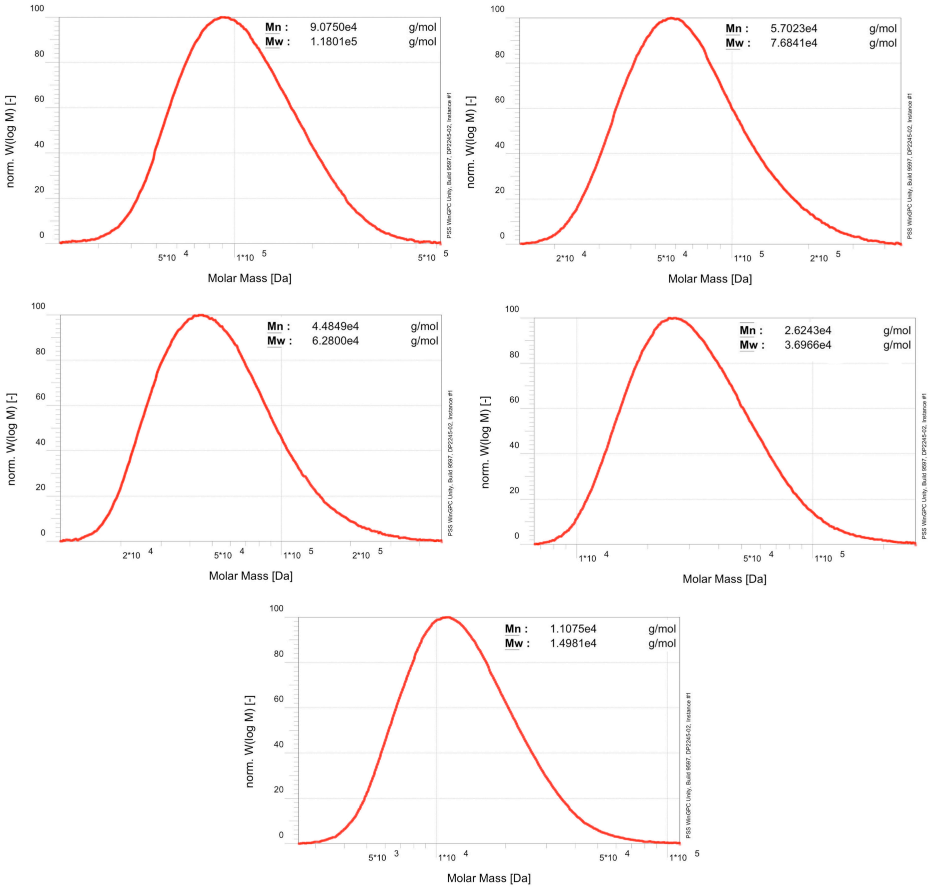

Figure 25 The five P3HT fractions used in this work

Solutions were prepared blending each polymer fraction with PCBM in a 1:1 ratio, in a 15 mg/mL concentration in *ortho*-dichlorobenzene (ODCB). The solar cells were prepared starting from indium tin oxide (ITO, 100 nm) coated glass plates that were successively cleaned in a soap solution, demineralized water and acetone, each for 10 min in an ultrasonic bath. This was followed by a cleaning step in boiling isopropanol for 10 min. A 30 nm thick poly(3,4-ethylenedioxythiophene)-polystyrenesulfonate (PEDOT–PSS) layer was spin-coated on the clean glass/ITO substrates. The substrates were dried for 20 min on a hot plate at 120 °C. The active layers were then spin-coated on top of the PEDOT–PSS layer and the spin speed was varied as such to keep the thickness constant at around 150 nm. The substrates were spin-coated for 20 s and slow dried for 1 h.

3. Main results

In this chapter the main results achieved are summarized in the form of a brief guide to the papers collected in the thesis addressing the following focus point:

I. *Is there a connection between the non-geminate recombination, the morphology of the active layer of solar cells and the amount of band gap trap states?*

II. *Which is the effect of changing the molecular weight of the donor polymer? What happens to the photovoltaic parameters? How is the crystallinity affected and how this reflects on non-geminate recombination?*

III. *What happens when a solar cell device is degraded under continuous light conditions and how does the degradation relate to the band gap trap states and recombination?*

IV. *Can the description of recombination kinetics in fully organic bulk heterojunction solar cells be extended to hybrid organic:inorganic solar cells?*

3.1. Focus point I: Effect of polymer crystallinity in P3HT:PCBM solar cells on band gap trap states and apparent recombination order

One of the main processes limiting solar cell performance is the non-geminate recombination of charge carriers. In recent years the recombination in a polymer-fullerene blend has been widely discussed in literature.[17-25] The Langevin model has been used, previously, to describe the non-geminate recombination process taking place in such solar cells.[26,27] It is a recombination process depending on the concentrations of free electrons and free holes in the device, being therefore bimolecular. Recently, several papers reported a recombination order higher than two in P3HT:PCBM solar cells.[29-31] This behavior was explained in the framework of the trap-assisted recombination model.[17,20] In this model the recombination coefficient, instead of being a constant as in the Langevin model, is assumed to depend on the concentration of charges. This is due to the dependence of the mobility on the charge carrier density caused by the presence of a tail of trapped states inside the gap.[23,32] The variation of the apparent recombination order between differently prepared devices most probably results from variations in the crystallinity of the photoactive layer causing different trap concentrations in these layers.[34] Although this assumption was derived from indirect studies on the effect of crystallinity on the recombination rate, there has been no systematic study linking the crystallinity of the active layer with the trap density and the recombination rate.[24,35-38]

Varying the temperature of a P3HT nanofiber casting dispersion, it is possible to consistently control the mass fraction f of highly crystalline nanofibrillar P3HT to the total P3HT content in the active layer of P3HT:PCBM solar cells.[92,112] This allowed us to make a systematic study of the apparent recombination order in function of the crystallinity of P3HT by means of TPV and TPC. The measurements have shown that the lower the crystallinity, the higher the apparent recombination order, as expected from the trap-assisted recombination model. In less crystalline P3HT, the concentration of traps is higher, most likely because of a shortening and a large variation of the conjugation length.[113,114] The reduction of the average conjugation length resulting from decreasing the P3HT fiber fraction in solar cell devices has been evidenced in a previous study from our group by a blue-shift of the charge-transfer absorption.[115] Noteworthy, even extrapolating the fit of the apparent recombination order vs fiber fraction, to a device with a fiber fraction of 1, the value of the slope does not reach the value of the recombination order expected in the absence of traps ($\lambda+1=2$). An explanation for this is that the fibers themselves are not completely crystalline. Since for the P3HT used in this study, a contour length l_n of 28 nm can be estimated, which is larger than the fiber width of ~20 nm [62] and also given the polydispersity of 1.80, many polymer chains incorporated into the fibers must give rise to dangling chain ends or chain folds for chains that are incorporated into the crystalline part of the fiber twice (or more). These chain folds and chain ends reduce the overall crystallinity of the fibers.[116] Following a study from Clark,[117] it is possible to estimate the crystalline part of P3HT fibers in *p*-xylene dispersion based on the UV–Vis absorption spectrum. This yielded a crystallinity of 65% for pure fibers dispersed in *p*-xylene. To get 100% crystalline polymer, a fiber fraction of

1.55 would be needed. Remarkably, the extrapolated recombination order is 2 at that same 1.55 fiber fraction, suggesting that if it would be possible to make completely crystalline P3HT (a single crystal), the recombination order would be two as in the Langevin model ($n_{free} > n_{trap}$). In practice, when we change the fiber fraction we are changing the relative weight of Langevin recombination and trap-assisted recombination in the solar cells.

To verify the hypothesis that the change in apparent recombination order is due to the change in the concentration of trap states inside the gap we performed admittance spectroscopy measurements [48,118,119] to investigate the density and energetic position of defect states within the gap of the absorber material. It is clear from the measurements that lower amounts of nanofibers induce a higher amount of defects. If we plot the apparent recombination order together with the integral of the traps as a function of crystallinity we obtain a correlation between the amount of fibers in the active layer, the apparent recombination order and amount of band gap traps.

For more details, check paper A included in the collection of papers: **D. Spoltore, W.D. Oosterbaan, S. Khelifi, J.N. Clifford, A. Viterisi, E. Palomares, M. Burgelman, L. Lutsen, D. Vanderzande, and J.V. Manca, *"Effect of Polymer Crystallinity in P3HT:PCBM Solar Cells on Band Gap Trap States and Apparent Recombination Order"* Advanced Energy Materials 3, 466 (2013)**

3.2. Focus point II: Effect of molecular weight on morphology and photovoltaic properties in P3HT:PCBM solar cells

After having studied the influence of different aggregation percentages in P3HT when used in a solar cell, we turned to study the effect of changing the molecular weight of the donor polymer: what happens to the photovoltaic parameters, how is the crystallinity affected and how this reflects on the non-geminate recombination.

Several studies have investigated the influence of varying MW on the photovoltaic properties of devices based on P3HT.[68,96-110] Schilinsky and coworkers varied the MW of P3HT from 2.2 to 11.3 kg/mol and found that higher molecular weight improves the performance of P3HT:PCBM based solar cells.[100] Hiorns et al. studied the variations in devices efficiency as a function of MW in the range 4.5 − 280 kg/mol,[101] finding the highest efficiency at an intermediate MW of M_n=14.8 kg/mol. Also, Ma and coworkers found an optimal photovoltaic performance at an intermediate value between M_n=13 kg/mol and M_n=62.5 kg/mol.[104] In contrast, Morana and coworkers obtained better efficiencies with high MW P3HT (M_n=160 kg/mol),[120] using chlorobenzene as solvent. Nicolet et al. performed an analysis of P3HT:PCBM phase diagrams showing the presence of an eutectic composition [108] and concluded that the higher the MW of P3HT, the higher the fraction of PCBM required to achieve optimal performance.

However, the regioregularity (RR) as well as the polydispersity index (PDI) often strongly varies for the different MW P3HT samples. This does not allow to completely disentangle the effect of solely the MW on the photovoltaic properties. The RR in particular has proven to have a strong effect on the solar cell performance and needs to be controlled carefully.[38] The different polymer fractions are usually obtained through different synthesis processes or repetitive soxhlet extractions. In the present work we introduce recycling Gel Permeation Chromatography (r-GPC) [111] as a versatile technique to fractionate a single master batch of donor polymer in order to obtain a systematic variation of MW with an almost constant PDI and RR.

Five fractions were prepared with differing MW (M_n=11 – 91 kg/mol) with an almost constant PDI and RR. Solar cells were made blending the different fractions with PCBM. We find that there is a strong correlation between MW and the photovoltaic properties. The open-circuit voltage (V_{OC}) increases with increasing M_n. This behavior is explained by measuring the energy of the charge transfer state (E_{CT}) with Fourier Transform Photocurrent Spectroscopy (FTPS). It has been shown in the past that there is a correlation between the E_{CT} and the V_{OC} of the solar cell.[121] The blue shift of E_{CT} with increasing M_n explain, therefore, the V_{OC} trend. In our attempts to link the observed change in E_{CT} as a function of MW to the film morphology, we find a correlation with the degree of crystallization of the polymer. The degree of polymer crystallinity is estimated by applying the Spano model [117,122-124] to the measured UV-visible spectra and performing Selected Area Electron Diffraction (SAED) and Rapid Heat Calorimetry (RHC) on the samples. The crystallinity of the polymer seems to increase going from high to low M_n with a maximum around 26 kg mol^{-1}. Also the short circuit current (J_{SC}) shows a clear trend with varying M_n, it increases with decreasing M_n. Charge Extration by Linearly Increasing

Voltage (CELIV), absolute absorption, photoluminescence and Transmission Electron Microscopy (TEM) measurements were performed in order to explain this trend. It is found that the reported trend in J_{SC} seems to be related to the increased absorption of lower M_n P3HT and to a higher phase separation in lower M_n improving the charge generation yeld. The apparent recombination order, which is linked to the morphology of the polymer:fullerene blend, is determined by using transient photovoltage (TPV) and photocurrent (TPC) techniques. Also the apparent recombination order shows a trend. It follows the crystallinity of the polymer fractions and seems to affect the fill factor. The charge density dependence of the recombination coefficient leads to different recombination current at different charge density (illumination) and therefore to different fill factors.[70,71,73] The minor trend observed in fill factor correlates with the apparent recombination order, reinforcing this view.

For more detail check the paper included in the collection of papers: **D. Spoltore, T. Vangerven, P. Verstappen, F. Piersimoni, S. Bertho, K. Vandewal, W. Maes, A. De Sio, L. Lutsen, D. Vanderzande, and J.V. Manca, *"Effect of molecular weight on morphology and photovoltaic properties in P3HT:PCBM solar cells"* Submitted to Advanced Energy Materials**

3.3. Focus point III: Effect of light induced degradation on electrical transport and charge extraction in polythiophene:fullerene solar cells

The stability of organic solar cells is a crucial parameter, as important as the efficiency. Extending the solar cell lifetime is fundamental to go toward the commercialization of these devices. A better understanding of the degradation mechanism is therefore necessary.

Herein, light induced device failure is investigated in standard devices ITO/PEDOT:PSS/P3HT:PCBM/Yb/Al kept in an inert nitrogen atmosphere. The samples were aged under continuous illumination with AM1.5 spectrum and 1 sun light intensity (constant temperature of 33°C-36°C) for different time durations in order to analyze the gradual degradation with advanced electrical characterization techniques. We observed two major electrical loss mechanisms in the P3HT:PCBM cells. First, the short-circuit current (J_{SC}) decreases abruptly in the first 250 h. Then, the loss in performance stabilizes until 900 h, when a second rapid decrease in performance sets in due to the reduction of fill factor (FF) (caused by the appearance of a S-shape in the current density-voltage (*J*-*V*) characteristic [61]).

To characterize the samples, External Quantum Efficiency (EQE), Fourier Transform Photocurrent Spectroscopy (FTPS), Charge Extraction by Linearly Increasing Voltage (CELIV), Transient Photovoltage and Photocurrent (TPV and TPC), Capacitance Voltage (C-V) and Admittance Spectroscopy (AS) measurements were performed in collaboration with Dr. S. Khelifi and Prof. M. Burgelman of UGent. Device modeling and simulation, performed by means of the software SCAPS (Solar Cell Capacitance Simulator),[48,125] led to deeper understanding of the lifetime-limiting mechanisms. Our electrical measurements could be reproduced with the fitting parameters provided mostly by the experimental data. The measurements and the modeling allowed us to attribute the first decrease to an increased *p*-type doping of the blend and a simultaneous increase of trap assisted recombination. This provoke a loss in the short-circuit current and in quantum efficiency by simultaneously reducing the charge carrier mobility and the electric field, due to a shrink of the space charge region. The reason for the origin of the increase in traps is still unclear. In a previous work we attributed this increase to an oxidation of the active layer.[48] It is worth mentioning that the acidic nature of PSS in the PEDOT:PSS layer could etch the ITO creating diffusion of indium, oxygen and other species into the active layer.[126,127] The presence of residual atmospheric gases, however, cannot be excluded even in inert atmosphere. The recombination current deduced from TPV and TPC measurements is higher in photo-degraded samples. The apparent recombination order can be deduced from the log-log plot of the small perturbation lifetime as a function of the charge density. From the slopes an apparent recombination order higher than two and increasing with the trap density in the band gap is reported, consistently with previous results.[128] The increase of recombination current delivers a loss in Voc. Increase in trap concentration to over 10^{15} cm^{-3} in aged cells leads to a decrease in V_{OC} of around 100 mV in agreement with the device measurements. To fully reproduce the V_{OC} degradation after 700 h illumination we also include the loss in the *CT* from 1.2 to 1.16 eV that might be related to morphological changes. Further decrease in V_{OC} after 1000 h is mainly caused by the appearance of the S-shape in the *J-V* characteristics. We used our model to assess the origin of the S-shape in the *J-V* graph of degraded cells. We attributed this characteristic feature to a reduced surface recombination velocity preventing a sufficient extraction/injection of carriers at the contacts.

In conclusion, we found that the photodegradation extended over a period of 1000 h following different stages. Until 250 h of illumination the devices exhibit an increase of *p*-type dopant concentration. We noted a tenfold increase of the deep trap density as detected by AS. Simultaneous alteration of these properties leads to non-homogenous electric field and explains the decrease in the short-circuit current and the EQE. The loss in V_{OC} is assigned to the increase of recombination due to traps together with a slight decrease in the CT after illumination ageing up to 700 h. Finally, we propose that the reduced surface recombination velocity at the cathode contact leads to the appearance of a kink in the *J-V* characteristic and to a strong reduction of the FF in our devices.

For more details check the paper included in the collection of papers: **S. Khelifi, E. Voroshazi, D. Spoltore, F. Piersimoni, S. Bertho, T. Aernouts, J. Manca, J. Lauwaert, H. Vrielinck, and M. Burgelman, *"Effect of light induced degradation on electrical transport and charge extraction in polythiophene:fullerene solar cells"* Submitted to Solar Energy Materials and Solar Cells**

3.4. Focus point IV: Generalized approach to the description of recombination kinetics in bulk heterojunction solar cells- extending from fully organic to hybrid solar cells

In this work it is demonstrated by means of impedance spectroscopy measurements under varying light intensity, a technique which delivers analogous results to TPV and TPC, that for hybrid solar cells based on ZnO nanorod arrays and P3HT, the mechanism that governs the V_{OC} is a strongly light intensity and charge carrier density dependent non-geminate recombination. Based on these results, it is shown that the approach used to describe recombination kinetics in P3HT:PCBM devices can be extended to hybrid solar cells. In order to clear up the analogy between hybrid and organic solar cells regarding recombination, we used a model developed for organic solar cells by the Durrant group. It is based on matching the flux of photogenerated charges with the flux of non-geminate recombination.[36] The total current in a solar cell can be considered as a sum of two contributions, namely the photocurrent (resulting from illumination) and, in opposite direction, the loss current.[36,129]

$$J(V) = J_{photo}(V) + J_{loss}(V) \tag{29}$$

The loss current J_{loss} can be estimated from the charge carrier density and lifetime under illumination:[36]

$$J_{loss} = ed\frac{n(V_{OC})}{\tau_n(V_{OC})} \tag{30}$$

Charge carrier density and lifetime are dependent on solar cell working conditions and they can be measured applying a small perturbation to a steady state.[130] The steady-state condition is varied changing the bias light applied on the cell, and therefore the V_{OC}. The small perturbation is given by the laser light in the case of TPV and TPC, while in impedance spectroscopy it is created by superimposing a small oscillating voltage Vac to the V_{OC}.[131] The relations between charge carrier density n and V_{OC} and small-perturbation lifetime τ and Voc therefore are the same as for TPV and TPC, Equation (18) and Equation (19). Inserting these two equations into Equation (30) and considering that the effective lifetime depends on the small-perturbation lifetime as $\tau_n = (1+\beta/\gamma)\tau_{\Delta n}$ [36,90] results in the following expression of the loss current:

$$J_{loss} = \frac{edn_0 e^{V_{OC}(\beta+\gamma)}}{(1+\beta/\gamma)\tau_{\Delta n_0}} \tag{31}$$

Taking into account that at open circuit conditions $J_{loss} \approx J_{SC}$ it is possible to derive an expression for V_{OC}:

$$V_{OC} = \frac{1}{(\beta+\gamma)} ln\left[\frac{(1+\beta/\gamma)\tau_{\Delta n_0} J_{SC}}{edn_0}\right] \tag{32}$$

Plotting n and τ as a function of V_{OC} and fitting n with Equation (19), we extract the values of n_0 and γ. Making a fit also for τ with Equation (19) it is possible to extract $\tau_{\Delta n_0}$ and β. Inserting these values in Equation (32) ultimately results in an independent prediction of V_{OC}, using exclusively the above mentioned circuit elements derived experimentally by means of impedance spectroscopy. This enables us to compare with V_{OC} values extracted directly from the corresponding J-V curves and, therefore, to test the applicability of the model to hybrid photovoltaic devices. The correlation between the measured and calculated values of V_{OC} was proven to be excellent, with an average deviation of 10 mV. This result gives strong confidence that the most essential concepts of recombination kinetics in organic photovoltaics are also valid in metal-oxide:polymer solar cells.

For more details, check the paper included in the collection of papers:

B. Conings, L. Baeten, H.-G. Boyen, D. Spoltore, J. D'Haen, M.K. Van Bael, and J.V. Manca, *"Generalized approach to the description of recombination kinetics in bulk heterojunction solar cells-extending from fully organic to hybrid solar cells"* Applied Physics Letters 100, 203905 (2012)

4. Summary and outlook

The general aim of this thesis work has been the study of the relation between morphology and recombination in polymer:fullerene solar cells, since both are crucial factors governing the photovoltaic parameters. The polymer:fullerene combination P3HT:PCBM has been chosen as the model system for this investigation since it is a well known material system and its morphology and crystallinity (e.g. fiber contents) can be varied.

Non-geminate recombination of charge carriers has received here particular attention as it has been proven, in the last years, to be one of the main loss pathways in organic solar cells. The open circuit voltage (V_{OC}) as well as the fill factor (FF) are mainly shaped by non-geminate recombination and by the relative weight of direct and trap-assisted recombination in the system studied.[70-72] In some polymer:fullerene blend it has been shown that the non geminate recombination is so strong to affect even the short circuit current (J_{SC}) while in P3HT based solar cells the sweep out of the charges is faster than recombination reducing the current loss for voltages close to zero.

To measure the mobility and the recombination behavior of solar cells, next to the already available measurement techniques at IMO, in this PhD-work several additional techniques have been introduced. For mobility measurements Charge Extraction by Linearly Increasing Voltage (CELIV) and photo-CELIV were introduced. They are relatively easy measurements to carry out but powerful as they allow the study of mobility in a real solar cell configuration. Other measurements techniques require to build samples with a different structure compared to a real solar cell (e.g. Space Charge Limited Current SCLC requires appropriate electrodes) or they provide the value of mobility in a different direction compared to the normal percolation path of a solar cell (e.g. Field Effect Transistor addresses planar transport instead of vertical transport). The main drawback of CELIV is that is not possible to assign the measured mobility to holes or electrons. A recent work assigned this mobility value to an ambipolar mobility (dominated by the main carrier). Our measurements on P3AT:PCBM systems compare well with SCLC measurements on hole only diodes suggesting the CELIV mobility in this system probes mainly the hole mobility.

To measure non-geminate recombination, Transient Photovoltage (TPV) and Transient Photocurrent (TPC) techniques were introduced, next to the above mentioned photo-CELIV. Using TPV and TPC is of particular interest as they are performed biasing the solar cell with a white light. This allows to probe the lifetime of carriers and the number of generated carriers at different quasi-Fermi level splitting.

Next to the general aim of the thesis formulated above, four specific research questions have been addressed in this work. In the following, from the experiments and the measurements performed, a summary is given of the answers obtained in this work to the formulated **research questions**:

I. *Is there a connection between the non-geminate recombination, the morphology of the active layer of solar cells and the amount of band gap trap states?*

By varying the mass fraction of highly crystalline nanofibrillar P3HT to the total P3HT content in P3HT:PCBM solar cells it has been possible to observe that decreasing the P3HT fiber fraction delivers a higher apparent recombination order. This phenomenon was assigned to the increasing of sub-band gap trap levels caused probably by a decreased conjugation length in less crystalline materials. The increase of the trap concentration was proved by admittance spectroscopy measurements. A correlation between the fraction of crystalline P3HT nanofibers, the apparent recombination order and the trap concentration in the band gap has been found. The apparent recombination order is higher than 2 also for a solar cell with a fiber fraction of 1. We suggested that this could be probably due to the lack of crystallinity of the fibers themselves, which was estimated to be 65%. The estimated degree of crystallinity of 65% for P3HT nanofibers suggests that within 100% crystalline P3HT the recombination order would be 2, a fully direct recombination with no trap assisted recombination contribution.

II. *Which is the effect of changing the molecular weight of the donor polymer? How do the photovoltaic parameters evolve? How is the crystallinity affected and how this reflects on non-geminate recombination?*

After having looked to the effect on recombination by changing the fiber content in P3HT:PCBM solar cells, we had a look to the effect of changing the molecular weight. Recycling GPC was used as a convenient technique to obtain different M_n polymer fractions from a single master batch of P3HT. The fractions showed an almost identical polydispersity and regioregularity, while in previous works it has been shown to be difficult to achieve this result. Therefore disentangling solely the effect of M_n in previous work was difficult as the influence of polydispersity and regioregularity was not fully taken into account. We saw in this work that varying M_n has an effect on the crystallinity of the polymer, delivering a red shift of E_{CT} with decreasing M_n. This shift has been proven to agree well with the shift in V_{OC}, supplying an explanation for the observed reduction of V_{OC} with decreasing the M_n. The M_n also affects the short circuit current delivered by the solar cells, mainly due to an increased light absorption for lower M_n P3HT, despite a decrease of CELIV mobility. The apparent recombination order follows the crystallinity of the polymer fraction and seems to affect the fill factor. The charge density dependence of the recombination coefficient leads to different recombination current at different charge density (illumination) and therefore to different fill factors.

III. *What happens when a solar cell device is degraded under continuous light conditions and how does the degradation relate to the band gap trap states and recombination?*

The stability of organic solar cells is a critical factor which needs to be considered in view of a future commercialization of this technology. We investigated the photo-degradation mechanisms under inert atmosphere of P3HT:PCBM solar cells, keeping an eye on the role of non-geminate recombination. We found that over a period of 1000 h the photo-degradation has different stages. In the first 250 h of illumination the devices exhibited an increase of *p*-type dopant concentration and a tenfold increase of the trap density. The alteration of these properties leads to a decrease of the mobility and a non-homogenous electric field, explaining the decrease in the short circuit current. The apparent recombination order starts to increase, probably due to the increased traps density and therefore of the trap assisted recombination causing a loss in V_{OC}. A rather stable zone for device properties and electron transport parameters follows until 700 h illumination. After this period the fill factor strongly reduces attributed to the reduced surface recombination velocity at the contacts.

IV. Can the description of recombination kinetics in fully organic bulk heterojunction solar cells be extended to hybrid organic:inorganic solar cells?

Making use of impedance spectroscopy measurements under varying light intensity we proved that for hybrid solar cells based on ZnO nanorod arrays and P3HT, the mechanism governing the V_{OC} is non-geminate recombination. The same approach used to describe recombination kinetics in fully organic P3HT:PCBM devices can be generalized and extended to hybrid solar cells. The working principles of photo excitation and recombination in hybrid solar cells seems the same as the one found for the model system P3HT:PCBM. This finding is achieved by extracting voltage dependent charge carrier densities and lifetimes by means of impedance spectroscopy, used as input parameters for a recombination model developed for purely organic solar cells. The predicted values for V_{OC} are accurate, therefore it is possible to extend the validity of the recombination model towards hybrid solar cells and, consequently, towards a more general applicability.

There are still a lot of research questions to address in the field of organic photovoltaic. In the last years, models have been presented to describe the non-geminate recombination in organic bulk heterojunction solar cells deriving from amorphous semiconductors. These models take into account the recombination of free with trapped charge carriers, beyond the recombination of free with free charges. The trapped charges are usually modeled with an exponential tail of trapped states tailing in the bandgap, like the simple model presented in paragraph 1.3.3.2. Anyway the real shape of these trapped states is still unclear. Gaussian distribution have been proposed as well as a combination of exponential and Gaussian distributions.[132] The shape of trap states density influences the apparent recombination order. It is important, therefore, to know this shape and to know the way the morphology of the film influence the shape, in order to control non-geminate recombination. It has been proposed, also, that the high recombination order cannot be explained solely by the charge carrier concentration dependent charge carrier mobility. If a charge carrier is trapped within one material phase far from the interface between the two phases, it has to be first released before it can recombine. The latter is an energy activated process and leads to a delay in recombination.[133,134] This delay results in the experiment as a reduced charge carrier decay in time and hence in an increased charge carrier recombination order. It is important to know if this phenomenon is present in organic BHJ.

The charge transfer state is commonly indicated as the intermediate state for two charges when they recombine. Therefore absorption/emission from this state is connected with the non-geminate recombination.

Quantitative investigations on the origin and impact of radiative and non-radiative recombination on the solar cell performance have been started only recently. It is, therefore, still an open field interesting to investigate to finally improve the devices performance.

Regarding the degradation of solar cells, it has been shown in our institute that PCBM in solar cells dimerize under illumination. This effect counteracts the phase segregation of P3HT and PCBM when exposed to thermal degradation. This phenomenon was not taken into account before and needs to be studied. In particular, in the framework of this thesis work, it would be interesting to study its influence on non-geminate recombination.

5. Nederlandse samenvatting

Het centrale thema doorheen dit werk is de relatie tussen de morfologie en recombinatie in polymeer:fullereen zonnecellen, aangezien beide verantwoordelijk zijn voor de prestaties van de zonnecel. Het polymeer:fullereen systeem, P3HT:PCBM, is gekozen als model systeem in dit onderzoek omdat het een wel gekend materiaal is en het ook een variatie van de morfologie en kristalliniteit (bv. nanovezel gehalte) toelaat. Gedurende de laatste jaren is de aandacht voor *non-geminate* recombinatie van ladingsdragers sterk toegenomen aangezien dit type van recombinatie grote verliezen in de performantie van zonnecellen veroorzaakt. Fotovoltaïsche parameters zoals de open-klem spanning (V_{oc}) en de vulfactor (*FF*) zijn sterk afhankelijk van *non-geminate* recombinatie en de verhouding van directe en *trap-assisted* recombinatie in P3HT:PCBM zonnecellen. [70-72] Voor sommige polymeer:fullereen systemen is aangetoond dat het effect van *non-geminate* recombinatie zo sterk is dat ook de kortsluitstroomdichtheid (J_{sc}) beïnvloed wordt. In P3HT gebaseerde zonnecellen vindt de extractie van de ladingen op een veel kortere tijdsschaal plaats dan de recombinatie, waardoor het verlies in stroomdichtheid verminderd wordt voor spanningen dicht bij het nulpunt. Dit werk introduceert, naast de reeds bestaande meettechnieken op IMO, verschillende nieuwe meettechnieken om de mobiliteit en het recombinatiegedrag van zonnecellen in kaart te brengen. *Charge Extraction by Linearly Increasing Voltage* (CELIV) en *photo*-CELIV zijn 2 technieken die geïntroduceerd werden. Deze technieken zijn relatief eenvoudig qua opbouw maar ontzettend krachtig, omdat ze toelaten de mobiliteit in een volledig werkende zonnecel op te meten. Andere meettechnieken vereisen namelijk een specifieke configuratie waarbij afgeweken moet worden van de werkelijke zonnecel-opbouw (bv. *Space Charge Limited Current* (SCLC) vereist speciale selectieve elektrodes) of de gemeten mobiliteitswaarde is voor ladingen die zich niet in de correcte richting verplaatsen zoals dat gebeurt in een echte zonnecel (bv. *Field Effect Transistor* (FET)-metingen meten enkel het planaire transport in plaats van het transport in de verticale richting). Het grootste nadeel van CELIV is dat het niet mogelijk is om de gemeten mobiliteit toe te wijzen aan positieve (gaten) of negatieve (elektronen) ladingen. Een recente studie kende deze mobiliteit toe aan een ambipolaire mobiliteit welke gedomineerd wordt door de ladingsdrager die het sterkst aanwezig is in het materiaal. Onze metingen op P3AT:PCBM systemen zijn zeer vergelijkbaar met SCLC metingen op *hole-only*-diodes, wat suggereert dat we met CELIV vooral de gatenmobiliteit meten. Om de *non-geminate* recombinatie te onderzoeken werden, buiten photo-CELIV, ook nog *Transient Photovoltage* (TPV) en *Transient Photocurrent* (TPC) geïntroduceerd. Deze technieken laten toe om de zonnecel te bestuderen onder invloed van een wit licht bias. Hierdoor is het mogelijk de levensduur alsook de generatie van de ladingsdragers te analyseren voor verschillende quasi-Fermi niveaus. Naast het algemene onderzoeksthema dat eerder werd geformuleerd, zijn vier onderzoeksvragen opgesteld. In de onderstaande paragrafen wordt een samenvatting gegeven van de experimenten en metingen met betrekking tot de **onderzoeksvragen:**

I. Is er een correlatie tussen non-geminate recombinatie, de morfologie van de actieve laag in de zonnecel en de hoeveelheid van "trap" toestanden in de bandkloof?

Variatie van de massa fractie van hoog kristallijn nanovezel gebaseerd P3HT met respect tot de totale P3HT inhoud in P3HT:PCBM zonnecellen, heeft tot een verschil in schijnbare recombinatie orde geleid. Vermindering van de P3HT vezel fractie leidt tot een hogere schijnbare recombinatie orde. Dit fenomeen werd toegeschreven aan een toename van de sub-bandkloof *trap* niveaus die waarschijnlijk veroorzaakt wordt door een afname in de conjugatie lengte in minder kristallijne materialen. De toename van de *trap* concentratie werd aangetoond met admittantie spectroscopie. Een correlatie tussen de fractie van de kristallijne P3HT nanovezels, de schijnbare recombinatie orde en de *trap* concentratie in de bandkloof werd gevonden. De schijnbare recombinatie orde is hoger dan 2, zelfs voor een zonnecel met een vezelfractie van 1. Wij suggereren dat dit te wijten is aan de kristalliniteit van de vezels zelf, welke volgens schattingen ongeveer 65% bedroeg. De geschatte graad van kristalliniteit van 65% voor P3HT nanovezels impliceert dat voor 100% kristallijne P3HT de directe recombinatie orde 2 zou moeten zijn, welke volledig gerelateerd is aan directe recombinatie met geen contributie van *trap assisted* recombinatie.

II. Wat is het effect van het moleculair gewicht van het donor polymeer op de fotovoltaïsche parameters en hoe wordt de kristalliniteit hierdoor beïnvloed? Wat gebeurt er met de non-geminate recombinatie indien het moleculaire gewicht aangepast wordt?

Nadat het effect van de hoeveelheid vezels onderzocht werd op recombinatie in P3HT:PCBM zonnecellen, is de invloed van het moleculaire gewicht bestudeerd. We hebben recyclerende gel permeatie chromatografie (r-GPC) gebruikt om verschillende M_n fracties te bekomen waarbij we vertrokken van één grote *master batch*. Belangrijk om op te merken is dat de fracties een zo goed als constante polydispersiteit en regioregulariteit vertoonden, terwijl uit verschillende studies in het verleden bleek dat dit zeer moeilijk te verkrijgen was. Daarom was het in het verleden ook zeer moeilijk om het effect van moleculair gewicht volledig los te kunnen maken van de invloed van de polydispersiteit en de regioregulariteit. In ons werk was er een duidelijk effect op de kristalliniteit van het polymeer, met een roodverschuiving van E_{CT} voor afnemend M_n. Deze verschuiving werd succesvol gecorreleerd met de verschuiving in V_{oc}, waardoor een verklaring gegeven kan worden aan de geobserveerde vermindering van V_{oc} met afnemend M_n. Het M_n beïnvloedt ook de kortsluitstroom-dichtheid van de zonnecel, wat verklaard kan worden door een verhoogde absorptie voor het lager M_n, ondanks een lagere CELIV mobiliteit. De schijnbare recombinatie orde volgt de kristalliniteit van de polymeerfractie en lijkt een invloed te hebben op de FF. De afhankelijkheid van de ladingsdichtheid op de recombinatie coëfficiënt leidt tot verschillende recombinatie stroomdichtheden voor verschillende ladingsdichtheden (onder belichting) en daarom tot andere vulfactoren.

III. Wat gebeurt er wanneer een zonnecel verouderd wordt onder continue lichtinval en in welke mate is degradatie gerelateerd aan "trap" toestanden en recombinatie?

De stabiliteit van organische zonnecellen is een kritische factor waar voldoende aandacht aan besteed dient te worden indien deze technologie commercieel wil doorbreken. We hebben de fotodegradatie mechanismen van P3HT:PCBM zonnecellen in een inerte atmosfeer onderzocht waarbij we nadrukkelijk op zoek gingen naar de rol van *non-geminate* recombinatie. De cellen werden verouderd over een periode van 1000 uren, waarbij opgemerkt werd dat de fotodegradatie doorheen verschillende fasen gaat. De zonnecellen vertoonden in de eerste 250 uren van belichting een toename van de *p-type* dopering concentratie en een tienvoudige toename in *trap* dichtheid. De verandering van deze eigenschappen leidt tot een afname van de mobiliteit en een niet-homogeen elektrisch veld, wat een verklaring biedt voor de vermindering van de stroom. De schijnbare recombinatie orde neemt hoogstwaarschijnlijk toe door de toenemende *trap* densiteit waardoor de *trap assisted* recombinatie toeneemt en verliezen veroorzaakt in V_{oc}. Tot ongeveer 700 uren belichting blijven de parameters van de zonnecel zeer stabiel, maar na deze periode wordt de FF sterk gereduceerd wat toegewezen kan worden aan de verminderde oppervlakte recombinatie snelheid aan de contacten.

IV. Is de beschrijving van de kinetiek van het recombinatiemechanisme in organische zonnecellen uitbreidbaar naar hybride organische:anorganische zonncellen?

We hebben impedantie spectroscopie onder variërende lichtintensiteiten gebruikt om aan te tonen, dat voor hybride zonnecellen (gebaseerd op arrays van ZnO nanostaafjes en P3HT), V_{oc} bepaald wordt door *non-geminate* recombinatie. De methode, die beschreven wordt voor de recombinatie kinetiek te bestuderen van volledig organische P3HT:PCBM zonnecellen, kan gebruikt en uitgebreid worden naar hybride zonnecellen. De werkingsprincipes voor de foto-excitatie en recombinatie in hybride zonnecellen lijken er hetzelfde uit te zien als voor het model systeem, P3HT:PCBM. Deze stelling wordt geargumenteerd door de spanningsafhankelijke ladingsdichtheid en levensduur te bepalen met impedantie spectroscopie, welke vervolgens gebruikt worden als *input* parameters voor een recombinatie model, dat zuiver ontworpen werd voor organische zonnecellen. De voorspelde waardes van V_{oc} zijn zeer accuraat, waardoor het recombinatie model ook toegepast kan worden voor hybride zonnecellen en dus ook algemeen toepasbaar is.

References

[1] M.A. Green, K. Emery, Y. Hishikawa, W. Warta, E.D. Dunlop, Solar cell efficiency tables (version 41), Prog. Photovolt: Res. Appl. 21 (2012) 1–11.

[2] http://www.nrel.gov/ncpv/images/efficiency_chart.jpg

[3] H. Akamatu, H. Inokuchi, Y. Matsunaga, Electrical conductivity of the perylene-bromine complex, Nature. 173 (1954) 168-169.

[4] G.A. Chamberlain, Organic solar cells: A review, Solar Cells. 8 (1983) 47–83.

[5] L. Sebastian, G. Weiser, One-dimensional wide energy bands in a polydiacetylene revealed by electroreflectance, Phys. Rev. Lett. 46 (1981) 1156–1159.

[6] C.W. Tang, Two-layer organic photovoltaic cell, Appl. Phys. Lett. 48 (1986) 183.

[7] N.S. Sariciftci, L. Smilowitz, A.J. Heeger, F. Wudl, Photoinduced electron transfer from a conducting polymer to buckminsterfullerene, Science. 258 (1992) 1474.

[8] C. Deibel, V. Dyakonov, Polymer–fullerene bulk heterojunction solar cells, Rep. Prog. Phys. 73 (2010) 096401.

[9] S.E. Shaheen, C.J. Brabec, N.S. Sariciftci, F. Padinger, T. Fromherz, J.C. Hummelen, 2.5% efficient organic plastic solar cells, Appl. Phys. Lett. 78 (2001) 841.

[10] F. Padinger, R. Rittberger, N. Sariciftci, Effects of postproduction treatment on plastic solar cells, Adv. Funct. Mater. 13 (2003) 85–88.

[11] J. Xue, B.P. Rand, S. Uchida, Mixed donor-acceptor molecular heterojunctions for photovoltaic applications. II. Device performance, Journal of Applied Physics 98 (2005) 124903–1 – 124903–9.

[12] J. Peet, J.Y. Kim, N.E. Coates, W.L. Ma, D. Moses, Efficiency enhancement in low-bandgap polymer solar cells by processing with alkane dithiols, Nature Materials. 6 (2007) 497–500.

[13] S.H. Park, A. Roy, S. Beaupré, S. Cho, N. Coates, J.S. Moon, et al., Bulk heterojunction solar cells with internal quantum efficiency approaching 100%, Nature Publishing Group. 3 (2009) 297–302.

[14] I.W. Hwang, D. Moses, A.J. Heeger, Photoinduced Carrier Generation in P3HT/PCBM Bulk Heterojunction Materials, J. Phys. Chem. C. 112 (2008) 4350–4354.

[15] H. Bässler, Charge transport in disordered organic photoconductors a Monte Carlo simulation study, Phys. Status Solidi B. 175 (1993) 15–56.

[16] S. Baranovski, Charge Transport in Disordered Solids with Applications in Electronics, Wiley, 2006.

[17] J. Nelson, Diffusion-limited recombination in polymer-fullerene blends and its influence on photocurrent collection, Phys. Rev. B. 67 (2003) 155209.

[18] A. Pivrikas, G. Juška, A. Mozer, M. Scharber, K. Arlauskas, N. Sariciftci, et al., Bimolecular Recombination Coefficient as a Sensitive Testing Parameter for Low-Mobility Solar-Cell Materials,

Phys. Rev. Lett. 94 (2005).

[19] G. Juška, G. Sliaužys, K. Genevičius, K. Arlauskas, A. Pivrikas, M. Scharber, et al., Charge-carrier transport and recombination in thin insulating films studied via extraction of injected plasma, Phys. Rev. B. 74 (2006) 115314.

[20] C.G. Shuttle, B. O'Regan, A.M. Ballantyne, J. Nelson, D. Bradley, J.R. Durrant, Bimolecular recombination losses in polythiophene: Fullerene solar cells, Phys. Rev. B. 78 (2008) 113201.

[21] C. Deibel, A. Wagenpfahl, V. Dyakonov, Origin of reduced polaron recombination in organic semiconductor devices, Phys. Rev. B. 80 (2009) 075203.

[22] R. Hamilton, C.G. Shuttle, B. O'Regan, T.C. Hammant, J. Nelson, J.R. Durrant, Recombination in Annealed and Nonannealed Polythiophene/Fullerene Solar Cells: Transient Photovoltage Studies versus Numerical Modeling, J. Phys. Chem. Lett. 1 (2010) 1432–1436.

[23] R.C.I. MacKenzie, T. Kirchartz, G.F.A. Dibb, J. Nelson, Modeling Nongeminate Recombination in P3HT:PCBM Solar Cells, J. Phys. Chem. C. 115 (2011) 9806–9813.

[24] S.R. Cowan, W.L. Leong, N. Banerji, G. Dennler, A.J. Heeger, Identifying a Threshold Impurity Level for Organic Solar Cells: Enhanced First-Order Recombination Via Well-Defined PC84BM Traps in Organic Bulk Heterojunction Solar Cells, Adv. Funct. Mater. 21 (2011) 3083–3092.

[25] T. Kirchartz, B. Pieters, J. Kirkpatrick, U. Rau, J. Nelson, Recombination via tail states in polythiophene:fullerene solar cells, Phys. Rev. B. 83 (2011) 115209.

[26] P. Langevin, Recombinaison et Mobilités des Ions dans les Gaz, Ann. Chim. Phys. 28 (1903) 433–530.

[27] M. Pope, C.E. Swenberg, Electronic processes in organic crystals and polymers, Oxford University Press, New York, NY, USA, 1999.

[28] M. Knipper, J. Parisi, K. Coakley, C. Waldauf, C.J. Brabec, V. Dyakonov, Impedance Spectroscopy on Polymer-Fullerene Solar Cells, Zeitschrift Fur Naturforschung a-Journal of Physical Sciences. 62 (2007) 490–494.

[29] G. Juška, K. Genevičius, N. Nekrasas, G. Sliaužys, G. Dennler, Trimolecular recombination in polythiophene: fullerene bulk heterojunction solar cells, Appl. Phys. Lett. 93 (2008) 143303.

[30] C. Deibel, A. Baumann, V. Dyakonov, Polaron recombination in pristine and annealed bulk heterojunction solar cells, Appl. Phys. Lett. 93 (2008) 163303.

[31] C.G. Shuttle, B. O'Regan, A.M. Ballantyne, J. Nelson, D.D.C. Bradley, J. de Mello, et al., Experimental determination of the rate law for charge carrier decay in a polythiophene: Fullerene solar cell, Appl. Phys. Lett. 92 (2008) 093311.

[32] C.G. Shuttle, R. Hamilton, J. Nelson, B.C. O'Regan, J.R. Durrant, Measurement of Charge-Density Dependence of Carrier Mobility in an Organic Semiconductor Blend, Adv. Funct. Mater. 20 (2010) 698–702.

[33] J.C. Blakesley, D. Neher, Relationship between energetic disorder and open-circuit voltage in bulk heterojunction organic solar cells,

Phys. Rev. B. 84 (2011) 075210.

[34] C.G. Shuttle, Recombination dynamics in polythiophene:fullerene solar cells, Imperial College, UK, 2009.

[35] T.M. Clarke, F.C. Jamieson, J.R. Durrant, Transient absorption studies of bimolecular recombination dynamics in polythiophene/fullerene blend films, The Journal of Physical Chemistry C. 113 (2009) 20934–20941.

[36] D. Credgington, R. Hamilton, P. Atienzar, J. Nelson, J.R. Durrant, Non-Geminate Recombination as the Primary Determinant of Open-Circuit Voltage in Polythiophene:Fullerene Blend Solar Cells: an Analysis of the Influence of Device Processing Conditions, Adv. Funct. Mater. 21 (2011) 2744–2753.

[37] A. Foertig, A. Baumann, D. Rauh, V. Dyakonov, C. Deibel, Charge carrier concentration and temperature dependent recombination in polymer-fullerene solar cells, Appl. Phys. Lett. 95 (2009) 052104.

[38] Y. Kim, S. Cook, S.M. Tuladhar, S.A. Choulis, J. Nelson, J.R. Durrant, et al., A strong regioregularity effect in self-organizing conjugated polymer films and high-efficiency polythiophene:fullerene solar cells, Nature Materials. 5 (2006) 197–203.

[39] T. Kirchartz, J. Nelson, Meaning of reaction orders in polymer:fullerene solar cells, Phys. Rev. B. 86 (2012) 165201.

[40] C.H. Peters, I.T. Sachs-Quintana, J.P. Kastrop, S. Beaupré, M. Leclerc, M.D. McGehee, High Efficiency Polymer Solar Cells with Long Operating Lifetimes, Advanced Energy Materials. 1 (2011) 491–494.

[41] M. Jørgensen, K. Norrman, S.A. Gevorgyan, T. Tromholt, B. Andreasen, F.C. Krebs, Stability of Polymer Solar Cells, Adv. Mater. 24 (2011) 580–612.

[42] H. Neugebauer, C.J. Brabec, J.C. Hummelen, R.A.J. Janssen, N.S. Sariciftci, Stability studies and degradation analysis of plastic solar cell materials by FTIR spectroscopy, Synthetic Metals. 102 (1999) 1002–1003.

[43] F. Padinger, T. Fromherz, P. Denk, C.J. Brabec, J. Zettner, T. HIERL, et al., Degradation of bulk heterojunction solar cells operated in an inert gas atmosphere : a systematic study, Synthetic Metals. 121 (2001) 1605–1606.

[44] J. Kroon, M. Wienk, W. Verhees, Accurate efficiency determination and stability studies of conjugated polymer/fullerene solar cells, Thin Solid Films. 403-404 (2002) 223–228.

[45] F. Krebs, J. Carle, N. Cruysbagger, M. Andersen, M. Lilliedal, M. Hammond, et al., Lifetimes of organic photovoltaics: photochemistry, atmosphere effects and barrier layers in ITO-MEHPPV:PCBM-aluminium devices, Solar Energy Materials and Solar Cells. 86 (2005) 499–516.

[46] M. Manceau, A. Rivaton, J.-L. Gardette, S. Guillerez, N. lemaitre, Light-induced degradation of the P3HT-based solar cells active layer, Solar Energy Materials and Solar Cells. 95 (2011) 1315–1325.

[47] M. Helgesen, M.V. Madsen, B. Andreasen, Thermally reactive

Thiazolo [5, 4-d] thiazole based copolymers for high photochemical stability in polymer solar cells, Polymer. 2 (2011) 2536-2542.

[48] S. Khelifi, K. Decock, J. Lauwaert, H. Vrielinck, D. Spoltore, F. Piersimoni, et al., Investigation of defects by admittance spectroscopy measurements in poly (3-hexylthiophene):(6,6)-phenyl C61-butyric acid methyl ester organic solar cells degraded under air exposure, J. Appl. Phys. 110 (2011) 094509.

[49] H. Neugebauer, C. Brabec, J.C. Hummelen, N.S. Sariciftci, Stability and photodegradation mechanisms of conjugated polymer/fullerene plastic solar cells, Solar Energy Materials and Solar Cells. 61 (2000) 35–42.

[50] G. Griffini, S. Turri, M. Levi, Degradation and stabilization of poly(3-hexylthiophene) thin films for photovoltaic applications, Polym. Bull. 66 (2010) 211–222.

[51] M. Manceau, A. Rivaton, J.L. Gardette, S. Guillerez, The mechanism of photo-and thermooxidation of poly (3-hexylthiophene)(P3HT) reconsidered, Polymer Degradation and Stability 94 (2009) 898‐907.

[52] H. Hintz, C. Sessler, H. Peisert, H.J. Egelhaaf, Wavelength-Dependent Pathways of Poly-3-hexylthiophene Photo-Oxidation, Chemistry of Materials 24 (2012) 2739.

[53] Z. Liang, A. Nardes, D. Wang, J.J. Berry, B.A. Gregg, Defect Engineering in π-Conjugated Polymers, Chem. Mater. 21 (2009) 4914–4919.

[54] S. Hoshino, M. Yoshida, S. Uemura, Influence of moisture on device characteristics of polythiophene-based field-effect transistors, Journal of Applied Physics 95 (2004) 5088.

[55] M. Abdou, F.P. Orfino, Y. Son, Interaction of oxygen with conjugated polymers: charge transfer complex formation with poly (3-alkylthiophenes), Journal of the American Chemical Society 119 (1997) 4518.

[56] E.J. Meijer, C. Detcheverry, P.J. Baesjou, Dopant density determination in disordered organic field-effect transistors, Journal of Applied Physics 93 (2003) 4831.

[57] E.J. Meijer, A. Mangnus, B.H. Huisman, G.T. Hooft, Photoimpedance spectroscopy of poly (3-hexyl thiophene) metal–insulator–semiconductor diodes, Synthetic Metals. 142 (2004) 53.

[58] C.K. Lu, H.F. Meng, Hole doping by molecular oxygen in organic semiconductors: Band-structure calculations, Phys. Rev. B. 75 (2007) 235206.

[59] H.H. Liao, C.M. Yang, C.C. Liu, S.F. Horng, Dynamics and reversibility of oxygen doping and de-doping for conjugated polymer, Journal of Applied Physics 103 (2008) 104506.

[60] M.O. Reese, A.M. Nardes, B.L. Rupert, Photoinduced degradation of polymer and polymer–fullerene active layers: experiment and theory, Advanced Functional Materials 20 (2010) 3476.

[61] E. Vörösházi, B. Verreet, T. Aernouts, Long-term operational lifetime and degradation analysis of P3HT: PCBM photovoltaic cells, Solar Energy Materials and Solar Cells 95 (2011) 1303.

[62] W.D. Oosterbaan, V. Vrindts, S. Berson, S. Guillerez, O. Douhéret,

B. Ruttens, et al., Efficient formation, isolation and characterization of poly(3-alkylthiophene) nanofibres: probing order as a function of side-chain length, J. Mater. Chem. 19 (2009) 5424.

[63] J.A. Merlo, C.D. Frisbie, Field effect conductance of conducting polymer nanofibers, J. Polym. Sci. B Polym. Phys. 41 (2003) 2674–2680.

[64] J.-C. Bolsée, W.D. Oosterbaan, L. Lutsen, D. Vanderzande, J. Manca, CAFM on conjugated polymer nanofibers: Capable of assessing one fiber mobility, Organic Electronics. 12 (2011) 2084–2089.

[65] J. Liu, M. Arif, J. Zou, S.I. Khondaker, L. Zhai, Controlling Poly(3-hexylthiophene) Crystal Dimension: Nanowhiskers and Nanoribbons, Macromolecules. 42 (2009) 9390–9393.

[66] J.A. Lim, F. Liu, S. Ferdous, M. Muthukumar, A.L. Briseno, Polymer semiconductor crystals, Materials Today. 13 (2010) 14–24.

[67] D.H. Kim, Y.D. Park, Y. Jang, S. Kim, K. Cho, Solvent Vapor-Induced Nanowire Formation in Poly(3-hexylthiophene) Thin Films, Macromol. Rapid Commun. 26 (2005) 834–839.

[68] J.-F. Chang, J. Clark, N. Zhao, H. Sirringhaus, D. Breiby, J. Andreasen, et al., Molecular-weight dependence of interchain polaron delocalization and exciton bandwidth in high-mobility conjugated polymers, Phys. Rev. B. 74 (2006) 115318.

[69] H. Sirringhaus, P. Brown, R. Friend, M. Nielsen, K. Bechgaard, B. Langeveld-Voss, et al., Two-dimensional charge transport in self-organized, high-mobility conjugated polymers, Nature. 401 (1999) 685–688.

[70] C.G. Shuttle, R. Hamilton, B.C. O'Regan, J.A. Nelson, J.R. Durrant, Charge-density-based analysis of the current–voltage response of polythiophene/fullerene photovoltaic devices, Proceedings of the National Academy of Sciences. 107 (2010) 16448–16452.

[71] R. Mauer, I.A. Howard, F. Laquai, Effect of Nongeminate Recombination on Fill Factor in Polythiophene/Methanofullerene Organic Solar Cells, J. Phys. Chem. Lett. 1 (2010) 3500–3505.

[72] D. Credgington, J.R. Durrant, Insights from Transient Optoelectronic Analyses on the Open-Circuit Voltage of Organic Solar Cells, J. Phys. Chem. Lett. 3 (2012) 1465–1478.

[73] G.F.A. Dibb, F.C. Jamieson, A. Maurano, J. Nelson, J.R. Durrant, Limits on Fill Factor in Organic Photovoltaics: Distinguishing Non-geminate and Geminate Recombination Mechanisms, J. Phys. Chem. Lett. (2013) 130205111718008.

[74] G. Juška, K. Arlauskas, M. Viliunas, J. Kocka, Extraction current transients: New method of study of charge transport in microcrystalline silicon, Phys. Rev. Lett. 84 (2000) 4946–4949.

[75] G. Juška, M. Viliunas, K. Arlauskas, N. Nekrasas, N. Wyrsch, L. Feitknecht, Hole drift mobility in μc-Si:H, J. Appl. Phys. 89 (2001) 4971.

[76] G. Juška, K. Genevičius, M. Viliunas, New method of drift mobility evaluation in [mu] c-Si: H, basic idea and comparison with time-of-flight, Journal of Non-Crystalline Solids 266-269 (2000) 331.

[77] G. Juška, K. Arlauskas, R. Österbacka, Time-of-flight measurements in thin films of regioregular poly (3-hexyl thiophene), Synthetic Metals. 109 (2000) 173.

[78] A. Mozer, N. Sariciftci, A. Pivrikas, R. Österbacka, G. Juška, L. Brassat, et al., Charge carrier mobility in regioregular poly(3-hexylthiophene) probed by transient conductivity techniques: A comparative study, Phys. Rev. B. 71 (2005) 035214.

[79] A. Pivrikas, N.S. Sariciftci, G. Juška, R. Österbacka, A review of charge transport and recombination in polymer/fullerene organic solar cells, Prog. Photovolt: Res. Appl. 15 (2007) 677–696.

[80] G. Juška, K. Arlauskas, M. Viliunas, K. Genevičius, R. Österbacka, H. Stubb, Charge transport in π-conjugated polymers from extraction current transients, Phys. Rev. B. 62 (2000) 16235–16238.

[81] K. Genevičius, R. Österbacka, G. Juška, K. Arlauskas, H. Stubb, Charge transport in π-conjugated polymers from extraction current transients, Thin Solid Films. 403 (2002) 415–418.

[82] G. Dennler, A.J. Mozer, G. Juška, A. Pivrikas, R. Österbacka, A. Fuchsbauer, et al., Charge carrier mobility and lifetime versus composition of conjugated polymer/fullerene bulk-heterojunction solar cells, Organic Electronics. 7 (2006) 229–234.

[83] S. Albrecht, W. Schindler, J. Kurpiers, J. Kniepert, J.C. Blakesley, I. Dumsch, et al., On the Field Dependence of Free Charge Carrier Generation and Recombination in Blends of PCPDTBT/PC70BM: Influence of Solvent Additives, J. Phys. Chem. Lett. (2012) 120209115459009.

[84] M. Schubert, E. Preis, J. Blakesley, P. Pingel, U. Scherf, D. Neher, Mobility relaxation and electron trapping in a donor/acceptor copolymer, Phys. Rev. B. 87 (2013) 024203.

[85] A. Mozer, Charge Transport and Recombination in Bulk Heterojunction Plastic Solar Cells, Johannes Kepler Universitat Linz, 2004.

[86] J. Lorrmann, B.H. Badada, O. Inganas, V. Dyakonov, C. Deibel, Charge carrier extraction by linearly increasing voltage: Analytic framework and ambipolar transients, J. Appl. Phys. 108 (2010) 113705.

[87] B.C. O'Regan, F. Lenzmann, Charge Transport and Recombination in a Nanoscale Interpenetrating Network of n-Type and p-Type Semiconductors: Transient Photocurrent and Photovoltage Studies of TiO 2/Dye/CuSCN Photovoltaic Cells, J. Phys. Chem. B. 108 (2004) 4342–4350.

[88] B. O’Regan, S. Veenstra, W. Verhees, Recombination kinetics of interpenetrating heterojunctions: comparison of dye sensitized and polymer solar cells, … Record of the Thirty …. (2005).

[89] B.C. O'Regan, S. Scully, A.C. Mayer, E. palomares, J. Durrant, The Effect of Al 2O 3Barrier Layers in TiO 2/Dye/CuSCN Photovoltaic Cells Explored by Recombination and DOS Characterization Using Transient Photovoltage Measurements, J. Phys. Chem. B. 109 (2005) 4616–4623.

[90] B.C. O'Regan, J.R. Durrant, P.M. Sommeling, N.J. Bakker, Influence of the TiCl4 Treatment on Nanocrystalline TiO2 Films in

Dye-Sensitized Solar Cells. 2. Charge Density, Band Edge Shifts, and Quantification of Recombination Losses at Short Circuit, J. Phys. Chem. C. 111 (2007) 14001–14010.

[91] A. Zaban, M. Greenshtein, J. Bisquert, Determination of the Electron Lifetime in Nanocrystalline Dye Solar Cells by Open-Circuit Voltage Decay Measurements, ChemPhysChem. 4 (2003) 859–864.

[92] S. Bertho, W.D. Oosterbaan, V. Vrindts, J. D'Haen, T.J. Cleij, L. Lutsen, et al., Controlling the morphology of nanofiber-P3HT:PCBM blends for organic bulk heterojunction solar cells, Organic Electronics. 10 (2009) 1248–1251.

[93] T.-A. Chen, X. Wu, R.D. Rieke, Regiocontrolled Synthesis of Poly(3-alkylthiophenes) Mediated by Rieke Zinc: Their Characterization and Solid-State Properties, J. Am. Chem. Soc. 117 (1995) 233–244.

[94] P. Vanlaeke, A. Swinnen, I. Haeldermans, G. Vanhoyland, T. Aernouts, D. Cheyns, et al., P3HT/PCBM bulk heterojunction solar cells: Relation between morphology and electro-optical characteristics, Solar Energy Materials and Solar Cells. 90 (2006) 2150–2158.

[95] J. Jo, S.-I. Na, S.-S. Kim, T.-W. Lee, Y. Chung, S.-J. Kang, et al., Three-Dimensional Bulk Heterojunction Morphology for Achieving High Internal Quantum Efficiency in Polymer Solar Cells, Adv. Funct. Mater. 19 (2009) 2398–2406.

[96] R.J. Kline, M.D. McGehee, E.N. Kadnikova, J. Liu, J.M.J. Fréchet, Controlling the Field-Effect Mobility of Regioregular Polythiophene by Changing the Molecular Weight, Adv. Mater. 15 (2003) 1519–1522.

[97] A. Zen, J. Pflaum, S. Hirschmann, W. Zhuang, F. Jaiser, U. Asawapirom, et al., Effect of Molecular Weight and Annealing of Poly(3-hexylthiophene)s on the Performance of Organic Field-Effect Transistors, Adv. Funct. Mater. 14 (2004) 757–764.

[98] C. Goh, R.J. Kline, M.D. McGehee, E.N. Kadnikova, J.M.J. Fréchet, Molecular-weight-dependent mobilities in regioregular poly(3-hexyl-thiophene) diodes, Appl. Phys. Lett. 86 (2005) 122110.

[99] R.J. Kline, M.D. McGehee, E.N. Kadnikova, J. Liu, J.M.J. Fréchet, M.F. Toney, Dependence of Regioregular Poly(3-hexylthiophene) Film Morphology and Field-Effect Mobility on Molecular Weight, Macromolecules. 38 (2005) 3312–3319.

[100] P. Schilinsky, U. Asawapirom, U. Scherf, M. Biele, C.J. Brabec, Influence of the Molecular Weight of Poly(3-hexylthiophene) on the Performance of Bulk Heterojunction Solar Cells, Chem. Mater. 17 (2005) 2175–2180.

[101] R.C. Hiorns, R. De Bettignies, J. Leroy, S. Bailly, M. Firon, C. Sentein, et al., High Molecular Weights, Polydispersities, and Annealing Temperatures in the Optimization of Bulk-Heterojunction Photovoltaic Cells Based on Poly(3-hexylthiophene) or Poly(3-butylthiophene), Adv. Funct. Mater. 16 (2006) 2263–2273.

[102] R. Joseph Kline, M.D. McGehee, M.F. Toney, Highly oriented crystals at the buried interface in polythiophene thin-film

transistors, Nature Materials. 5 (2006) 222–228.

[103] M. Brinkmann, P. Rannou, Effect of Molecular Weight on the Structure and Morphology of Oriented Thin Films of Regioregular Poly(3-hexylthiophene) Grown by Directional Epitaxial Solidification, Adv. Funct. Mater. 17 (2007) 101–108.

[104] W. Ma, J.Y. Kim, K. Lee, A.J. Heeger, Effect of the Molecular Weight of Poly(3-hexylthiophene) on the Morphology and Performance of Polymer Bulk Heterojunction Solar Cells, Macromol. Rapid Commun. 28 (2007) 1776–1780.

[105] M. Brinkmann, P. Rannou, Molecular Weight Dependence of Chain Packing and Semicrystalline Structure in Oriented Films of Regioregular Poly(3-hexylthiophene) Revealed by High-Resolution Transmission Electron Microscopy, Macromolecules. 42 (2009) 1125–1130.

[106] M. Koppe, C.J. Brabec, S. Heiml, A. Schausberger, W. Duffy, M. Heeney, et al., Influence of Molecular Weight Distribution on the Gelation of P3HT and Its Impact on the Photovoltaic Performance, Macromolecules. 42 (2009) 4661–4666.

[107] O.G. Reid, J.A.N. Malik, G. Latini, S. Dayal, N. Kopidakis, C. Silva, et al., The influence of solid-state microstructure on the origin and yield of long-lived photogenerated charge in neat semiconducting polymers, J. Polym. Sci. B Polym. Phys. 50 (2011) 27–37.

[108] C. Nicolet, D. Deribew, C. Renaud, G. Fleury, C. Brochon, E. Cloutet, et al., Optimization of the Bulk Heterojunction Composition for Enhanced Photovoltaic Properties: Correlation between the Molecular Weight of the Semiconducting Polymer and Device Performance, J. Phys. Chem. B. 115 (2011) 12717–12727.

[109] P. Kohn, S. Huettner, H. Komber, V. Senkovskyy, R. Tkachov, A. Kiriy, et al., On the role of single regio-defects and polydispersity in regioregular poly (3-hexylthiophene): Defect distribution, synthesis of defect-free chains and a simple model for the determination of crystallinity, J. Am. Chem. Soc. 134 (2012) 4790.

[110] S. Engmann, V. Turkovic, P. Denner, H. Hoppe, G. Gobsch, Optical order of the polymer phase within polymer/fullerene blend films, J. Polym. Sci. B Polym. Phys. 50 (2012) 1363–1373.

[111] S. Van Mierloo, A. Hadipour, M.-J. Spijkman, N. Van den Brande, B. Ruttens, J. Kesters, et al., Improved Photovoltaic Performance of a Semicrystalline Narrow Bandgap Copolymer Based on 4 H-Cyclopenta[2,1- b:3,4- b′]dithiophene Donor and Thiazolo[5,4-d]thiazole Acceptor Units, Chem. Mater. 24 (2012) 587–593.

[112] S. Bertho, W.D. Oosterbaan, V. Vrindts, J.-C. Bolsée, F. Piersimoni, D. Spoltore, et al., Poly (3-alkylthiophene) Nanofibers for Photovoltaic Energy Conversion, Adv. Mater. Res. (Durnten-Zurich, Switz.). 324 (2011) 32–37.

[113] R. Schmechel, H. von Seggern, Electronic traps in organic transport layers, Phys. Stat. Sol. (a). 201 (2004) 1215–1235.

[114] U. Zhokhavets, T. Erb, G. Gobsch, M. Al-Ibrahim, O. Ambacher, Relation between absorption and crystallinity of poly (3-hexylthiophene)/fullerene films for plastic solar cells, Chemical Physics Letters. 418 (2006) 347–350.

[115] K. Vandewal, W.D. Oosterbaan, S. Bertho, V. Vrindts, A. Gadisa, L. Lutsen, et al., Varying polymer crystallinity in nanofiber poly(3-alkylthiophene): PCBM solar cells: Influence on charge-transfer state energy and open-circuit voltage, Appl. Phys. Lett. 95 (2009) 123303.

[116] P. Kohn, S. Huettner, H. Komber, V. Senkovskyy, R. Tkachov, A. Kiriy, et al., On the Role of Single Regiodefects and Polydispersity in Regioregular Poly(3-hexylthiophene): Defect Distribution, Synthesis of Defect-Free Chains, and a Simple Model for the Determination of Crystallinity, J. Am. Chem. Soc. 134 (2012) 4790–4805.

[117] J. Clark, J.-F. Chang, F.C. Spano, R.H. Friend, C. Silva, Determining exciton bandwidth and film microstructure in polythiophene films using linear absorption spectroscopy, Appl. Phys. Lett. 94 (2009) 163306.

[118] A. Campbell, D. Bradley, D. Lidzey, Space-charge limited conduction with traps in poly (phenylene vinylene) light emitting diodes, J. Appl. Phys. 82 (1997) 6326.

[119] V. Dyakonov, D. Godovsky, J. Meyer, J. Parisi, C. Brabec, N. Sariciftci, et al., Electrical admittance studies of polymer photovoltaic cells, Synthetic Metals. 124 (2001) 103–105.

[120] M. Morana, P. Koers, C. Waldauf, M. Koppe, D. Muehlbacher, P. Denk, et al., Organic Field-Effect Devices as Tool to Characterize the Bipolar Transport in Polymer-Fullerene Blends: The Case of P3HT-PCBM, Adv. Funct. Mater. 17 (2007) 3274–3283.

[121] K. Vandewal, K. Tvingstedt, A. Gadisa, O. Inganäs, J.V. Manca, On the origin of the open-circuit voltage of polymer--fullerene solar cells, Nature Materials. 8 (2009) 1–6.

[122] F.C. Spano, Modeling disorder in polymer aggregates: The optical spectroscopy of regioregular poly(3-hexylthiophene) thin films, J. Chem. Phys. 122 (2005) 234701.

[123] F.C. Spano, Absorption in regio-regular poly(3-hexyl)thiophene thin films: Fermi resonances, interband coupling and disorder, Chemical Physics. 325 (2006) 22–35.

[124] J. Clark, C. Silva, R.H. Friend, F.C. Spano, Role of intermolecular coupling in the photophysics of disordered organic semiconductors: aggregate emission in regioregular polythiophene, Phys. Rev. Lett. 98 (2007) 206406.

[125] M. Burgelman, P. Nollet, S. Degrave, Modelling polycrystalline semiconductor solar cells, Thin Solid Films. 361 (2000) 527–532.

[126] J.C. Scott, J.H. Kaufman, P.J. Brock, R. DiPietro, J. Salem, J.A. Goitia, Degradation and failure of MEH-PPV light-emitting diodes, J. Appl. Phys. 79 (1996) 2745.

[127] M.P. De Jong, L.J. Van Ijzendoorn, M.J.A. de Voigt, Stability of the interface between indium-tin-oxide and poly(3,4-ethylenedioxythiophene)/poly(styrenesulfonate) in polymer light-emitting diodes, Appl. Phys. Lett. 77 (2000) 2255.

[128] D. Spoltore, W.D. Oosterbaan, S. Khelifi, J.N. Clifford, A. viterisi, E. Palomares, et al., Effect of Polymer Crystallinity in P3HT: PCBM Solar Cells on Band Gap Trap States and Apparent Recombination Order, Advanced Energy Materials. 3 (2013) 466–471.

[129] J. Bisquert, G. Garcia-Belmonte, On Voltage, Photovoltage, and Photocurrent in Bulk Heterojunction Organic Solar Cells, J. Phys. Chem. Lett. 2 (2011) 1950–1964.

[130] J. Bisquert, F. Fabregat-Santiago, I. Mora-Seró, G. Garcia-Belmonte, S. Giménez, Electron Lifetime in Dye-Sensitized Solar Cells: Theory and Interpretation of Measurements, J. Phys. Chem. C. 113 (2009) 17278–17290.

[131] W.L. Leong, S.R. Cowan, A.J. Heeger, Differential Resistance Analysis of Charge Carrier Losses in Organic Bulk Heterojunction Solar Cells: Observing the Transition from Bimolecular to Trap-Assisted Recombination and Quantifying the Order of Recombination, Advanced Energy Materials. 1 (2011) 517–522.

[132] R.C.I. MacKenzie, C.G. Shuttle, M.L. Chabinyc, J. Nelson, Extracting Microscopic Device Parameters from Transient Photocurrent Measurements of P3HT:PCBM Solar Cells, Advanced Energy Materials. 2 (2012) 662–669.

[133] A. Baumann, T.J. Savenije, D.H.K. Murthy, M. Heeney, V. Dyakonov, C. Deibel, Influence of Phase Segregation on Recombination Dynamics in Organic Bulk-Heterojunction Solar Cells, Adv. Funct. Mater. 21 (2011) 1687–1692.

[134] C. Deibel, A. Baumann, V. Dyakonov, Photogeneration and Recombination in Polymer Solar Cells, Physics of Organic Semiconductors, Second Edition. (n.d.) 575–602.

Collection of papers

On the following pages the papers included in this thesis are collected.

Paper A

D. Spoltore, W.D. Oosterbaan, S. Khelifi, J.N. Clifford, A. Viterisi, E. Palomares, M. Burgelman, L. Lutsen, D. Vanderzande, and J.V. Manca, *"Effect of Polymer Crystallinity in P3HT:PCBM Solar Cells on Band Gap Trap States and Apparent Recombination Order"* Advanced Energy Materials 3, 466 (2013)

Effect of Polymer Crystallinity in P3HT:PCBM Solar Cells on Band Gap Trap States and Apparent Recombination Order

Donato Spoltore, Wibren D. Oosterbaan, Samira Khelifi, John N. Clifford, Aurelien Viterisi, Emilio Palomares, Marc Burgelman, Laurence Lutsen, Dirk Vanderzande, and Jean Manca*

The non-geminate recombination of charge carriers in polymer-fullerene solar cells has been modeled in the last few years with a trap-assisted recombination model, which states that the apparent recombination order depends on the concentration of trapped charges tailing into the band gap. Higher concentrations of trapped charges lead to higher apparent recombination orders. In this work, the mass fraction *f* of highly crystalline nanofibrillar P3HT to the total P3HT content in P3HT:PCBM solar cells is consistently varied, controlling the temperature of a nanofibers-P3HT casting dispersion. A systematic study of the apparent recombination order, measured with a transient photovoltage technique, as a function of *f* is presented. A correlation is shown between the apparent recombination order, the P3HT crystallinity, and the trap concentration in the band gap measured with an admittance spectroscopy technique.

1. Introduction

Organic solar cells have seen increasing interest in recent years due to the potential for low cost production, with efficiencies reaching lately 10%.[1] Better understanding of the fundamental physical properties of organic solar cells is necessary to go further towards the commercialization of such devices. One of the main processes limiting solar cell performance is the non-geminate recombination of charge carriers. In recent years the recombination in a polymer-fullerene blend has been widely discussed in literature.[2–10] The Langevin model has been used to describe the non-geminate recombination processes taking place in such solar cells.[11,12] This is a second order recombination process depending on the concentrations of free electrons and free holes in the device. The recombination rate is linked to these concentrations through a recombination coefficient, which is proportional to the charge carrier mobility. Lately, several papers reported a recombination order higher than two in P3HT:PCBM solar cells.[13–15] Durrant, Nelson and coworkers explained this phenomenon in the framework of a trap-assisted recombination model,[2,5] where they attest that the recombination process is a second order bimolecular type, with a recombination coefficient depending on the concentration of charges. This is due to the dependence of mobility on the charge carrier density caused by the presence of a tail of trapped states inside the gap.[8,16] The variation of the apparent recombination order between differently prepared devices most probably results from variations in the crystallinity of the photoactive layer causing different trap concentrations in these layers.[17] Although this assumption was derived from indirect studies on the effect of crystallinity on the recombination rate, there has been no systematic study published to date, that links the crystallinity of the active layer with the trap density and the recombination rate.[9,18–21]

In the present study we have utilized a method to consistently control the mass fraction of P3HT fibers in the active layer of P3HT:PCBM solar cells.[22,23] This allowed us to make a systematic study of the apparent recombination order in function of the crystallinity of P3HT by means of a transient photovoltage technique.[15,24] We also measured the amount of hole traps present in the energy gap of active layers using admittance spectroscopy[25–27] and we showed that there is a correlation between the crystallinity of the material, the apparent recombination order and the amount of traps present in the active layer.

2. Theory

The continuity equation for electrons in a solar cell is:

$$\frac{dn}{dt} = -\frac{1}{q}\frac{dj_n}{dx} + G - R \qquad (1)$$

D. Spoltore, W. D. Oosterbaan, L. Lutsen,
Prof. D. Vanderzande, Prof. J. V. Manca
Institute for Materials Research (IMO)
Universiteit Hasselt
Division IMOMEC, IMEC
Wetenschapspark 1, 3590 Diepenbeek, Belgium
E-mail: donato.spoltore@uhasselt.be

S. Khelifi, Prof. M. Burgelman
Department of Electronics and Information Systems (ELIS)
University of Gent
Sint-Pietersnieuwstraat 41, 9000 Gent, Belgium

J. N. Clifford, A. Viterisi, Prof. E. Palomares
Institute of Chemical Research of Catalonia (ICIQ)
Avda. Països Catalans 16, 43007 Tarragona, Spain

Prof. E. Palomares
Institut Català de Recerca I Estudis Avançats (ICREA)
Avda. Lluís Companys 23, 80810 Barcelona, Spain

DOI: 10.1002/aenm.201200674

where n is the electron concentration, q the elementary charge, j_n the electron current, G the generation rate and R the recombination rate. In organic semiconductors the non-geminate recombination rate has been represented using a bimolecular Langevin model:[11,12]

$$R = k_L \left(np - n_i^2\right) \cong k_L \cdot n^2 \tag{2}$$

Assuming equal electron and hole concentations $n = p$, and neglecting the intrinsic charge concentration n_i, the recombination coefficient k_L can be written, in the framework of the Langevin model, as:

$$k_L = \frac{q}{\varepsilon}\left(\mu_h + \mu_e\right) \tag{3}$$

where ε is the dielectric constant of the material and μ_h and μ_e are the hole and electron mobility, respectively. It is a very simple model considering recombination as a diffusive process in which the charges recombine when they find each other (direct recombination). In P3HT:PCBM recombination orders higher than 2 were found.[13–15] The explanation given by Durrant, Nelson et al. is that the recombination coefficient k depends on the concentration of charge carriers n. In this case we can write the recombination rate as:

$$R = k(n) \cdot n^2 \propto k_0 \cdot n^{\lambda+1} \tag{4}$$

where $\lambda + 1$ is an empirical reaction order (the apparent recombination order) with respect to n and k_0 is the constant part of the recombination coefficient. Measuring the recombination at open circuit using a transient photovoltage technique,[15,24] $\frac{1}{q}\frac{dj_n}{dx}$ is almost zero and cancels with the spatial derivative of the hole current. Therefore:

$$\frac{dn}{dt} = G - R \tag{5}$$

The decay dynamics can then be expressed as:[5]

$$\frac{dn}{dt} \approx -\frac{n^{\lambda+1}}{(\lambda+1)\,\tau_{\Delta n_0} n_0^{\lambda}} \tag{6}$$

and the recombination coefficient can be written as:[5]

$$k\,(n) \approx -\frac{n^{\lambda-1}}{(\lambda+1)\,\tau_{\Delta n_0} n_0^{\lambda}} \tag{7}$$

where $\tau_{\Delta n0}$ (the small perturbation lifetime in dark), n_0 and λ are determined experimentally.

The dependence of the recombination coefficient on the charge carrier concentration can be explained in the framework of the multiple trapping model.[2] The charge transport in this kind of materials is due to hopping between localized states of the density of states, the total charge carrier concentration can be thought of as being composed in part of free charges and in part of trapped charges in the tail of the density of states. By assigning a constant mobility μ_0 to the free carriers and zero mobility to the trapped carriers, the average carrier mobility can be written, for electrons, as:[8,28]

$$\mu(n) = \mu_{0,e}\frac{n_{free}}{n_{free} + n_{trap}} = \mu_{0,e}\frac{n_{free}}{n_{tot}} \tag{8}$$

Substituting **Equation (8)** in **Equation (3)** and using **Equation (4)**, the recombination rate can be rewritten as:

$$\begin{aligned} R &\cong \frac{q}{\varepsilon}\left(\mu_h\,(p) + \mu_e\,(n)\right) \cdot n_{tot} \cdot p_{tot} \\ &= \frac{q}{\varepsilon}\left(\mu_{0,h} \cdot p_{free} \cdot n_{tot} + \mu_{0,e} \cdot n_{free} \cdot p_{tot}\right) \end{aligned} \tag{9}$$

If $n_{trap} > n_{free}$, as might be the case under standard organic solar cells working conditions, we can approximate the previous equation as:[8]

$$R \cong \frac{q}{\varepsilon}\left(\mu_{0,h} \cdot p_{free} \cdot n_{trap} + \mu_{0,e} \cdot n_{free} \cdot p_{trap}\right) \tag{10}$$

So recombination can be thought of as being dominated by free carriers recombining with trapped carriers. If we make the simplified assumption of a symmetric device (with equal hole and electron densities) and assume charge distributions like:[10,28]

$$n_{free} \propto e^{\frac{qV}{2k_BT}} \tag{11}$$

$$n_{trap} \propto e^{\frac{qV}{2E_T}} = n_{free}^{\frac{k_BT}{E_T}} \tag{12}$$

where E_T is the Urbach energy of the trap distribution, we can draw an expression of the apparent recombination order for the particular case of a symmetric device with an exponential distribution of trap states:[10]

$$R \propto n_{free} \cdot p_{trap} = n_{trap}^{\frac{E_T}{k_BT}+1} \propto n^{\lambda+1} \tag{13}$$

This apparent recombination order should not be interpreted as a physical mechanism of recombination, but it gives a useful indication of the amount of traps in the device.

3. Experimental Section and Discussion

P3HT:PCBM solar cells were prepared using poly(3-hexylthiophene) (P3HT) synthesized by the Rieke method,[29,30] with regioregularity >94.5% and molar mass of $M_n = 23.7\ Kg\ mol^{-1}$ (polydispersity index of 1.80) as determined by analytical size exclusion chromatography (SEC) in chlorobenzene *vs* polystyrene standards. The P3HT nanofiber dispersion was prepared by slowly cooling a warm P3HT solution in a bad solvent (*p*-xylene) to room temperature.[30] [6,6]-Phenyl-C_{61}-butyric acid methyl ester (PCBM) was added to the fiber dispersion in a 1:1 weight ratio and the dispersion was stirred for 24h. The fiber fraction, defined by the weight of the nanofibers over the total polymer weight, was varied via temperature control of the fiber dispersion and was determined by UV–vis spectroscopy in solution, following the procedure described by Bertho et al.[22,23] Because PCBM inhibits P3HT crystallization during spin coating,[31,32] and neither thermal annealing nor slow drying

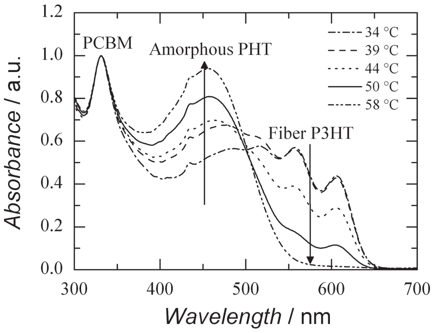

Figure 1. UV–vis absorption spectra of P3HT:PCBM 1:1 in p-xylene recorded for several dispersion temperatures.

was applied, the fiber fraction in the solid-state spin-coated films was approximated by the one determined by UV–vis in dispersion (**Figure 1**). Solar cell preparation was done following the same procedure described elsewhere,[22,23,33] using Ca capped with Al as top negative electrode. The overall efficiencies of the studied devices measured under standard condition are around 2%. Detailed results about morphology and device parameters are described elsewhere.[22] Transient photo-voltage (TPV) and transient photo-current (TPC) measurements[15,24] were carried out on these samples in the IMO laboratory (Hasselt university, Belgium). For the TPV measurements the devices were kept at open circuit while being illuminated with a white light bias, the intensity of which was used to control the open circuit voltage V_{OC}. A small optical perturbation was applied using a nitrogen pumped dye laser with wavelength of 500 nm resulting in a voltage transient with an amplitude $\Delta V << V_{oc}$. In this way the measurements were carried out in the small perturbation regime with the transient showing the shape of a single exponential (pseudo first order behavior).[15,24] In this case the dependence of the small perturbation carrier lifetime on V_{OC} (varied by varying the bias light) is:[15]

$$\tau_{\Delta n} = \tau_{\Delta n_0} e^{-\beta Voc} \tag{14}$$

For the TPC measurements the devices were kept in short circuit condition under dark and a single current transient resulting from the same laser pulse used in the TPV measurement was recorded. Integrating this current transient in time and using the voltage transient amplitude coming from TPV allows to calculate the differential capacitance defined as $C = \Delta Q/\Delta V$, where ΔQ is the current integral. Using a differential charging technique it is possible to calculate the charge carrier concentration in the sample as:[15]

$$n = \frac{1}{Aqd} \int_0^{V_{oc}} C\,dV = n_0 e^{\gamma^{V_{oc}}} \tag{15}$$

where A is the device area, d is the device thickness, n_0 is the carrier concentration prefactor, and γ is a constant. Linearizing Equation (5) and using Equation (4) the rate of decrease of the pulse-induced excess charge density can be expressed as:[34,35]

$$\frac{d\Delta n}{dt} \cong -\frac{dR}{dn} \cdot \Delta n = -k_0 \cdot (\lambda + 1) \cdot n^{\lambda} \cdot \Delta n \tag{16}$$

Therefore, the time evolution of Δn is exponential and the lifetime is given by $\tau_{\Delta n} = \left(\frac{dR}{dn}\right)^{-1}$ for each steady state. This implies, using Equation (16), Equation (4) and Equation (5):

$$\frac{dn}{dt} \cong \frac{d\Delta n}{dt} \cdot \frac{n}{\Delta n \cdot (\lambda + 1)} \tag{17}$$

which is a known result in the study of rate constants for higher order reactions.[15] Replacing Equation (14), Equation (15) and Equation (16) into Equation (17) we finally obtain Equation (6). Integrating Equation (6):[5]

$$t \cong \left(n^{-\lambda} - n_{t=0}^{-\lambda}\right) \cdot \frac{(\lambda + 1) \cdot \tau_{\Delta n_0} \cdot n_0^{\lambda}}{\lambda} \propto n^{-\lambda} \tag{18}$$

where $n_{t\,=\,0}$ is the initial charge density. The value of $-\lambda$ is readily accessible by taking the slope of the log-log plot of the small perturbation lifetime *vs* the charge density (Equation (18)). In the case of strictly bimolecular recombination λ is expected to be 1. However, since in the presence of traps the recombination coefficient depends on the charge carrier concentration, slopes with $\lambda > 1$ were found (**Figure 2**). The slope of the log-log plot of the recombination coefficient k *vs* the charge carrier density n is equal to $\lambda - 1$. In the case of strictly bimolecular recombination the recombination coefficient is expected to be a constant while in this case it's not, also because of the presence of traps (**Figure 3**). The slopes observed in Figure 2 and Figure 3 ($\lambda > 1$) confirm that the recombination coefficient is charge density dependent, consistent with the presence of traps in the band gap, the density of which is seen to decrease with increasing crystallinity. From these values we can calculate the

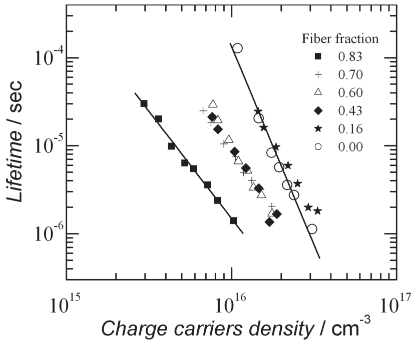

Figure 2. Small perturbation lifetime vs charge carrier density for devices with P3HT fiber fractions in the range 0 to 0.83.

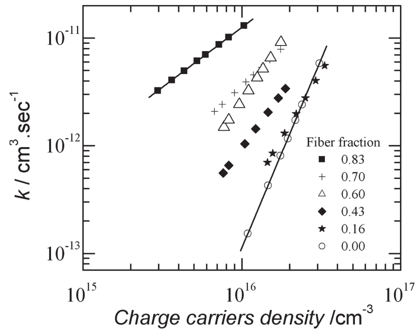

Figure 3. Recombination coefficient vs charge carrier density for devices with P3HT fiber fractions in the range 0 to 0.83.

apparent recombination order ($\lambda + 1$) and plot it vs the crystallinity of the active layer (**Figure 4**). The lower the crystallinity, the higher the apparent recombination order. This is attributed to a tail of trap states inside the band gap. In less crystalline P3HT the concentration of traps is higher most likely because of a broader distribution of the HOMO/LUMO energy levels, caused by the many structural imperfections (turns, backbone twists, etc.) which shorten and give a large variation to the conjugation length.[36,37] The reduction of the average conjugation length resulting from decreasing the P3HT fiber fraction in solar cell devices has been evidenced in a previous study from our group by a red-shift of the charge-transfer absorption.[33] Noteworthy, even if we extrapolate the fit to a device with a fiber fraction of 1, the value of the slope does not reach the value of the recombination order expected in the absence of traps ($\lambda + 1 = 2$). An explanation for this is that the fibers themselves are not completely crystalline, but consist of a crystalline inner part and an amorphous outer part. In the crystalline part, the extended polymer chains are packed in a parallel fashion, perpendicular to the long axis of the fiber.[38] Since for the P3HT used in this study, a contour length l_n of 28 nm can be estimated, which is larger than the fiber width of ~20 nm[30] and also given the rather large polydispersity of 1.80, many polymer chains incorporated into the fibers must give rise to dangling chain ends or chain folds for chains that are incorporated into crystalline part of the fiber twice (or more). These chain folds and chain ends in the outer part of the fiber and, to a lesser degree, regioregularity defects in the polymer chain reduce the overall crystallinity of the fibers.[39] Following a study from Clark,[40] it is possible to estimate the crystalline part of P3HT fibers in *p*-xylene dispersion based on the UV–vis absorption spectrum. The theoretical spectrum of aggregated P3HT has zero intensity below 443 nm. Therefore, assuming that all absorption between 300 and 350 nm is due to amorphous P3HT and knowing the corresponding absorption spectra of an equally concentrated solution of well-dissolved P3HT and a dispersion of isolated P3HT fibers both in *p*-xylene,[30] it is possible to estimate the non-crystalline part of the fiber. This yielded a crystallinity of 65% for pure fibers dispersed in *p*-xylene. To get 100% crystalline polymer, a fiber fraction of 1.55 would be needed. Remarkably, the extrapolated recombination order is 2 at that same 1.55 fiber fraction, suggesting that if it would be possible to make completely crystalline P3HT (a single crystal) the recombination order would be two as in the Langevin model ($n_{free} > n_{trap}$). The idea is that a perfectly crystalline polymer would have apparent recombination order 2 like in the Langevin model, while completely amorphous material would have a high apparent recombination order connected to a trap assisted recombination. When we change the fiber fraction we are changing the relative weight of the two phenomena in the solar cells. It should be noticed here that the values for λ in conventionally made P3HT:PCBM solar cells found in literature ranges from 1.4 to 3.3.[17,18,21] To verify the hypothesis that the change in apparent recombination order in these cells is due to the change in the concentration of trap states inside the gap we performed admittance spectroscopy measurements to investigate the density and energetic position of defect states within the gap of the absorber material. Despite this technique has been used extensively for inorganic materials,[41–43] only few studies on this technique have been reported on organic solar cells.[25–27] The measurements have been carried out in ELIS laboratory (Gent university, Belgium) by means of an impedance analyzer, using a small *ac* signal. The temperature dependent measurements have been done using a cryostat within the range of 100K to 300K. The energetic distribution of defects $N_t(E)$ was determined from the measured capacitance frequency data $C(f, T)$ using the model of Walter et al.[42] In this analysis, the defect distribution is related to the derivative of the capacitance with respect to the frequency:

$$N_t\,(E_\omega) = -\frac{V_{bi}}{q\,W}\frac{dC}{d\omega}\frac{\omega}{kT} \tag{19}$$

where V_{bi} is the built in voltage, W is the width of the space charge region and the energy position $E\omega$ is proportional to $ln(\omega)$ according to:

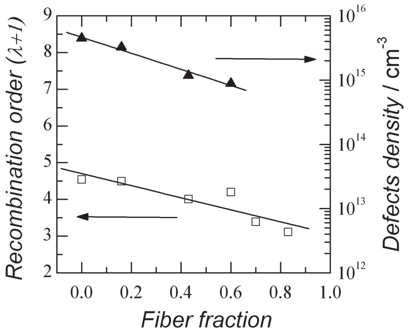

Figure 4. The apparent recombination order plotted together with the integral of the trap density as functions of the P3HT nanofiber fraction in films.

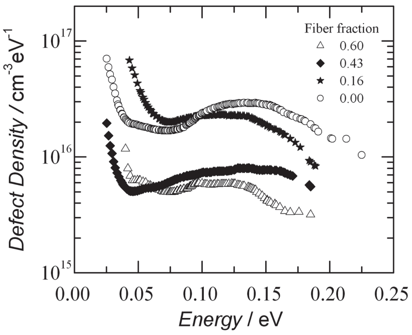

Figure 5. Defects density distribution for samples with different P3HT nanofiber fractions. Each curve represents the results of several temperature measurements (temperature range 100°K–300°K) merged with a special algorithm.[46]

$$E_\omega = kTln\left(\frac{2v_0}{\omega}\right) \tag{20}$$

v_0 is an attempt-to-escape frequency and ω is the angular frequency. More details can be found elsewhere[27] while the results are shown in **Figure 5**. A similar distribution of traps was found in literature, measured with a thermally stimulated current (TSC) technique.[44] The traps look to have a far more complicated distribution in energy than the simple exponential distribution of Equation (12). It looks as if there is an additional Gaussian distribution of traps around 0.1–0.15 eV. The presence of this additional Gaussian distribution of trapped states is not strange as structural defects are not necessarily restricted to the formation of tail states alone. If a specific kind of structural defect occurs with enhanced probability, it may result in more or less discrete trap states inside the gap.[36] The presence of exponential plus Gaussian trap states in P3HT:PCBM solar cells has been pointed out also in recent theoretical works.[8,45] In the most recent paper the trap states are initially modeled with an exponential tail, by varying the shape of the tail a better fit was reached on their experimental data. The best fit was reached modeling the trap states as a series of Gaussian-shaped features inside the gap, it was suggested to use the exponential model only as a first approximation. Indeed, Equation (13) is an approximation as it is derived in the simplified case of a totally symmetric device, when both electron and hole concentrations are equal and both increase with half of the voltage (quasi-Fermi level splitting). Moreover, the characteristic energies of the trap distributions for electrons and holes are considered the same, deep traps are not taken into account and the shape of the tail of trap states is considered perfectly exponential. In any case, the total amount of traps does play a role in determining the apparent recombination order as the mobility is hindered by the presence of traps. We integrated, therefore, the density of traps in energy and plotted the result vs the fiber fraction. It is clear that lower amounts of nanofibers induce a higher amount of defects. If we plot the apparent recombination order together with the integral of the traps in Figure 5 as a function of crystallinity we obtain a correlation between the amount of fibers in the active layer, the apparent recombination order and the change in the amount of band gap traps (Figure 4).

4. Conclusion

In conclusion, the mass fraction of highly crystalline nanofibrillar P3HT to the total P3HT content in P3HT:PCBM solar cells was varied by temperature control of the nanofibers-P3HT casting dispersion. Decreasing the fiber fraction has shown to deliver a higher apparent recombination order. This phenomenon was assigned to the increasing of sub-band gap trap levels caused probably by a decreased conjugation length in less crystalline materials. The increase of the trap concentration was proved by an admittance spectroscopy technique. A clear correlation between the fraction of crystalline P3HT nanofibers, the apparent recombination order and the trap concentration in the band gap has been found. The apparent recombination order is higher than 2 also for a solar cell with a fiber fraction of 1. This is probably due to the lack of crystallinity of the fibers themselves, which was estimated to be 65%. The estimated degree of crystallinity of 65% for P3HT nanofibers suggests that within 100% crystalline P3HT the recombination order would be 2, like in a fully bimolecular model.

Acknowledgements

The authors acknowledge the Interreg-project ORGANEXT and the IWT-SBO-project Polyspec for funding. The authors are grateful to Dr. Eng. Sabine Bertho for help, Dr. Eng. Hans Moons for reading the paper, Dr. Eng. Koen Vandewal and Dr. Thomas Kirchartz for useful discussion.

Received: August 26, 2012
Revised: September 17, 2012
Published online:

---

[1] M. A. Green, K. Emery, Y. Hishikawa, W. Warta, E. D. Dunlop, *Prog. Photovoltaics* **2011**, *20*, 12.
[2] J. Nelson, *Phys. Rev. B* **2003**, *67*, 155209.
[3] A. Pivrikas, G. Juška, A. Mozer, M. Scharber, K. Arlauskas, N. Sariciftci, H. Stubb, R. Österbacka, *Phys. Rev. Lett.* **2005**, *94*, 176806.
[4] G. Juška, G. Sliaužys, K. Genevičius, K. Arlauskas, A. Pivrikas, M. Scharber, G. Dennler, N. Sariciftci, R. Österbacka, *Phys. Rev. B* **2006**, *74*, 115314.
[5] C. G. Shuttle, B. O'Regan, A. M. Ballantyne, J. Nelson, D. Bradley, J. R. Durrant, *Phys. Rev. B* **2008**, *78*, 113201.
[6] C. Deibel, A. Wagenpfahl, V. Dyakonov, *Phys. Rev. B* **2009**, *80*, 075203.
[7] R. Hamilton, C. G. Shuttle, B. O'Regan, T. C. Hammant, J. Nelson, J. R. Durrant, *J. Phys. Chem. Lett.* **2010**, *1*, 1432.
[8] R. C. I. MacKenzie, T. Kirchartz, G. F. A. Dibb, J. Nelson, *J. Phys. Chem. C* **2011**, *115*, 9806.
[9] S. R. Cowan, W. L. Leong, N. Banerji, G. Dennler, A. J. Heeger, *Adv. Funct. Mater.* **2011**, *21*, 3083.
[10] T. Kirchartz, B. Pieters, J. Kirkpatrick, U. Rau, J. Nelson, *Phys. Rev. B* **2011**, *83*, 115209.

[11] P. Langevin, *Ann. Chim. Phys* **1903**, *28*, 433.

[12] M. Pope, C. E. Swenberg, *Electronic Processes in Organic Crystals and Polymers*, Oxford University Press, New York, NY, USA, **1999**.

[13] G. Juška, K. Genevičius, N. Nekrasas, G. Sliaužys, G. Dennler, *Appl. Phys. Lett.* **2008**, *93*, 143303.

[14] C. Deibel, A. Baumann, V. Dyakonov, *Appl. Phys. Lett.* **2008**, *93*, 163303.

[15] C. G. Shuttle, B. O'Regan, A. M. Ballantyne, J. Nelson, D. D. C. Bradley, J. de Mello, J. R. Durrant, *Appl. Phys. Lett.* **2008**, *92*, 093311.

[16] C. G. Shuttle, R. Hamilton, J. Nelson, B. C. O'Regan, J. R. Durrant, *Adv. Funct. Mater.* **2010**, *20*, 698.

[17] C. G. Shuttle, *Recombination Dynamics in Polythiophene:Fullerene Solar Cells*, Imperial College, London **2009.**

[18] T. M. Clarke, F. C. Jamieson, J. R. Durrant, *J. Phys. Chem. C* **2009**, *113*, 20934.

[19] D. Credgington, R. Hamilton, P. Atienzar, J. Nelson, J. R. Durrant, *Adv. Funct. Mater.* **2011**, *21*, 2744.

[20] A. Foertig, A. Baumann, D. Rauh, V. Dyakonov, C. Deibel, *Appl. Phys. Lett.* **2009**, *95*, 052104.

[21] Y. Kim, S. Cook, S. M. Tuladhar, S. A. Choulis, J. Nelson, J. R. Durrant, D. D. C. Bradley, M. Giles, I. McCulloch, C.-S. Ha, M. Ree, *Nat. Mater.* **2006**, *5*, 197.

[22] S. Bertho, W. D. Oosterbaan, V. Vrindts, J. D'Haen, T. J. Cleij, L. Lutsen, J. Manca, D. Vanderzande, *Org. Electron.* **2009**, *10*, 1248.

[23] S. Bertho, W. D. Oosterbaan, V. Vrindts, J.-C. Bolsée, F. Piersimoni, D. Spoltore, J. D'Haen, L. Lutsen, D. Vanderzande, J. V. Manca, *Adv. Mater. Res. (Durnten-Zurich, Switz.)* **2011**, *324*, 32.

[24] B. C. O'Regan, S. Scully, A. C. Mayer, E. Palomares, J. Durrant, *J. Phys. Chem. B* **2005**, *109*, 4616.

[25] A. Campbell, D. Bradley, D. Lidzey, *J. Appl. Phys.* **1997**, *82*, 6326.

[26] V. Dyakonov, D. Godovsky, J. Meyer, J. Parisi, C. Brabec, N. Sariciftci, J. Hummelen, *Synth. Met.* **2001**, *124*, 103.

[27] S. Khelifi, K. Decock, J. Lauwaert, H. Vrielinck, D. Spoltore, F. Piersimoni, J. Manca, A. Belghachi, M. Burgelman, *J. Appl. Phys.* **2011**, *110*, 094509.

[28] J. C. Blakesley, D. Neher, *Phys. Rev. B* **2011**, *84*, 075210.

[29] T.-A. Chen, X. Wu, R. D. Rieke, *J. Am. Chem. Soc.* **1995**, *117*, 233.

[30] W. D. Oosterbaan, V. Vrindts, S. Berson, S. Guillerez, O. Douhéret, B. Ruttens, J. D'Haen, P. Adriaensens, J. Manca, L. Lutsen, D. Vanderzande, *J. Mater. Chem.* **2009**, *19*, 5424.

[31] P. Vanlaeke, A. Swinnen, I. Haeldermans, G. Vanhoyland, T. Aernouts, D. Cheyns, C. Deibel, J. D'Haen, P. Heremans, J. Poortmans, J. V. Manca, *Sol. Energy Mater. Sol. Cells* **2006**, *90*, 2150.

[32] J. Jo, S.-S. Kim, S.-I. Na, B.-K. Yu, D.-Y. Kim, *Adv. Funct. Mater.* **2009**, *19*, 866.

[33] K. Vandewal, W. D. Oosterbaan, S. Bertho, V. Vrindts, A. Gadisa, L. Lutsen, D. Vanderzande, J. V. Manca, *Appl. Phys. Lett.* **2009**, *95*, 123303.

[34] B. C. O'Regan, J. R. Durrant, P. M. Sommeling, N. J. Bakker, *J. Phys. Chem. C* **2007**, *111*, 14001.

[35] A. Zaban, M. Greenshtein, J. Bisquert, *ChemPhysChem* **2003**, *4*, 859.

[36] R. Schmechel, H. von Seggern, *Phys. Stat. Sol. A* **2004**, *201*, 1215.

[37] U. Zhokhavets, T. Erb, G. Gobsch, M. Al-Ibrahim, O. Ambacher, *Chem. Phys. Lett.* **2006**, *418*, 347.

[38] K. J. Ihn, J. Moulton, P. Smith, *J. Polym. Sci. B Polym. Phys.* **1993**, *31*, 735.

[39] P. Kohn, S. Huettner, H. Komber, V. Senkovskyy, R. Tkachov, A. Kiriy, R. H. Friend, U. Steiner, W. T. S. Huck, J. U. Sommer, *J. Am. Chem. Soc.* **2012**, *134*, 4790.

[40] J. Clark, J.-F. Chang, F. C. Spano, R. H. Friend, C. Silva, *Appl. Phys. Lett.* **2009**, *94*, 163306.

[41] D. Losee, *J. Appl. Phys.* **1975**, *46*, 2204.

[42] T. Walter, R. Herberholz, C. Muller, H. Schock, *J. Appl. Phys.* **1996**, *80*, 4411.

[43] S. Khelifi, A. Belghachi, J. Lauwaert, K. Decock, J. Wienke, R. Caballero, C. A. Kaufmann, M. Burgelman, *Energy Proc.* **2010**, *2*, 109.

[44] J. Schafferhans, A. Baumann, A. Wagenpfahl, C. Deibel, V. Dyakonov, *Org. Electron.* **2010**, *11*, 1693.

[45] R. C. I. MacKenzie, C. G. Shuttle, M. L. Chabinyc, J. Nelson, *Adv. Energy Mater.* **2012**, *2*, 662.

[46] K. Decock, S. Khelifi, M. Burgelman, *EU PVSEC Proc.* **2011**, 2922.

Paper B

D. Spoltore, T. Vangerven, P. Verstappen, F. Piersimoni, S. Bertho, K. Vandewal, W. Maes, A. De Sio, L. Lutsen, D. Vanderzande, and J.V. Manca, *"Effect of molecular weight on morphology and photovoltaic properties in P3HT:PCBM solar cells"* Submitted to Advanced Energy Materials

DOI: 10.1002/aenm.((please add manuscript number))
Article type: Full Paper

Effect of molecular weight on morphology and photovoltaic properties in P3HT:PCBM solar cells

Donato Spoltore, Tim Vangerven, Pieter Verstappen, Fortunato Piersimoni, Sabine Bertho, Koen Vandewal, Niko Van den Brande, Bruno Van Mele, Wouter Maes, Antonietta De Sio, Jürgen Parisi, Laurence Lutsen, Dirk Vanderzande and Jean V. Manca*

D. Spoltore, T. Vangerven, F. Piersimoni, S. Bertho, Prof. J. V. Manca
Hasselt University, Campus Diepenbeek, Institute for Materials Research (IMO), Materials Physics, Wetenschapspark 1, 3590 Diepenbeek, Belgium
E-mail: donato.spoltore@uhasselt.be

P. Verstappen, Prof. W. Maes, Prof. D. Vanderzande
Hasselt University, Campus Diepenbeek, Institute for Materials Research (IMO), Design & Synthesis of Organic Semiconductors (DSOS), Agoralaan-Building D, 3590 Diepenbeek, Belgium

Pieter Verstappen, Prof. W. Maes, Prof. D. Vanderzande, Prof. L. Lutsen, Prof. J. V. Manca
IMEC, Division IMOMEC, Wetenschapspark 1, 3590 Diepenbeek, Belgium

K. Vandewal
Department of Materials Science and Engineering, Stanford University, Stanford, CA 94305, USA

N. Van den Brande, Prof. B. Van Mele
Department of Physical Chemistry and Polymer Science, Faculty of Engineering Sciences, Vrije Universiteit Brussel, Pleinlaan 2, 1050 Brussels, Belgium

A. De Sio, Prof. J. Parisi
Institute of Physics, Carl von Ossietzky University, 26111 Oldenburg, Germany

Keywords: molecular weight, crystallinity, recycling gel permeation chromatography

The molecular weight (MW) of poly(3-hexylthiophene) has already been indicated as an important factor influencing the photovoltaic properties of bulk heterojunction organic solar cells based on this material. However, since different synthetic processes or repetitive soxhlet extractions – generally applied to obtain the different MW batches under study – result in samples with simultaneously varying regioregularity (RR) and polydispersity (PDI) as well, it has not been possible yet to find an unambiguous correlation between MW alone and the photovoltaic performance. In the present work recycling gel permeation chromatography is introduced as a versatile technique to fractionate the donor polymer and thereby obtain a systematic variation of molecular weight (M_n=11 – 91 kg mol^{-1}) with an almost constant PDI and RR. There is indeed a strong correlation between molecular weight and the photovoltaic properties. Polymer crystallinity and conjugation length are evaluated by several techniques such as Spano analysis of UV-Vis spectra, rapid heat-cool calorimetry and selected area electron diffraction, and are found to be deeply affected by MW. This in turn influences the behavior of the charge transfer state energy, measured via Fourier transform photocurrent spectroscopy, and therefore the open-circuit voltage. The short circuit current also shows a dependence on MW, mainly due to the change in absorption coefficient. The apparent recombination order, which is linked to the morphology of the polymer:fullerene blend, is determined using transient photovoltage and photocurrent techniques and also shows a correlation with polymer crystallinity. Finally, a correlation between recombination and fill factor is also suggested.

1. Introduction

Organic solar cells are gaining increasing interest as a promising alternative to silicon-based solar cells due to their beneficial optical, electronic and mechanical properties.[1-4] The possibility to use some of their inherent interesting properties like the high absorption coefficients, the prospect of easier and cheaper processing combined with the possibility of building flexible, integrated and light weight solar cell modules, has pushed the research on organic photovoltaics forward in the last years. This allowed to reach lab record power conversion efficiencies of over 10%.[5] Despite this impressive progress in device efficiency, a better understanding of their fundamental physical properties is necessary to increase this efficiency further and move towards the commercialization of such devices.

In this paper, we focus on the effect of the molecular weight (MW) of the donor polymer in polymer:fullerene bulk heterojunction solar cells. Several studies have already investigated the influence of varying MW on the photovoltaic properties of devices based on poly(3-hexylthiophene) (P3HT).[6-21] Schilinsky and coworkers varied the MW of P3HT from 2.2 to 11.3 kg mol^{-1} and observed that higher molecular weight improves the performance of P3HT:PCBM based solar cells.[10] Hiorns et al. studied the variations in device efficiency as a function of MW in the range 4.5 − 280 kg mol^{-1},[12] finding the highest efficiency at an intermediate MW of M_n=14.8 kg mol^{-1}. Also, Ma and coworkers found an optimal photovoltaic performance at an intermediate value between M_n=13 kg mol^{-1} and M_n=62.5 kg mol^{-1}.[15] In contrast, Morana and coworkers obtained better efficiencies with high MW P3HT (M_n=160 kg mol^{-1}),[22] using chlorobenzene as solvent. Nicolet et al. performed an analysis of P3HT:PCBM phase diagrams, showing the presence of an eutectic composition[19] and concluded that the higher the MW of P3HT, the higher the fraction of PCBM required to achieve optimal performance.

However, in these previous studies the regioregularity (RR) as well as the polydispersity index (PDI) often strongly varies for the different MW P3HT samples. This does not allow to completely disentangle the effect of solely the MW on the photovoltaic properties. The RR in particular has been proven to have a strong effect on solar cell performance and needs to be controlled carefully.[23] The polymer fractions are usually obtained through different synthetic protocols - also resulting in varying degrees of purity - or repetitive soxhlet extractions. In the present work we introduce recycling Gel Permeation Chromatography (r-GPC)[24] as a versatile technique to fractionate a single master batch of donor polymer, affording a systematic variation of MW with an almost constant PDI and RR. Five fractions were prepared with differing MW (M_n=11 – 91 kg mol^{-1}, Table 1). Solar cells were made by blending the different fractions with PCBM. To reach an optimal morphology, an high boiling solvent, namely *ortho*-dichlorobenzene, was used and slow drying was applied instead of thermal annealing to avoid possible differences in optimal annealing temperature. We observed that there is a strong correlation between MW and the photovoltaic properties. The behavior of the open-circuit voltage (V_{OC}) is explained by measuring the energy (E_{CT}) of the charge transfer (CT) state with Fourier Transform Photocurrent Spectroscopy (FTPS). In our attempts to link the observed change in CT-state energy as a function of MW to the film morphology, we found a correlation with the crystallinity of the polymer. The crystallinity is estimated by applying the Spano model[25-28] to the measured UV-visible spectra and performing Selected Area Electron Diffraction (SAED) and Rapid Heat Calorimetry (RHC) on the samples. Also the short circuit current (J_{SC}) showed a clear trend with varying Mn. Charge Extration by Linearly Increasing Voltage (CELIV) and absolute absorption measurements were performed to explain this trend. Moreover, the apparent recombination order, which is linked to the morphology of the polymer:fullerene blend, was determined by transient photovoltage (TPV) and photocurrent (TPC) techniques. A correlation between recombination and fill factor was also suggested.

We believe that the focus of this work, keeping (virtually) constant the PDI and RR and using an optimal high boiling processing solvent with slow drying, helps to clarify the true effect of the MW of the donor polymer.

2. Results and discussion

2.1. Photovoltaic properties

A clear trend in the photovoltaic parameters was observed with increasing M_n (**Figure 1**): the V_{OC} increases (by 0.06 V), while J_{SC} and efficiency decrease with increasing M_n. The fill factor (FF) remains rather constant, slightly increasing when lowering M_n, and shows a peak at the mean value of M_n. The highest efficiency was obtained for the lowest MW polymer, in contrast to the common belief that high MW is required to ensure high solar cell efficiency. A similar trend has been previously observed,[15] while in other works an opposite trend was observed.[10,19] It must, however, be noted that in these cases besides MW, also RR and PDI are varying substantially.

In the next paragraphs, we provide an interpretation of the observed relation between photovoltaic parameters and MW by investigating absorption spectra, crystallinity and Voc on one hand, and mobility, fraction of absorbed sunlight versus short circuit current and recombination on the other hand.

2.2. Crystallinity vs M_n

Figure 1 shows that the V_{OC} increases with increasing M_n, whereas one would intuitively expect more crystallinity in polymers with higher MW, resulting in a smaller V_{OC} (vide infra). To check the degree of crystallinity of the polymer fractions, UV-Vis spectra of the neat polymer films were initially taken (Figure 2) and analyzed using the model developed by Spano et al,[25-28] following the procedure described in the paper of Turner and coworkers.[29] In this model the absorption spectrum of P3HT is explained by a weakly interacting H-aggregate model. The model can provide the degree of excitonic coupling within the aggregates, which is connected to the conjugation length and crystalline quality. The exciton bandwidth W can be determined from the UV-Vis spectra by using **Equation (1)**.

$$\frac{A_{0-0}}{A_{0-1}} = \left(\frac{1 - 0.24 \cdot W/E_p}{1 + 0.073 \cdot W/E_p}\right)^2 \tag{1}$$

where E_p is the intermolecular vibrational energy, taken to be 0.179 eV assuming that the C=C symmetric stretch dominates the electronic transition coupling.[27] W has been shown to be inversely proportional to the number of planarized interacting chain segments.[28,29]

The model can also provide the fraction of the film made up of aggregates (**Equation (2)**).

$$A \propto \sum_{m=0} \left(\frac{e^{-S}S^{m}}{m!}\right)\left(1-\frac{We^{-S}}{2E_{p}}G_{m}\right)^{2}\Gamma\left(\hbar\omega-E_{0-0}-mE_{p}\right) \qquad (2)$$

where A is the absorbance, S is the Huang-Rhys factor, m and n are differing vibrational levels, $E_{0\text{-}0}$ is the 0-0 transition energy and σ is the Gaussian linewidth. G_m can be expressed as:

$$G_{m} = \sum_{n(\neq m)} \frac{S^{n}}{n!\,(n-m)} \qquad (3)$$

From the optical analysis we can see that lowering M_n diminishes W (Figure 2), a trend which has been observed before.[30] Only the lowest M_n fraction shows again an increasing W. A specular trend seems to apply to the fraction of aggregated polymer in the studied films (**Figure 4**), calculated using **Equation (2)** and **Equation (3)**. Both the crystalline quality of the polymer and the amount of aggregated polymer seems to increase going from high to low M_n with a maximum around 26 kg mol^{-1}.

This trend can be explained as follows: P3HT chains form typically fibers with a height of ~4 nm, a length of a few microns and a width of ~20 nm (contour length).[31] Chang and coworkers[11] suggest that for the low MW (MW < 22 kD), with chain lengths shorter than the contour length, there is a higher probability that more than one molecule is folded into a cross section perpendicular to the axis of the fiber, leading to defective crystals, less interacting polymer chain segments and an increasing W. In the intermediate MW group (29–52 kD), the polymer chains are long enough to fold into lamellae without chain ends inside the crystals. In this regime, the polymer chains within the crystal are expected to be the most planar with the lowest number of defect sites and lower W. Once the chain lengths are significantly longer than the contour length (MW > 76 kD), the polymer chain needs to either reenter the same fiber at some distance along the axis of the fiber or fold into another fiber. In this way, the number of molecules linking different fibers is enhanced. On the other hand, the more pronounced polymer entanglement during growth and the percentage of chain segments located on the disordered surface of fibers might lead to an overall higher degree of conformational disorder, producing chains containing kinks, bends and twists. Consequently, the highest MW fibers are expected to have a higher W.

The spectral analysis of the blend UV-Vis spectra showed a similar trend in W as in the neat polymer films: an increase in W with increasing M_n as shown in **Figure 3**. Making use of the PCBM:PS absorption curve of the Turner paper, we calculated the fraction of aggregated polymer also for the blend films. Even for the blends a specular trend compared to W is present, just like in the case of neat polymer fractions (**Figure 4**).

To obtain further (thermal) information about the type and quality of the P3HT crystals as a function of M_n, Rapid Heat-Cool DSC (RHC) was performed, measuring the melting peak temperature and melting enthalpy of the neat polymer films.[32] Two extra fractions with a different M_n, 7 (PDI 1.07) and 14 kg mol^{-1} (PDI 1.18) respectively, were included to further elucidate the trends seen. In **Figure 5** a complex behavior is seen for the fractions studied, which can be divided into 2 distinct limiting regimes (M_n < 14 kg mol^{-1} and M_n > 26 kg mol^{-1}, respectively) with a transient regime in between.

At M_n values below 14 kg mol^{-1}, crystals with a lower peak temperature of melting are found, indicating an effect of crystal lamellar thickness L_d. This can be explained by the formation of extended chain crystals with a value of L_d increasing with M_n. The higher melting enthalpies found in this regime indicate a higher crystal fraction. This first regime at very low M_n is clearly different from these at higher M_n. Above a critical value for M_n, found in literature to be 10 to 15 kg mol^{-1},[33,34] chain folding should occur which leads to a more constant value for L_d and thus for the peak temperature of melting (in case of a constant supercooling in the preceding cooling). Due to the chain folding, giving rise to less perfect lamellar crystals, slightly lower melting enthalpies are found compared to the extended chain crystals. From 26 kg mol^{-1} on, the interconnection of neighboring lamellar domains induces a less perfect crystal fraction. Moreover, the melt viscosity is higher for these higher molecular weight fractions of P3HT. This increase in viscosity leads to a decrease of chain mobility and induces slower kinetics of crystallisation with a higher supercooling during cooling. The result is a further decrease of melting peak temperature and melting enthalpy with increasing M_n of P3HT.

The trends in thermal properties as observed in **Figure 5** are in agreement with the spectral analysis *after* the onset of chain folding. A higher M_n is found to lead to lower crystal quality, as shown by the trends in melting enthalpy and melting peak temperature for values of M_n beyond ca. 14 kg mol^{-1}. It should be noted that interlamellar connectivity in P3HT probably gets prominent from values of M_n above ca. 26 kg mol^{-1}.

The observed trend is confirmed by Selected Area Electron Diffraction (SAED). The SAED patterns (**Figure 6**) showed two peaks, one related to the crystalline phase of PCBM and one related to the crystalline part of P3HT. Also in these measurements it is possible to see that the lower M_n fraction has the largest SAED peak being, therefore, the more crystalline, while the highest M_n fraction has the lower peak having, therefore, a smaller crystalline ratio.

2.3. V_{OC} and E_{CT} versus M_n

In organic solar cells it has been shown that there is a correlation between the energy of the charge transfer state (E_{CT}) and the V_{OC} of the solar cell.[35] An inverse dependency between the E_{CT} and the crystalline polymer fraction in a P3HT-fibers:PCBM blend has also already been reported.[36] Preparing samples with different ratios of crystalline and amorphous polymer fractions,[37,38] it was shown that the higher the crystalline fraction, the lower the E_{CT} and V_{OC}. The E_{CT} can be obtained via a sensitive measurement of the EQE spectrum by Fourier Transform Photocurrent Spectroscopy (FTPS)[39] in the low energy region where the relevant CT optical transitions occur. The spectra in **Figure 7**, normalized to the PCBM peak, show that the charge transfer (CT) state energy shows a blue shift with increasing M_n. The E_{CT} is obtained by fitting the CT band with a Gaussian as described in[40]. The E_{CT} follows the same trend of the V_{OC} (**Figure 8**).

A closer look at the FTPS-EQE spectra, shown in **Figure 7**, reveals that the CT absorption band comprises two distinct peaks. The highest energy one, centered around 1.6 eV, has a comparable energy as the CT absorption band of an amorphous regiorandom P3HT:PCBM blend (added in the picture). The low energy band, centered around 1.2 eV, therefore, seems related to the crystalline part of the polymer. Fitting the EQE curves with two Gaussians, one centered in the regiorandom-like zone and one centered in the crystalline-like zone, we can see that there is a trend also in the relative intensity of the two peaks. The regiorandom-like peak, which goes down in intensity with decreasing M_n, and the other peak that increases in intensity with decreasing the M_n. The relative contribution to the current given by the amorphous P3HT rises for increasing MW, while the crystalline contribution diminishes (**Figure 9**).

The FTPS results are a further indication that with increasing M_n there is a larger fraction of amorphous mixed polymer:fullerene phase as compared to crystalline phase present. Furthermore, based on the earlier mentioned relation between E_{CT} and V_{OC}, we can explain the observed increasing trend of V_{OC} with increasing M_n as shown in **Figure 8**.

2.4. Mobility and Current

To have a complete overview on the solar cells properties we measured also the charge mobility, by means of the Charge Extraction by Linearly Increasing Voltage (CELIV) technique.[41] With this technique, the measured mobility is in the direction perpendicular to the film surface, which is most relevant for the real solar cell operation mode. The mobilities as a function of M_n are shown in Figure 10, revealing that the mobility generally increases with increasing MW. It is not possible with CELIV to discern whether the measured mobility is actually the electron or hole mobility, but our findings are in agreement with Space Charge Limited Current hole mobility measurements reported in literature.[8] The reported trend of increasing mobility with increasing molecular weight is however anticorrelated with the short circuit current behavior, which decreases with increasing M_n (**Figure 1**).[42]

In order to better understand the trend in J_{SC}, we looked at the absorption coefficient of the five fractions (Figure 11). To estimate the amount of photons absorbed by the solar cells, it is possible to multiply the solar spectrum by the absorbance of the solar cell and integrate over the energies (**Equation (4)**).

$$\#\ of\ photons = \int \Phi(E) \cdot A(E)\, dE = \int \Phi(E)(1 - e^{-\alpha 2d})\, dE \qquad (4)$$

where Φ(E) is the solar spectrum, A(E) is the fraction of absorbed photons, α is the absorption coefficient and d is the thickness of the solar cell (multiplied by two to take into account the reflection of light from the back electrode). This approach neglects interference effects and only gives a rough estimate for the total fraction of absorbed photons. Multiplying the number of absorbed photons calculated in this way by the electron charge we obtain the maximum attainable current in the solar cells. It can be seen (Figure 12) that the lower M_n fractions absorb more photons than the higher M_n fractions, so the maximum attainable current is higher for lower M_n P3HT. This can explain the current behavior: even if the higher MW polymer has a higher hole mobility, it absorbs less photons and therefore yields less current. In literature, there are various reports stating that more crystalline polymers have a higher absorption coefficient in the IR, where the solar spectrum contains more photons.[23,43]

Another possible phenomenon influencing the current could be an increased phase separation in the lower M_n films, delivering an improved charge generation yield but less excitons reaching the interface.[15] In literature,[44,45] it is possible to find a similar behavior in P3HT:PCBM cells casted from chlorobenzene (CB). Before annealing, the 2 phases are finely intermixed and the current is low, while the V_{OC} is higher. After annealing, the 2 phases are more segregated and the current is much higher with a concomitant decrease in V_{OC}. In our case evidence for the increased phase separation is obtained by photoluminescence (PL) measurements (Figure 13). The PL is more quenched for the higher M_n indicating a finer intermixing, while in lower M_n the quenching is lower (as for the case of P3HT:PCBM cells casted from CB). The quenching was calculated dividing the PL of the blend films by the PL of the respective neat polymer film. Every PL measurement was normalized to the absorption of the film at the excitation wavelength (500 nm).

Additional evidence of the different extent of separation of the two phases in the five blends can be inferred from TEM images (**Figure 14**). We observed that for low M_n P3HT there is a higher degree of phase segregation. Polymer fibers can be seen in all the samples.

In summary, the reported trend in J_{SC} seems related to the increased absorption of lower M_n P3HT and to a more coarse phase separation improving the charge extraction yield.

2.5. Recombination

The recombination dynamics of free charge carriers in the devices as a function of M_n are measured by Transient Photo Voltage (TPV) and Transient Photo Current (TPC). The non-geminate recombination rate is a loss process involving two free charge carriers and can be expressed empirically as **Equation (5)**.

111111111111111111114111111

$$R = k(n) \cdot n^2 = k_0 \cdot n^{\lambda+1} \quad (5)$$

where n is the charge carriers density, k(n) is the recombination coefficient depending on n and λ+1 is the apparent recombination order.[46,47] For the TPV measurements the devices were kept at open circuit while being illuminated with a white light bias, the intensity of which was used to control the open circuit voltage V_{OC}. A small optical perturbation was applied using a Nd:YAG laser with a wavelength of 532 nm and a pulse duration of 5 ns, resulting in a voltage transient with an amplitude $\Delta V << V_{OC}$. In this way the measurements were carried out in the small perturbation regime with the transient showing the shape of a single exponential (pseudo first order behavior). For the TPC measurements the devices were kept in short circuit conditions under dark and a single current transient resulting from the same laser pulse used in the TPV measurement was recorded. Integrating this current transient in time and using the voltage transient amplitude coming from TPV allows, using a differential charging technique, to calculate the charge carrier concentration in the sample. Also in the recombination coefficient measurements there is a trend. It has been shown in the past that the degree of phase segregation in P3HT:PCBM blends influences the intensity of this parameter.[48] The more the two phases are segregated, the lower the intensity of the recombination coefficient is, since the charges have less chance to meet each other at a decreased amount of interface (Figure 15).

From the slope of the recombination coefficient versus charge carriers density it is possible to measure the apparent recombination order, λ+1, which has been related to the crystallinity of the material.[23,47,49] The apparent recombination order is also following the conjugation length as derived by the optical model (Figure 16).

It has been shown in the past that the fill factor in P3HT:PCBM solar cells is mainly shaped by non geminate recombination.[50,51] It is possible, therefore, that the change in apparent recombination order is influencing the fill factor. The charge density dependence of the recombination coefficient leads to a different recombination current at different charge density (illumination) and therefore to different fill factors.[50-52] A similar effect has been observed in temperature dependent recombination measurements.[52] Also in our case the minor trend in fill factor correlates with the recombination order, reinforcing this view.

3. Conclusion

In conclusion, recycling GPC was used as a convenient technique to obtain different M_n polymer fractions from a single master batch of P3HT. The fractions showed an almost identical PDI and RR, which in previous works has been shown to be difficult to achieve and therefore their effects on photovoltaic performance were not taken fully into account. In this way, it is possible to disentangle exclusively the effect of the variation of M_n for a polymer used as donor material in a BHJ solar cell. The variation of M_n has been shown to affect the crystallinity of the polymer, delivering a red shift of E_{CT} with decreasing M_n. This shift has been proven to agree well with the shift in V_{OC}, supplying an explanation for the observed reduction of V_{OC} with decreasing M_n. The M_n also affects the short circuit current delivered by the solar cells, mainly due to an increased light absorption for lower M_n P3HT, despite a decrease of CELIV mobility. The apparent non-geminate recombination order follows the crystallinity of the polymer fractions and seems to affect the fill factor. In summary, for the studied P3HT:PCBM system, the optimal M_n for device performance seems to be around 26 kg/mol. The influence of M_n should therefore well been taken into account when designing organic solar cells due to its strong effects on the morphology of polymer:fullerene active layers and on the resulting photovoltaic parameters and the underlying electro-optical properties.

1313131313131313131313134131313

4. Experimental Section

Materials: Starting from a single master batch of commercial P3HT from Rieke Metals (M_n = 27 kg mol^{-1}, PDI = 2.3, RR = 91-94%), five fractions were obtained using recycling GPC (Table 1). The polymer was fractionated via a JAI LC-9110Next recycling preparative HPLC equipped with JAIGEL-2H and 3H columns.[24] The obtained fractions have different MW (M_n ranging from 11 to 91 kg mol^{-1}) and almost the same PDI (~1.4) and RR (~90%). The regioregularities of the different P3HT fractions were determined via ^{1}H NMR spectroscopy, as described elsewhere.[31] It has to be noted here that, depending on the applied baseline correction, RR values around 94% were obtained for all samples. The minor trend (if any) observed remained, however, identical.

Preparation of solar cells: Solutions were prepared blending each polymer fraction with [6,6]-phenyl-C_{61}-butyric acid methyl ester (PCBM) in a 1:1 ratio, in a 15 mg mL^{-1} concentration in *ortho*-dichlorobenzene (ODCB). The solar cells were prepared starting from indium tin oxide (ITO, 100 nm) coated glass plates that were successively cleaned in a soap solution, demineralized water and acetone, each for 10 min in an ultrasonic bath. This was followed by a cleaning step in boiling isopropanol for 10 min. A 30 nm thick poly(3,4-ethylenedioxythiophene)-polystyrenesulfonate (PEDOT–PSS) layer was spin-coated on the clean glass/ITO substrates. The substrates were dried for 20 min on a hot plate at 120 °C. The active layers were then spin-coated on top of the PEDOT–PSS layer and the spin speed was varied as such to keep the thickness constant at around 150 nm. The substrates were spin-coated for 20 s and slow dried for 1 h.

Preparation of TEM samples: In order to have a look at the bulk morphology of the active layer with Transmission Electron Microscopy (TEM), films of the P3HT:PCBM blends were prepared. For this purpose, layers identical to the active layers of the solar cells were produced on glass substrates and were put on a copper TEM grid (3.05 mm diameter, 400 mesh, supplied by EMS) after etching with hydrofluoric acid. Bright Field TEM images and Selected Area Electron Diffraction (SAED) patterns were recorded on different parts of the substrate to verify that they were representative for the whole sample. The measurements were performed with a Tecnai G2 Spirit Twin.

Preparation of TEM samples: UV-Vis samples were prepared for neat polymer and blend films. For this purpose, layers identical to the active layers of the solar cells were produced on glass substrates. UV-Visible spectroscopy was then performed on a Varian Cary 500 UV-Vis-NIR spectrophotometer (scan rate 600 nm min^{-1}).

Thermal analysis: Rapid heat-cool DSC experiments were performed on a prototype RHC of TA Instruments, specifically designed for operation at high scanning rates, and equipped with a Liquid Nitrogen cooling. Experiments were conducted using Neon (6 ml min^{-1}) as a purge gas. Aluminum RHC crucibles weighing less than 2 mg were filled with sample masses in the range of 200 - 250 µg. Melting temperatures and melting enthalpies presented are the result of non-isothermal heating experiments performed at 500 K min^{-1} following a cooling of 250 K min^{-1}.

Acknowledgements

The authors would like to acknowledge the Interreg Euregio-Maas-Rijn project 'ORGANEXT' and the IWT- SBO-project Polyspec for funding.

Received: ((will be filled in by the editorial staff))
Revised: ((will be filled in by the editorial staff))
Published online: ((will be filled in by the editorial staff))

[1] C. Deibel, V. Dyakonov, *Rep. Prog. Phys.* **2010**, *73*, 096401.
[2] F. C. Krebs, *Polymeric solar cells: Materials, design, manufacture,* DEStech Publications, Lancaster, PA, USA **2010**.
[3] J. Nelson, *Materials Today* **2011**, *14*, 462.
[4] M. T. Dang, L. Hirsch, G. Wantz, J. D. Wuest, *Chem. Rev.* **2013**, *113*, 3734.
[5] M. A. Green, K. Emery, Y. Hishikawa, W. Warta, E. D. Dunlop, *Prog. Photovolt: Res. Appl.* **2012**, *21*, 1.
[6] R. J. Kline, M. D. McGehee, E. N. Kadnikova, J. Liu, J. M. J. Fréchet, *Adv. Mater.* **2003**, *15*, 1519.
[7] A. Zen, J. Pflaum, S. Hirschmann, W. Zhuang, F. Jaiser, U. Asawapirom, J. P. Rabe, U. Scherf, D. Neher, *Adv. Funct. Mater.* **2004**, *14*, 757.
[8] C. Goh, R. J. Kline, M. D. McGehee, E. N. Kadnikova, J. M. J. Fréchet, *Appl. Phys. Lett.* **2005**, *86*, 122110.
[9] R. J. Kline, M. D. McGehee, E. N. Kadnikova, J. Liu, J. M. J. Fréchet, M. F. Toney, *Macromolecules* **2005**, *38*, 3312.
[10] P. Schilinsky, U. Asawapirom, U. Scherf, M. Biele, C. J. Brabec, *Chem. Mater.* **2005**, *17*, 2175.
[11] J.-F. Chang, J. Clark, N. Zhao, H. Sirringhaus, D. Breiby, J. Andreasen, M. Nielsen, M. Giles, M. Heeney, I. McCulloch, *Phys. Rev. B* **2006**, *74*, 115318.
[12] R. C. Hiorns, R. De Bettignies, J. Leroy, S. Bailly, M. Firon, C. Sentein, A. Khoukh, H. Preud'homme, C. Dagron-Lartigau, *Adv. Funct. Mater.* **2006**, *16*, 2263.
[13] R. Joseph Kline, M. D. McGehee, M. F. Toney, *Nature Materials* **2006**, *5*, 222.
[14] M. Brinkmann, P. Rannou, *Adv. Funct. Mater.* **2007**, *17*, 101.
[15] W. Ma, J. Y. Kim, K. Lee, A. J. Heeger, *Macromol. Rapid Commun.* **2007**, *28*, 1776.
[16] M. Brinkmann, P. Rannou, *Macromolecules* **2009**, *42*, 1125.
[17] M. Koppe, C. J. Brabec, S. Heiml, A. Schausberger, W. Duffy, M. Heeney, I. McCulloch, *Macromolecules* **2009**, *42*, 4661.
[18] O. G. Reid, J. A. N. Malik, G. Latini, S. Dayal, N. Kopidakis, C. Silva, N. Stingelin, G. Rumbles, *J. Polym. Sci. B Polym. Phys.* **2011**, *50*, 27.
[19] C. Nicolet, D. Deribew, C. Renaud, G. Fleury, C. Brochon, E. Cloutet, L. Vignau, G. Wantz, H. Cramail, M. Geoghegan, G. Hadziioannou, *J. Phys. Chem. B* **2011**, *115*, 12717.
[20] P. Kohn, S. Huettner, H. Komber, V. Senkovskyy, R. Tkachov, A. Kiriy, R. H. Friend, U. Steiner, W. T. S. Huck, J. U. Sommer, *J. Am. Chem. Soc.* **2012,** *134,* 4790.
[21] S. Engmann, V. Turkovic, P. Denner, H. Hoppe, G. Gobsch, *J. Polym. Sci. B Polym. Phys.* **2012**, *50*, 1363.
[22] M. Morana, P. Koers, C. Waldauf, M. Koppe, D. Muehlbacher, P. Denk, M. Scharber, D. Waller, C. Brabec, *Adv. Funct. Mater.* **2007**, *17*, 3274.
[23] Y. Kim, S. Cook, S. M. Tuladhar, S. A. Choulis, J. Nelson, J. R. Durrant, D. D. C.

Bradley, M. Giles, I. McCulloch, C.-S. Ha, M. Ree, *Nature Materials* **2006**, *5*, 197.
[24] S. Van Mierloo, A. Hadipour, M.-J. Spijkman, N. Van den Brande, B. Ruttens, J. Kesters, J. D'Haen, G. Van Assche, D. M. de Leeuw, T. Aernouts, J. Manca, L. Lutsen, D. J. Vanderzande, W. Maes, *Chem. Mater.* **2012**, *24*, 587.
[25] F. C. Spano, *J. Chem. Phys.* **2005**, *122*, 234701.
[26] F. C. Spano, *Chemical Physics* **2006**, *325*, 22.
[27] J. Clark, C. Silva, R. H. Friend, F. C. Spano, *Phys. Rev. Lett.* **2007**, *98*, 206406.
[28] J. Clark, J.-F. Chang, F. C. Spano, R. H. Friend, C. Silva, *Appl. Phys. Lett.* **2009**, *94*, 163306.
[29] S. T. Turner, P. Pingel, R. Steyrleuthner, E. J. W. Crossland, S. Ludwigs, D. Neher, *Adv. Funct. Mater.* **2011**, *21*, 4640.
[30] P. Pingel, A. Zen, R. D. Abellón, F. C. Grozema, L. D. A. Siebbeles, D. Neher, *Adv. Funct. Mater.* **2010**, *20*, 2286.
[31] W. D. Oosterbaan, V. Vrindts, S. Berson, S. Guillerez, O. Douhéret, B. Ruttens, J. D'Haen, P. Adriaensens, J. Manca, L. Lutsen, D. Vanderzande, *J. Mater. Chem.* **2009**, *19*, 5424.
[32] F. Demir, N. Brande, B. Mele, S. Bertho, D. Vanderzande, J. Manca, G. Assche, *J Therm Anal Calorim* **2011**, *105*, 845.
[33] A. Zen, M. Saphiannikova, D. Neher, J. Grenzer, S. Grigorian, U. Pietsch, U. Asawapirom, S. Janietz, U. Scherf, I. Lieberwirth, G. Wegner, *Macromolecules* **2006**, *39*, 2162.
[34] J. Liu, M. Arif, J. Zou, S. I. Khondaker, L. Zhai, *Macromolecules* **2009**, *42*, 9390.
[35] K. Vandewal, K. Tvingstedt, A. Gadisa, O. Inganäs, J. V. Manca, *Nature Materials* **2009**, *8*, 1.
[36] K. Vandewal, W. D. Oosterbaan, S. Bertho, V. Vrindts, A. Gadisa, L. Lutsen, D. Vanderzande, J. V. Manca, *Appl. Phys. Lett.* **2009**, *95*, 123303.
[37] S. Bertho, W. D. Oosterbaan, V. Vrindts, J. D'Haen, T. J. Cleij, L. Lutsen, J. Manca, D. Vanderzande, *Organic Electronics* **2009**, *10*, 1248.
[38] S. Bertho, W. D. Oosterbaan, V. Vrindts, J.-C. Bolsée, F. Piersimoni, D. Spoltore, J. D'Haen, L. Lutsen, D. Vanderzande, J. V. Manca, *Adv. Mater. Res. (Durnten-Zurich, Switz.)* **2011**, *324*, 32.
[39] K. Vandewal, L. Goris, I. Haeldermans, M. Nesládek, K. Haenen, P. Wagner, J. Manca, *Thin Solid Films* **2008**, *516*, 7135.
[40] K. Vandewal, K. Tvingstedt, A. Gadisa, O. Inganäs, J. V. Manca, *Phys. Rev. B* **2010**, *81*, 125204.
[41] A. Pivrikas, N. S. Sariciftci, G. Juška, R. Österbacka, *Prog. Photovolt: Res. Appl.* **2007**, *15*, 677.
[42] R. Noriega, J. Rivnay, K. Vandewal, F. P. V. Koch, N. Stingelin, P. Smith, M. F. Toney, A. Salleo, *Nature Materials* **2013** *Accepted*.
[43] M. Kurniawan, T. Salim, K. F. Tai, S. Sun, E. J. Sie, X. Wu, E. K. L. Yeow, C. H. A. Huan, Y. M. Lam, T. C. Sum, *J. Phys. Chem. C* **2012**, *116*, 18015.
[44] T. M. Clarke, A. M. Ballantyne, J. Nelson, D. D. C. Bradley, J. R. Durrant, *Adv. Funct. Mater.* **2008**, *18*, 4029.
[45] F. C. Jamieson, E. B. Domingo, T. McCarthy-Ward, M. Heeney, N. Stingelin, J. R. Durrant, *Chemical Science* **2012**, *3*, 485.
[46] T. Kirchartz, B. Pieters, J. Kirkpatrick, U. Rau, J. Nelson, *Phys. Rev. B* **2011**, *83*, 115209.
[47] D. Spoltore, W. D. Oosterbaan, S. Khelifi, J. N. Clifford, A. viterisi, E. Palomares, M. Burgelman, L. Lutsen, D. Vanderzande, J. Manca, *Advanced Energy Materials* **2013**, *3*, 466.
[48] R. Hamilton, C. G. Shuttle, B. O'Regan, T. C. Hammant, J. Nelson, J. R. Durrant, *J.*

Phys. Chem. Lett. **2010**, *1*, 1432.
[49] T. M. Clarke, F. C. Jamieson, J. R. Durrant, *The Journal of Physical Chemistry C* **2009**, *113*, 20934.
[50] C. G. Shuttle, R. Hamilton, B. C. O'Regan, J. A. Nelson, J. R. Durrant, *Proceedings of the National Academy of Sciences* **2010**, *107*, 16448.
[51] G. F. A. Dibb, F. C. Jamieson, A. Maurano, J. Nelson, J. R. Durrant, *J. Phys. Chem. Lett.* **2013**, *4*, 803.
[52] R. Mauer, I. A. Howard, F. Laquai, *J. Phys. Chem. Lett.* **2010**, *1*, 3500.

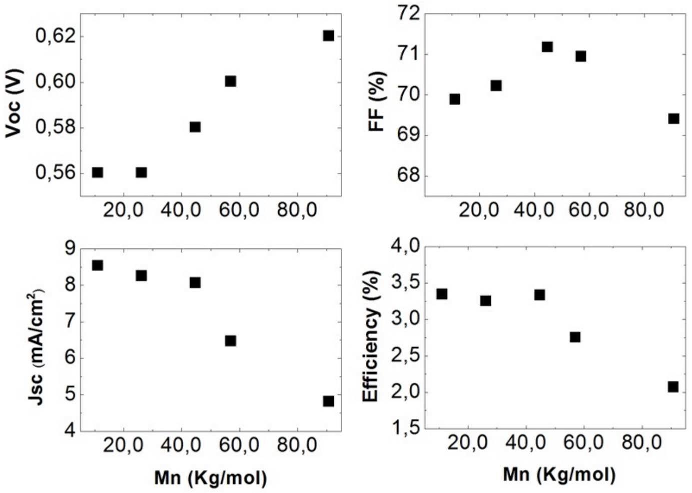

Figure 1 Photovoltaic parameters for the solar cells as a function of molecular weight

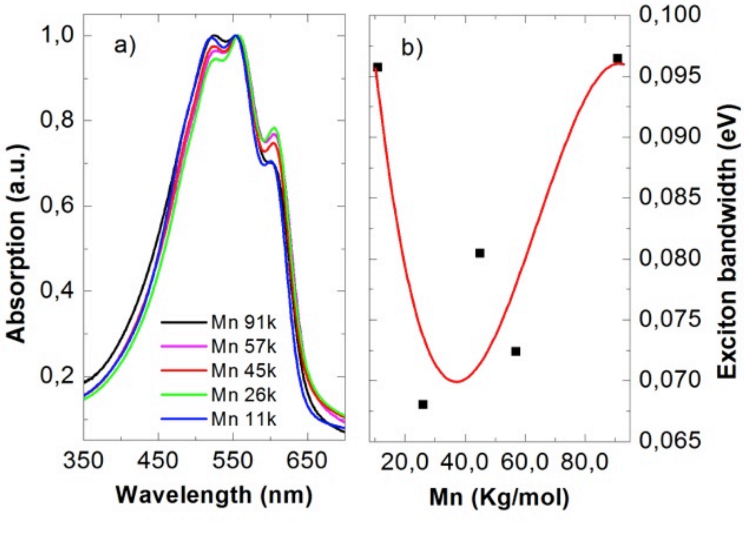

Figure 2 a) UV-Vis spectra of the neat polymer fractions with different MW. b) Exciton bandwidth W for the five polymer fractions (the red line serves as a guide to the eye only)

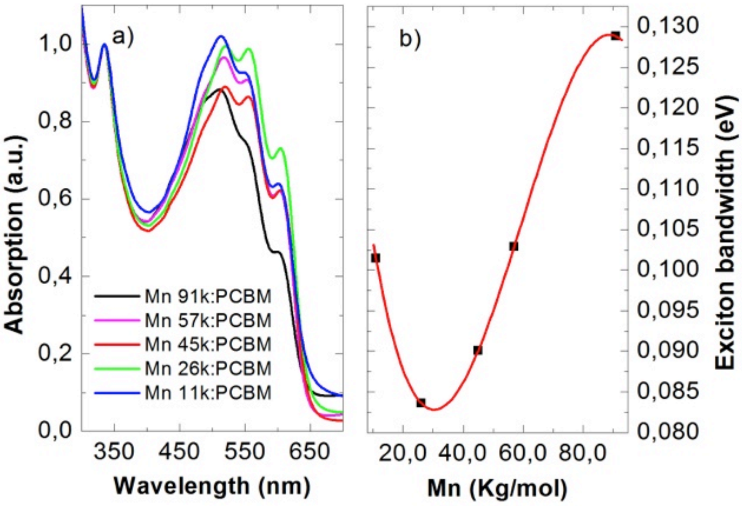

Figure 3 a) UV-Vis spectra of the polymer fractions blended with PCBM. b) Exciton bandwidth W for the five polymer fractions blended with PCBM (the red line serves as a guide to the eye only)

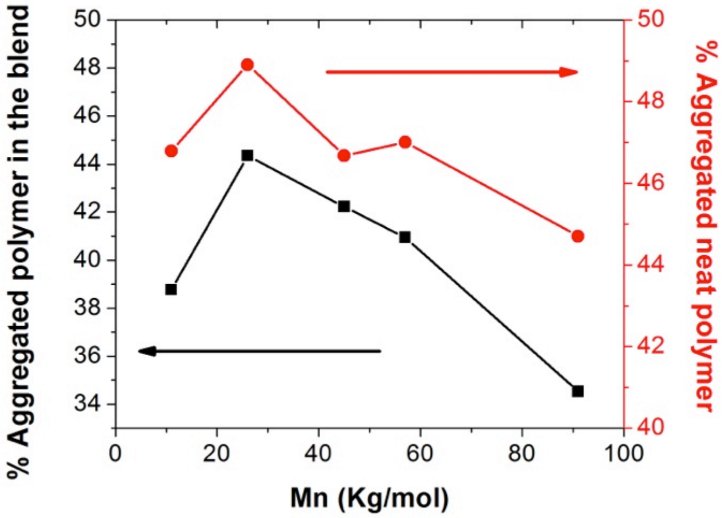

Figure 4 Fraction of aggregated polymer over the total polymer, in neat polymer films and in blend films

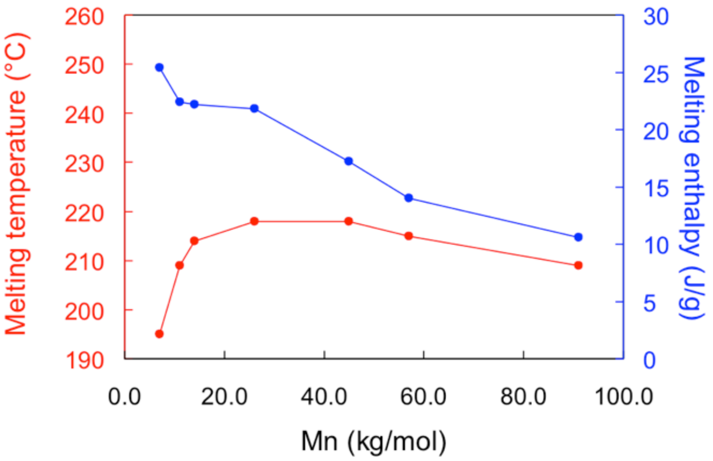

Figure 5 RHC measurements of the different MW P3HT fractions

212121212121212121214212121

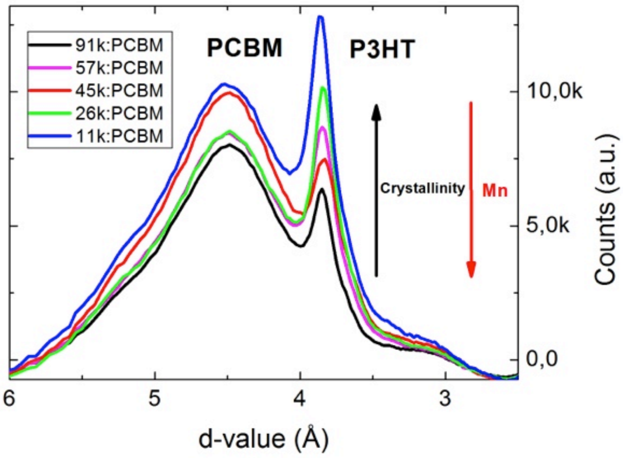

Figure 6 SAED patterns of the five P3HT fractions blended with PCBM

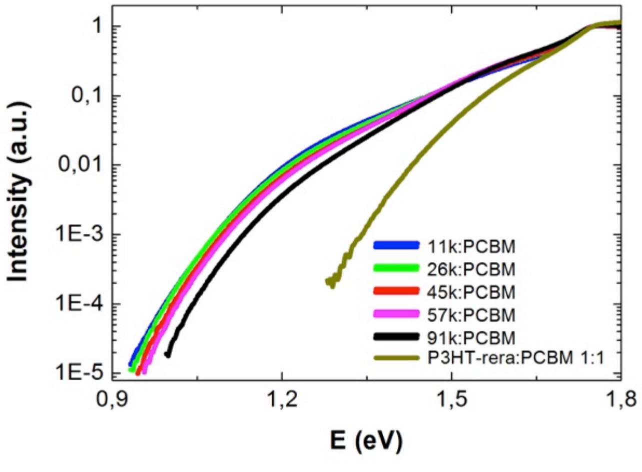

Figure 7 FTPS spectra for the studied blends (a regiorandom P3HT:PCBM curve was added, showing the resemblance with the right side peak of the fractionated P3HT samples)

222222222222222222224222222

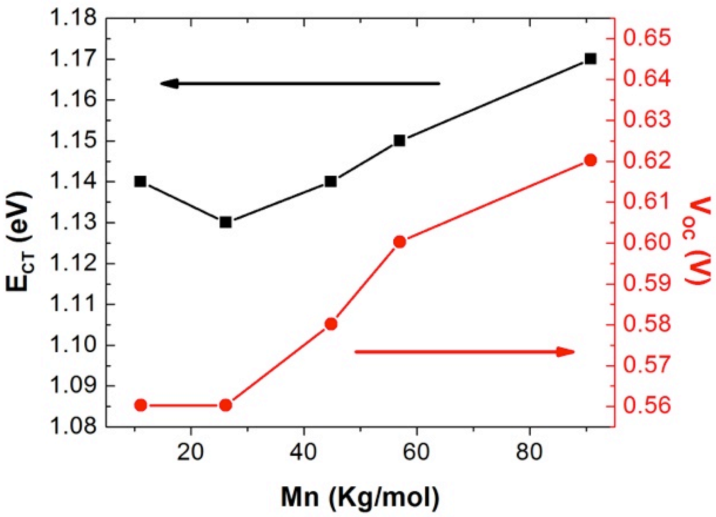

Figure 8 CT energies of the five blends (the values result from a fit of the FTPS spectra) and the relative V_{OC}

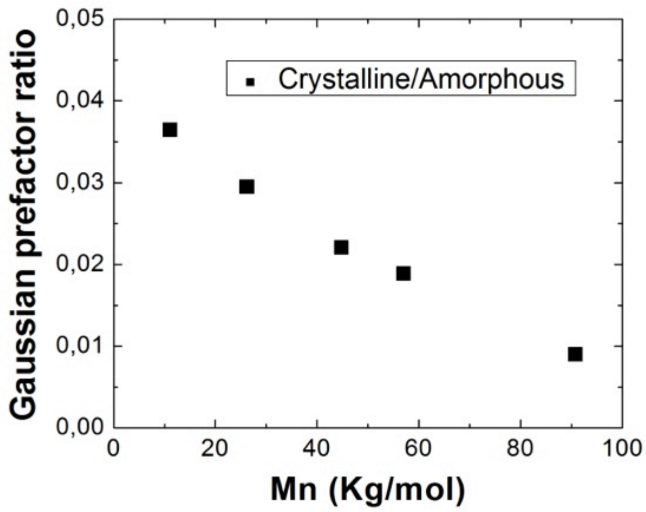

Figure 9 Relative intensity of the Gaussians fit to the FTPS spectra

232323232323232323234232323

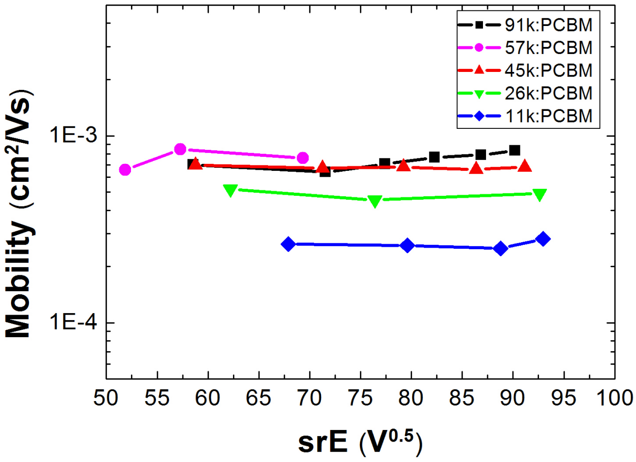

Figure 10 CELIV mobility of the five P3HT:PCBM blends

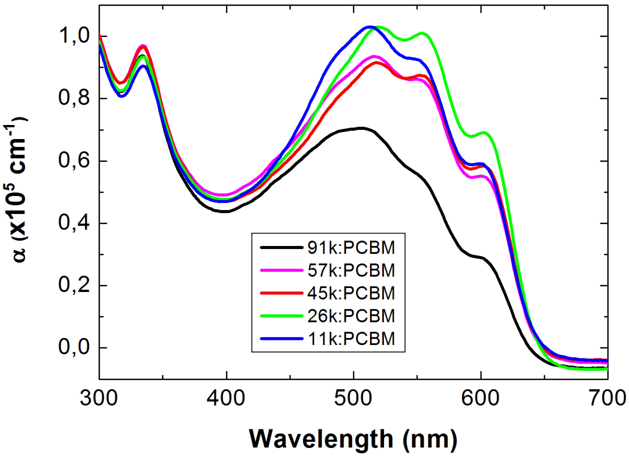

Figure 11 Absorption coefficients of the five P3HT fractions blended with PCBM

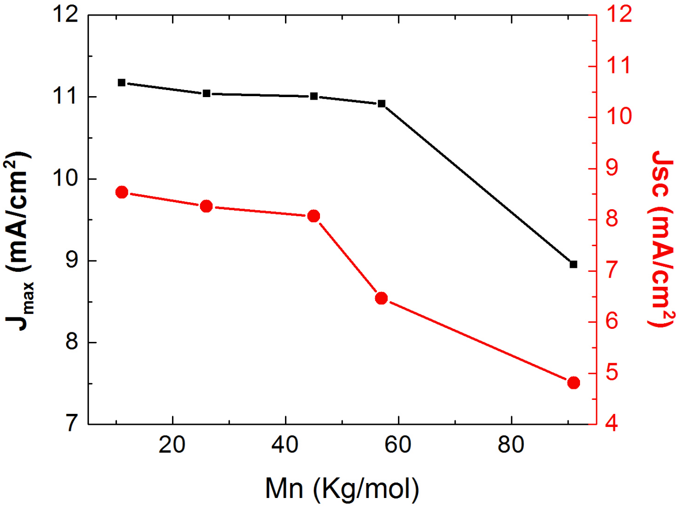

Figure 12 Maximum current attainable, considering only the photon absorption and the relative J_{SC}

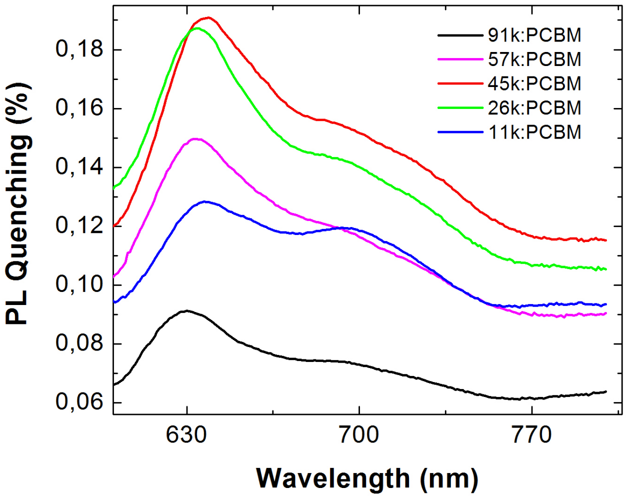

Figure 13 Photoluminescence of the blends, with more efficient quenching as the M_n of the donor polymer is increased

252525252525252525254252525

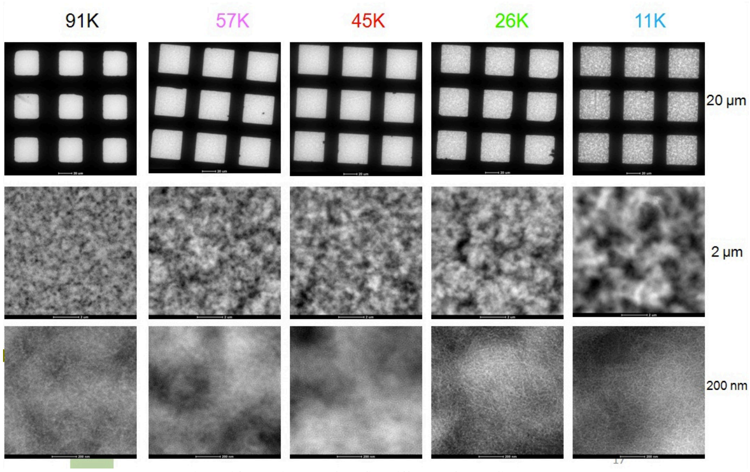

Figure 14 TEM images of the five different P3HT:PCBM blends

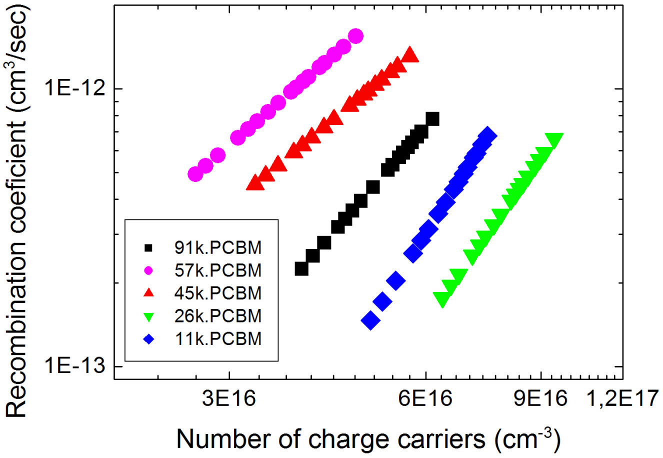

Figure 15 Recombination coefficients of the five P3HT:PCBM blends

262626262626262626264262626

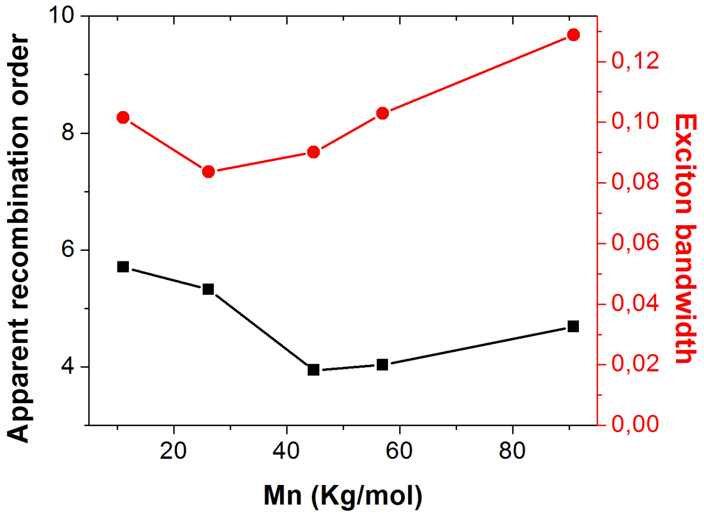

Figure 16 Apparent recombination order λ+1 derived from the slope of the recombination coefficient vs charge carrier density (which is λ-1) and exciton bandwidth W for the five different fractions

Samples	M_n (kg mol^{-1})	PDI	RR
1	11	1.35	90%
2	26	1.41	91%
3	45	1.40	91%
4	57	1.35	89%
5	91	1.30	89%

Table 1 Number average molecular weight (M_n), polydispersity index (PDI) and regioregularity (RR) of the investigated P3HT fractions

272727272727272727274272727

Paper C

S. Khelifi, E. Voroshazi, D. Spoltore, F. Piersimoni, S. Bertho, T. Aernouts, J. Manca, J. Lauwaert, H. Vrielinck, and M. Burgelman, ***"Effect of light induced degradation on electrical transport and charge extraction in polythiophene:fullerene solar cells"*** **Submitted to Solar Energy Materials and Solar Cells**

Effect of light induced degradation on electrical transport and charge extraction in polythiophene:fullerene solar cells

S. Khelifi[a,*], E. Voroshazi[c], D. Spoltore[b], F. Piersimoni[b], S. Bertho[b],T. Aernouts[c], J. Manca[b], J. Lauwaert[d], H. Vrielinck[d], and Marc Burgelman[a]

[a] Department of Electronics and Information Systems (ELIS), University of Gent, Sint-Pietersnieuwstraat 41, B-9000 Gent, Belgium

[b] Institute of Materials Research, University of Hasselt, Wetenschapspark 1, B-3590 Diepenbeek, Belgium

[c] Imec, Organic Photovoltaics, Polymer & Molecular Electronics, Kapeldreef 75, B-3001 Leuven, Belgium

[d] Department of Solid State Sciences, University of Gent, Krijgslaan 281-S1, B-9000 Gent, Belgium

[*] email: samira.khelifi@elis.ugent.be

Abstract

We investigate the photodegradation in inert atmosphere of P3HT:PCBM heterojunction solar cells under continuous illumination using advanced electrical characterization and a device modeling tool. Our results indicate that different failure mechanisms contribute to the performance loss. The first 250 hours of illumination induced *p*-type doping and recombination related to traps in the blend which mainly decreases the short-circuit current and the efficiency of the cells. Device modeling and simulation allowed us to prove that increased *p*-type doping of the blend provoke the loss in the short-circuit current and the quantum efficiency by simultaneously reduction of charge carrier mobility and the electric field together with a shrink of the space charge region. Transmission electron microscopy (TEM) measurements reveal a change in the blend morphology upon long illumination times manifested by phase segregation in the blend. The reduction in the open-circuit voltage is reported to be related to a slight reduction of the charge transfer energy (CT) upon 700 h of illumination ageing. Final failure mechanism observed upon 1000 h of illumination, is the reduction of charge extraction caused by a reduced surface recombination velocity at the contacts.

1. Introduction

Organic solar cells (OSCs) based on P3HT:PCBM (poly 3-hexylthiophene:[6,6]-phenyl-C61-butyric acid methyl ester) are widely investigated in terms of device stability and degradation [1]. Among the failure mechanisms, photodegradation of the active layer forms the most complex stability problem, since most of the organic polymers are unstable under UV illumination when exposed to ambient atmosphere. This process is further complicated in the presence of oxygen, water as these stress factors can cause both photo-oxidation of the polymer as well as degradation at the interfaces of the device.

In a study of photo and thermo-oxidation of poly (3-hexylthiophene), Manceau et al [2], showed that modifications of the chemical structure of P3HT occur during the degradation which results in the formation of numerous oxidized species affecting the properties of the materials. In a recent study by Hintz et al [3], where samples were degraded under controlled atmospheric conditions (dry synthetic air and relative humidity < 2%), it was shown that illumination with wavelength close to the absorption maximum of the polymer leads to a break in the pi-conjugated system, and the primary attack takes place at the polymer backbone. Besides chemical degradation of the compounds, trap formation can be a major source of instability and deteriorate charge carrier mobility and exciton diffusion length [4]. Polymers exhibit a reversible *p*-type doping whose density increases upon exposure to air or moisture [5] due to charge reaction with oxygen in dark and under light exposure [6-10] .

Degradation in OSCs depends not only on the organic materials but also on the device architecture. Current device lifetime is not limited by photo-oxidation of the polymer or the fullerene but by the failure at the photo-active layer/electrode interfaces. Indeed, Reese et al [11], reported that P3HT:PCBM active layers under prolonged illumination of 1000 h at one sun intensity and under inert conditions, without additional layers exhibited no photo-oxidation, in contrast to complete devices were the photodegradation is caused by charge collection layers and interfaces [12].

In a previous work[13], we have showed that P3HT:PCBM devices degraded under air exposure exhibit a *p*-type doping of the blend, which was related to reaction of the active layer with oxygen. The doping concentration increased in the degraded sample, leading to degradation of the mobility and of the device performance.

Herein we aim to gain a better understanding of the light induced device failure of standard architecture devices. We aged the cells with the following device stack ITO/poly(3,4-ethylenedioxythiophene) poly(styrenesulfonate)) PEDOT:PSS/ P3HT:PCBM/ Yb/Al under 1 sun intensity and AM1.5G spectrum illumination for different duration to be able to analyze their gradual degradation by advanced electrical characterization techniques. Device modeling and simulation assisted us in deepening our understanding of the lifetime-limiting mechanisms. We set a SCAPS (Solar Cell Capacitance Simulator) [13,14] problem definition that can both qualitatively and quantitatively reproduce our electrical measurements with the fitting parameters provided mostly by the experimental data. The model is based on the drift-diffusion simulations taking into account multi-charge states recombination process described by Sah-Shockley statistics [15-17].

We noted two major electrical loss mechanisms in the P3HT:PCBM cells when degraded under illumination in nitrogen atmosphere as shown in Figure 1.a. First, the short-circuit current (J_{sc}) decreases exponentially in the first 100 h. Followed by a slow linear performance loss prior to a rapid decrease of the fill factor (*FF*) after 1000 h due to the appearance of the S-shape in the current density-voltage (*J*-*V*) characteristic [12] as illustrated in Figure .1b. The solar cells parameters for the samples investigated in this work before and after the ageing are presented in Table 1.

2. Sample preparation and electrical characterization

2.1.1 Sample preparation

Standard solar cells have been prepared on glass substrate coated with patterned indium-tin-oxide (ITO). A PEDOT:PSS hole transport layer (HTL) was spin-coated on the cleaned and patterned ITO substrate giving a 35-40 nm thick layer. The samples were subsequently annealed in nitrogen at 130°C for 10 min to remove excess water. All further steps of processing were carried out in an inert nitrogen atmosphere. P3HT and PCBM in a 1:1weight ratio were used to prepare a solution of 25mg/ml in ortho-dichlorobenzene. The solution was stirred inside a glovebox at 80 °C and filtered with a 5µm PTFE filter prior to use. The active layer was spin-coated at 800 rpm for 60s to give a ~250-270 nm thick layer. The samples were subsequently heated at 130 °C for 10 min to achieve an optimal morphology. Finally, 40 nm Yb and 150 nm Al were deposited by evaporation at 1.5 Å/s without breaking the vacuum. The metals evaporated through a shadow mask defined twelve cells on each substrate. No further passivation or encapsulation layers are applied on the devices before the ageing.

2.1.2 Ageing conditions

Devices are processed, characterized and aged in nitrogen atmosphere and were never exposed to air. The samples were continuously illuminated by a metal halide lamp with AM1.5 spectrum and 1 sun light intensity. The current-voltage characteristic of the device was measured every 30 min with a Keithley 2400. The samples were left in open-circuit conditions between the measurements. The temperature of the samples during the illumination was 33-36 °C as measured at the substrate backside. These ageing conditions correspond to

ISOS-L2 protocol [18]. The samples were removed after 50 h, 125 h, 250 h, 700 h, 900 h and 1050 h from the continuous illumination setup and stored in dark and at room temperature.

To allow the device characterization in air, devices were encapsulated using a glass cavity attached with UV cross-linked adhesive with low water permeation rate, leaving the electrical contacts accessible.

2.2 Electrical characterization

After the illumination ageing the encapsulated samples were characterized using current voltage *(J-V)* quantum efficiency (*EQE*), Fourier-transform photocurrent spectroscopy (FTPS) [19,20], charge extraction by linearly increased voltage (CELIV) [21], transient photo-voltage and photo-current (TPV and TPC) [22], capacitance-voltage (*C-V*) and admittance spectroscopy (AS) *(C-f-T)* measurements [13,23].

The *EQE* spectra were performed using a halogen lamp via a monochromator and a silicon photodiode as a reference. For the FTPS measurements, a modulated illumination beam of a thermo electron Nicolte 8700 FTIR with an external detector option was used [19,20].

For transient photo-voltage (TPV) measurements, the cells were kept at open-circuit and illuminated with white light bias and a small optical perturbation was applied using a nitrogen pumped dye laser with a wavelength of 500 nm. For the transient photo-current measurements (TPC) the cells were kept in short circuit condition under dark and a single current transient from the same laser pulse used in TPV was applied [22].

Capacitance voltage and admittance spectroscopy measurements were carried out using a HP 4192 A LF impedance analyzer. The temperature dependent measurements have been done using a cold finger cryostat within a temperature range 100-300 K [13].

The morphology of the devices was studied by transmission electron microscopy (TEM). The measurements were performed with a Philips CM12-STEM. The active layers were isolated by etching with hydrofluoric acid (HF) to remove the glass substrate and then put on a copper TEM-grid.

3. Results and discussion

3.1 Device degradation:

We observed two major degradation loss processes in P3HT:PCBM cells when illuminated continuously in nitrogen atmosphere. The evolution of solar cell parameters normalized to their initial value as function of illumination time is represented in Figure 1a. First, the J_{sc} decreases exponentially in the first 200 h due to the degradation of the active layer as suggested by the capacitance and admittance spectroscopy that follows. Second, the rapid drop of the *FF* is activated after 700 h, which is linked to the degradation of the metal/organic interface. Devices aged for 1000 h exhibit a characteristic kink in the *J-V* curve as shown in Figure. 1b. The cell performances are also reported in Table 1.

3.2 Failure process in the first hours of illumination

3.2.1. Capacitance voltage (*C-V*) measurements

The capacitance-voltage measurements were performed at f = 10 kHz. The apparent doping profile was calculated from the Mott-Schottky plot ($1/C_j^2$ vs. V) of capacitance voltage C_j as [13,24]

$$C_j = \frac{\varepsilon_0 \varepsilon}{W} = \sqrt{\frac{q \varepsilon_0 \varepsilon N_{ap}}{2\left(V_{bi} - V\right)}} \tag{1}$$

thus

$$\frac{d\left(1/C_j^2\right)}{dV} = -\frac{2}{q \varepsilon_0 \varepsilon N_{ap}\left(W\right)} \tag{2}$$

where V_{bi} is the built-in voltage, W is the depletion layer width, ε_0 is the permittivity of vacuum, ε is the relative dielectric constant of the blend, q is the elementary charge and N_{ap} is the apparent doping profile in the depleted layer.

The apparent doping profile calculated using Eq.(1) and (2) is displayed in Figure 2. The doping profile was nonuniform and shows an increase in the concentration and a narrowing of the space charge region due to the light induced ageing. The same observations were reported previously in samples aged under air exposure and were assigned to an increase of a *p*-type doping in the active layer caused by the presence of oxygen-related traps [13].

3.2.3 Defect investigation using admittance spectroscopy (AS) measurements

Defect investigation was performed by analyzing the capacitance frequency spectra *C-f-T* using the derivative of the capacitance with respect to the frequency as [13,25]

$$N_t(E_\omega) = -\frac{V_{bi}}{qW}\frac{dC}{d\omega}\frac{\omega}{kT} \tag{3}$$

where ω is the angular frequency $\omega = 2\pi f$ (f is the frequency).

The energy position E_ω is proportional to ω as

$$E_\omega = kT \ln\left(\frac{2\nu_0}{\omega}\right) \tag{4}$$

where ν_0 is an attempt-to-escape frequency, which is the product of the thermal velocity, the capture cross section of carriers and the effective density of states in the valence or conduction band (HOMO or LUMO) as given by Eq.

$$\nu_0 = v_{th}\sigma_{n,p}N_{v,c} \quad (5)$$

The defect distribution calculated for samples at different staged of degradation are presented in Figure 3. Initially, the density of states (DOS) spectra is composed of two overlapping peaks with different energy positions and concentrations. These freshly prepared samples exhibit a broader spectrum than the aged one indicating a broad energetic trap distribution. The activation energies and the attempt-to-escape frequency values extracted from the Arrhenius plot of the capacitance derivative [13], were in the range of $E_A \sim$ 93-100 meV and $\nu_0 \sim 10^8$ Hz for the peak with lower energy and $E_A \sim$ 167-190 meV and $\nu_0 \sim 2\times10^7$ Hz for the peak with higher energy respectively. A rapid increase of the defect density was observed after 250 h of illumination and evolves little afterwards.

By comparing the values of the attempt-to-escape frequency of the two peaks detected in samples before and after the ageing, we concluded that the increase of the defect density occurs in the deeper trap with activation energy 167-190 meV, while the trap with lower activation energy is no longer visible over 700 h.

However it is still unclear whether the increase of traps in the samples was caused by impurities diffusion out from the ITO anode, a process which is much faster under illumination, or simply by structural changes in the blend material.

It is worth mentioning that, the acidic nature of PSS in the PEDOT: PSS layer is expected to etch the ITO which can create diffusion of indium, oxygen and other species into the HTL and the active layer [26,27], also to the presence of residual atmospheric gases cannot be excluded even in inert atmosphere.

3.3. Failure process upon long-term illumination

3.3.1 Quantum efficiency and Fourier transform photocurrent spectroscopy

External quantum efficiency and Fourier transform photocurrent spectroscopy measurements were performed on samples aged at different illumination duration, one freshly prepared device was also added for comparison. The results are shown in Figure 4a and b respectively. The CT values as extracted from the FTPS measurements are shown in Figure 4b.

The *EQE* and FTPS measurements showed a strong reduction in the spectral response shape in the samples aged under continuous illumination for 700 h and a reduction of the peak at ~ 2.3 eV (~ 540 nm), together with a slight decrease in interface charge transfer energy (CT) (~ ΔE_{CT} = 30 meV). This behavior was not observed in previous studies, for devices aged until 500 h [12].

Figure 5 shows TEM images for samples freshly prepared and aged for 900 h. Phase segregation was observed after 700 h of light exposure, and also appearance of dark spots which could be due to the aggregation of PCBM [28], despite the low temperature during the illumination exposure [12]. In this case, excitons may be lost because the donor/acceptor domains became larger compared to the exciton diffusion length which is typically around ~ 12 nm [29]. Furthermore, morphology re-organization can strongly alter the charge carrier mobility corroborating with the mobility reduction observed in the admittance spectroscopy spectra in section 3.2.3.

3.3.2 Recombination of charge carriers during the photodegradation

In order to investigate the recombination loss in the photo-degraded sample we performed transient photo-voltage (TPV) and transient photo-current (TPC) measurements [22]. The recombination current deduced from TPV and TPC measurements is presented in Figure 6 for samples freshly prepared and aged for 1050 h. As it can be seen, higher recombination current was reported in the photo-degraded samples.

The apparent recombination order $\lambda+1$ can be deduced from the slope of the log-log plot of the small perturbation lifetime as function of the charge density [22] shown in Figure 7. The slopes deduced from the plot give values of $\lambda+1$ higher than 2 and increase with the traps density in band gap, consistent with the results reported previously [22]. Several authors reported a recombination order higher than two in P3HT:PCBM solar cells, and it was linked to trap assisted recombination effect [30,31].

4.1 Modelling and simulation results

To confirm that the degradation of the various electrical transport properties we indentified is the origin of the device failure, we performed numerical simulation using the software SCAPS [14,16]. In our modelling, we applied the effective medium model which is characterized by an averaging of the material parameters of the polymer and the fullerene [13,32]. It is worth to mention that setting up a problem in any simulation program means finding a large number of parameters that can simulates as good as possible the measurements. Typically the number of parameters is very high, even if some parameters are known from literature; those related to traps in organic solar cells are rare.

The parameters used in the simulation are listed in Table 2. Most of the parameters used in the simulation were defined from measurements, such as carriers mobility (Extracted from CELIV), band gap energy (extracted from FTPS), and carrier capture cross sections (extracted from AS) [13]. The absorption coefficient vs. wavelength was measured at Imec.

We have included two recombination processes in our calculations, radiative recombination (Langevin recombination), given by Eq.(6) and non-radiative recombination in multi-level defects described by Sah-Shockley statistics where many states may have more than one charge states [15-17,33].

$$U_{rad} = k\left(pn - n_i^2\right) \tag{6}$$

With n and p electrons and holes concentration, n_i intrinsic carrier density and radiative k recombination coefficient.

The traps were introduced as a multivalent double acceptor level with a Gaussian distribution of energy states in the gap, at 93 meV and 167 meV, and exponential grading dependent on position.

In this section, the main parameters which have been changed during the simulation are the traps concentration and the carriers mobility, unless otherwise notified. We used for the fresh device ($N_t = 4\times10^{15}$ cm^{-3} and $\mu = 10^{-3}$ cm^2/V.s) and for the aged device ($N_t = 4\times10^{16}$ cm^{-3} and $\mu = 10^{-4}$ cm^2/V.s).

Figure 8 a and b display the Mott-Schottky plot and the apparent doping profile calculated by varying the trap density in the multivalent defect. The model is in good agreement with the measurement results. Both behaviors were reproduced, the nonuniformity of the doping profile and also the narrowing of the depletion layer due to an increase of the density of traps as observed in the *C-V* measurements.

We also calculated the defect distribution from the *C-f-T* simulation. The results are presented in Figure 9 assuming a tenfold increase of traps concentrations N_t in the aged device. As observed from the measurements, by increasing the defect concentration of the traps, the peak with lower activation energy is no longer visible in the admittance spectra. This is obvious, since after increasing the doping in the blend, and degradation of holes mobility, we have the situation where the defect response of the trap at $E_t \sim 0.093$ eV is faster than the free holes response during the admittance spectroscopy measurements, then only one peak will be visible in the *AS* spectra and thus the one at $E_t \sim 0.167$ eV [13].

Assuming a decrease in the hole mobility and an increased of the *p*-type doping in the blend by 10 order of magnitude, due to the presence of traps, we were also able to reproduce the decrease of the *EQE* in the photo-degraded sample as presented in Figure 10. The decrease in the quantum efficiency (and in J_{sc}) can be explained by the reduction of the internal electric field due to the degradation of mobility and the doping of the active layer. Initially the electric field near the anode is 10^4 V/cm and homogenously increases towards the cathode due to a presence of a space charge region created by the flow of holes (formation of a Schottky barrier). In degraded cells the electric field decreases in the active layer below 10^3 V/cm due to the increase of the *p*-type doping in the blend as can be seen in Figure.11.

To explain the influence of the degraded charge carrier transport on other device parameters, we calculated the variation of recombination current as function of V_{oc} for different trap concentrations and assuming different radiative recombination coefficients for aged and fresh samples. The results are shown in Figure 12. An increase of recombination current is caused by an increase of the holes concentrations caused by the *p*-type doping of the blend. By increasing the light intensity, the excess carrier concentration increases which also increase the reaction order.

The loss in the V_{oc} has also been studied in the photo-degraded devices. Figure 13 displays the effect of traps concentration on the non-radiative recombination current and the open-circuit voltage. Increase in trap concentration to over 10^{15} cm^{-3} in aged cells leads to a decrease in V_{oc} of around 100 mV in agreement with the device measurement. To fully reproduce the device failure after 700 h illumination we also include the loss in the *CT* from 1.2 to 1.16 eV which might be related to morphological changes. Further decrease in V_{oc} after 1000 h is mainly caused by the appearance of the S-shape in the *J-V* characteristic.

The V_{oc} exhibits a reduction of 50 mV until 250 h of illumination and then approaches 100 mV, after exposure to 1000 h, as seen in Table .1. Thus, we conclude that the slight reduction in the V_{oc} is caused in the first 250 h of illumination by the increase of recombination due to the trap states, then a decrease in the *CT* upon 900 h of photodegradation, probably caused by the fullerene aggregation.

These degraded transport properties have little influence on the FF of the cells, suggesting that an additional failure mechanism occurs upon 900 h illumination provoking the failure of the FF. We used our model to assess the origin of the S-shape at V_{oc} in *J-V* graph of degraded cells. This characteristic feature in the *J-V* graph has already been reported in OSCs and was ascribed to various factors which often linked to charge extraction problem due to the presence of an extraction/ injection barrier [34-36], and formation of interface states. However, a reduced surface recombination for majority carriers was reported to create S-shape *J-V* characteristics, since it prevents a sufficient extraction/injection of carriers at the interface active layer/metal [34,37].

Figure.14a and b show the illuminated *J-V* characteristics for devices before and after the ageing respectively, calculated for different majority surface recombination velocities for holes and electrons. As one can see, both reduced majority surface recombination for holes at the anode and electrons at the cathode gives an inflection point of the *J-V* curve close to the open-circuit voltage, which causes a kink in *J-V* reducing the fill factor. However, we could reproduce the S-shape *J-V* characteristics in the photo-degraded samples, by assuming a reduction in the surface recombination velocity for majority carriers at the cathode (electrons) S_n = 10^{-4} cm/s. Assuming a reduced surface recombination for majority carriers at the anode (holes) is manifested by a strong roll over, a behavior which was not observed in our measurements. Moreover, the degradation of the reactive low work-function cathode is more likely in these standard configuration devices could be provoked by residual humidity of the PEDOT:PSS layer accelerated by the illumination ageing.

Conclusions

The photo-degradation mechanisms under inert atmosphere of standard P3HT:PCBM solar cells have been investigated using numerous electrical characterization techniques and numerical device modeling.

Within this work we found out that the photodegradation extended over a period of 1000 h follows different stages. We gained detailed insight into the gradual degradation of the electrical transport and charge extraction by ageing devices under continuous illumination for different duration. After 50 h of illumination the devices exhibit an increase of *p*-type dopant concentration and upon continued exposure to illumination, we noted tenfold increase of the deep trap density after 250 h as detected by AS. Simultaneous alteration of these properties leads to non-homogenous electric field and explain the decrease in the short-circuit current and the *EQE* we could quantitatively reproduce this loss in *EQE* provided the input of *CV* and *AS* measurements.

Upon this initial degradation, both the device properties and electron transport parameters remain stable until 700 h illumination. After this period we detected note reduction in the CT energy linked probably to the change in the active layer morphology as shown by TEM.

The loss in V_{oc} is assigned to the increase of recombination due to traps together with this slight decrease in the CT after illumination ageing up to 700 h.

The degradation in the active layer is mainly caused by photoxidation of the blend, and an increase of traps density as detected by admittance spectroscopy technique, with higher concentration in the aged samples.

Finally, we propose that the reduced surface recombination velocity at the cathode contact leads to the appearance of a kink in the J-V characteristic and strong reduction of the FF in our devices illuminated for more than 1000 h.

We conclude that the photodegradation in the devices is caused in a first stage, by the deterioration of transport properties of the active layer due to the increased density of deep traps in the blend and a p-type doping of the active layer, while in a second stage of the failure the degradation of the charge extraction dominates the device failure.

Also, we were able to prove using our model that the drop in the FF is due to a poor collection of carriers at the cathode manifested by a low surface recombination for majority carriers (electrons).

Acknowledgments

The authors would like to acknowledge the IWT-SBO project PolySpec financed by the Institute of Science and Technology, as well as the Research Foundation-Flanders for financial support.

References

[1] M. Jørgensen, K. Norrman, S. A. Gevorgyan, T. Tromholt, B. Andreasen, and F. C. Krebs, Adv. Mater, 24, 580 (2012).

[2] M. Manceau, A. Rivaton, J-.L. Gardette, S. Guillerez, N. Lamaitre, Polymer degradation and stability, 94, 898 (2009)

[3] H. Hintz, C. Sessler, H. Peisert, H-.J. Egelhaaf and T. Chassé, Chem. Mater, 24, 2739 (2012).

[4] Z. Liang, A. Nardes, D. Wang, J.J. Berry, and B.A. Gregg, Chem. Mater. 20, 6307 (2008).

[5] S. Hoshino, M. Yoshida, S. Uemura, T. Kodzasa, N. Takada, T. Kamata, and K. Yase, J. Appl. Phys. 95, 5088 (2004)

[6] M.S.A. Abdou, F.P. Orfino, Y. Son, and S. Holdcroft, J. Am. Chem. Soc, 119, 4518 (1997).

[7] E. J. Meijer, A.V. G. Mangnus, B.-H. Huisman, G. W. t Hooft, D. M. de Leeuw, and T. M. Klapwijk, Synth. Met. 142, 53 (2004).

[8] E.J. Meijer, C. Detcheverry, P.J. Baesjou, E. Van Veenendaal, D.M. de Leeuw, and T.M. Klapwijk, J. App. Phys, 93, 4831 (2003).

[9] H.-H. Liao, C.-M. Yang, C.-C. Liu, S.-F. Horng,H.-F. Meng, J.-T. Shy, J. App. Phys, 103, 104506 (2008).

[10] C.-K. Lu and H.-F. Meng, Phys. Rev. B, 75 235206 (2007).

[11] M.O. Reese, A.M. Nardes, B.L. Rupert, R.E. Larsen, D.C. Olson, M.T. Llyod, S. E. Shaheen, D.S. Ginley, G. Rumbles and N. Kopidakis, Adv. Func.Mater, 20, 3476 (2010).

[12] E. Voroshazi, B. Verreet, T. Aernouts, P. Heremans, Sol. Energy. Mater. Sol. Cells, 95, 1303 (2011).

[13] S. Khelifi, K. Decock, J. Lauwaert, H. Vrielinck, D. Spoltore, F. Piersimoni, J. Manca, A. Belghachi, M. Burgelman, J. Appl. Phys, 110, 094509-1, (2011)

[14] M. Burgelman, P. Nollet, and S. Degrave, Thin solid films, 361-362, 527 (2000).

[15] C.-T. Sah and W. Shockley, Phys. Rev, 109, 1103 (1958).

[16] K. Decock, S. Khelifi, and M. Burgelman, Thin Solid Films, 519, 7481 (2011).

[17] T. Kirchartz, B. E. Pieters, J. Kirkpatrick, U. Rau, J. Nelson, Phys. Rev. B, 83, 115209-1 (2011)

[18] M.O. Reese et al., Solar energy materials and solar cells, 95, 1253 (2011).

[19] K. Vandewal, L. Goris, I. Haeldermans, M. Nesladek, K. Haenen, P. Wagner, and J.Manca, Thin Solid Films, 516, 7135 (2008).

[20] F. Piersimoni, S. Chambon, K. Vandewal, R. Mens, T. Boonen, A. Gadisa, M. Izquierdo, S. Filippone, B. Ruttens, J. D'Haen, N. Martin, L. Lutsen, D. Vanderzande, P. Adriaensens ortunato, and J. Manca, J. Phys.Chem. C 15, 10873 (2011).

[21] A. Pivrikas, N.S. Sariciftci, G. Juška, and R. Österbacka, Prog. Photovolt: Res.Appl. 15, 677 (2007).

[22] D. Spoltore, W.D. Oosterbaal, S. Khelifi, J.N. Clifford, A. Viterisi, E. Palomares, M. Burgelman, L. Lutsen, D. Vanderzande, J. Manca, Adv.Energy. Mater, (2012), doi:10.1002/aenm.201200674

[23] S. Khelifi, A. Belghachi, J. Lauwaert, K. Decock, J. Wienke, R. Caballero, C.A. Kaufmann, and M. Burgelman, Energy. Proc, 2, 109 (2010).

[24] S. Khelifi, J. Marlein, M. Burgelman, A. Belghachi, Proceeding of 23rd *European Photovoltaic Solar Energy Conference*, Valencia, 2165-2169 (2008).

[25] T. Walter, R. Herberholtz, C. Müller, and H.-W. Schock, J. Appl. Phys, 80, 4411 (1996).

[26] J.C. Scott, J. H. Kaufman, P. J. Brock, R. DiPietro, J. Salem, and J.A. Goitia, J. Appl. Phys, 79, 2745 (1996).

[27] M.P. de Jong, L. J. Van IJzendoorn, and M. J. A. de Voigt, Appl. Phys. Lett, 77, 2255 (2000).

[28] S. Bertho, G. Janssen, T. J. Cleij, B. Conings, W. Moons, A. Gadisa, J. D'Haen, E. Goovaerts, L. Lutsen, J. Manca, D. Vanderzande, Sol. Energy. Mater. Sol. Cells, 92, 753 (2008)

[29] P.E. Shaw, A. Ruseckas, and I.D.W. Samuel, Adv. Mater, 20, 3516 (2008).

[30] J. Nelson, Phys. Rev. B, 67, 155209 (2003)

[31] C. G. Shuttle, B. O'Regan, A. M. Ballantyne, J. Nelson, D. Bradley, J. R. Durrant, Phys. Rev. B, 78, 113201 (2008)

[32] M. Burgelman, B. Minnaert, C. Grasso, "Device modeling of nanostructured solar cells" in "Nanostructured materials for solar energy conversion" edited by T. Soga, (Elsevier, 2006).

[33] R. E. I. Schropp and M. Ziman, Amorphous and crystalline silicon solar cells: Modeling, materials and device technology, (Kluwer Academic Publishers 1998).

[34] M. Glatthaar, M. Riede, N. Keegan, K. Sylvester-Hvid, B. Zimmermann, N. Niggemann, H. Hinsch, A. Gombert, Sol. Energy. Mater. Sol. Cells, 91, 390 (2007).

[35] A. Kumar, S. Sista, Y. Yang, J. Appl. Phys, 105, 094512 (2009)

[36] W. Tress, K. Leo, M. Riede, Adv. Fun. Mater, 21, 2140 (2011)

[37] A. Wagenpfahl, D. Rau, M. Binder, C. Deibel, and V. Dyakonov, Phys. Rev. B., 82, 115306 (2010).

Table 1

Table 1 Solar cells parameters measured before and after the ageing under 100 mW/cm^2 AM1.5.

Illumination duration	V_{oc} (mV)	J_{sc} (mA/cm^2)	FF (%)	η (%)
0 h	580±3.3	8.6±0.23	57±2.7	2.9±0.20
50 h	556±7.0	7.8±0.10	57±2.3	2.5±0.14
250 h	497±3.4	5.0±0.14	58±0.8	1.4±0.04
700 h	495±3.6	4.5±0.22	57±0.8	1.3±0.06
1050 h	459±5.5	3.7±0.20	29±5.5	0.5±0.11

Table 2

Table 2 A summary of the standard cell parameters used in SCAPS simulation

Parameter	Symbol	Value	Unit
Thickness	d	300	nm
Bandgap	E_g	1.2	eV
Effective density of states	N_c, N_v	10^{19}	cm^{-3}
Electron mobility	μ_n	10^{-3}	cm^2/V.s
Hole mobility	μ_p	10^{-3}	cm^2/V.s
Dielectric constant	ε	3.5	
Metal work function at anode	ϕ_p	4.75	eV
Metal work function at cathode	ϕ_n	4.2	eV
Electron capture cross section	σ_n	10^{-17}	cm^2
Hole capture cross section	σ_p	5×10^{-18}-9×10^{-19}	cm^2

Figure 1a

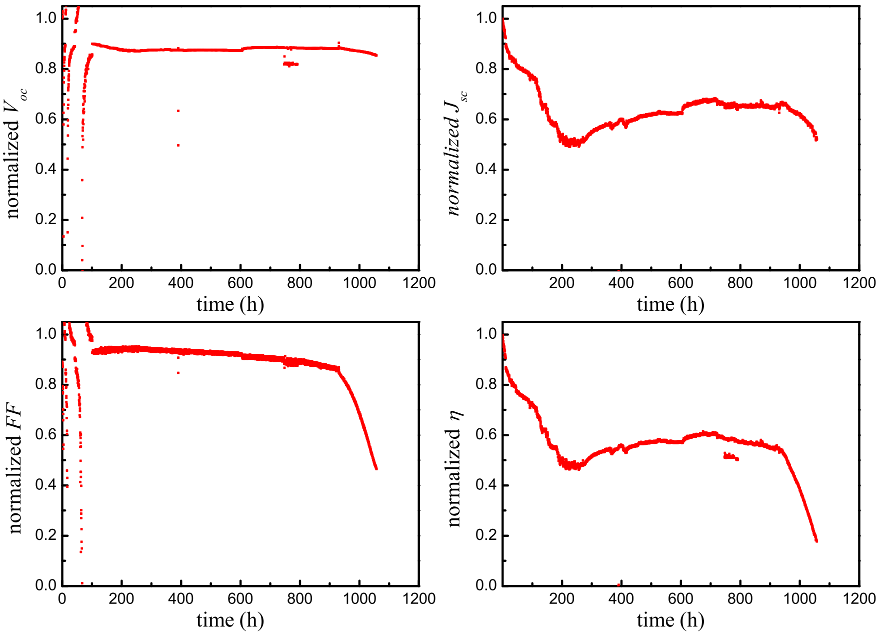

1.0
0.8
0.6
0.4
0.2
0.0
normalized V_{oc}
0
200
400
600
800
1000
1200
time (h)
normalized J_{sc}
200
400
600
800
1000
1200
time (h)
normalized FF
0
200
400
600
800
1000
1200
time (h)
normalized η
200
400
600
800
1000
1200
time (h)

Figure 1b

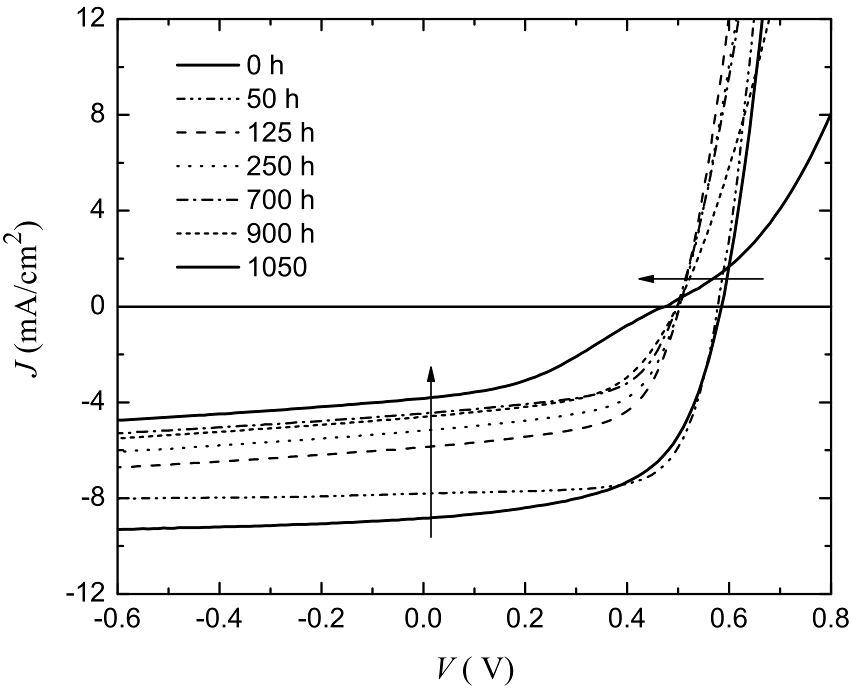

12
8
4
0
-4
-8
-12
-0.6
-0.4
-0.2
0.0
0.2
0.4
0.6
0.8
J (mA/cm^2)
V (V)
0 h
50 h
125 h
250 h
700 h
900 h
1050

Figure 2

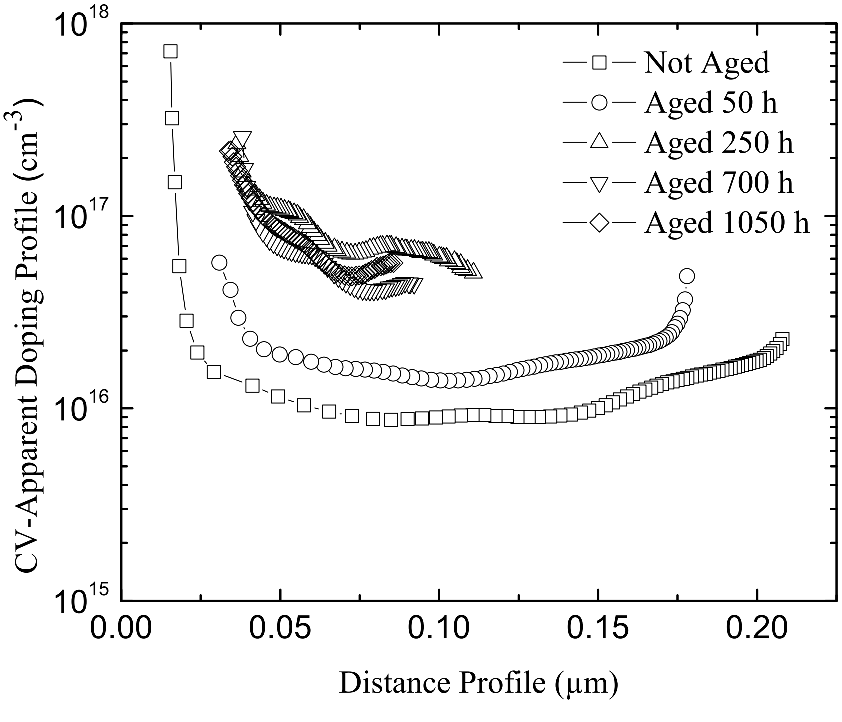
10^{18}
10^{17}
10^{16}
10^{15}
0.00
0.05
0.10
0.15
0.20
CV-Apparent Doping Profile (cm^{-3})
Distance Profile (μm)
Not Aged
Aged 50 h
Aged 250 h
Aged 700 h
Aged 1050 h

Figure 3

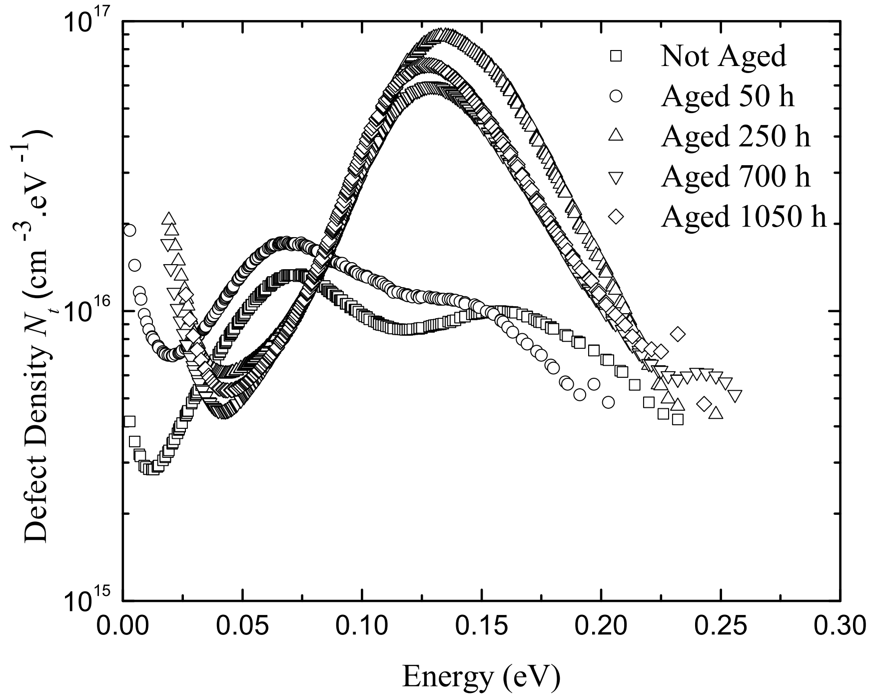
10^{17}
10^{16}
10^{15}
0.00
0.05
0.10
0.15
0.20
0.25
0.30
Energy (eV)
Defect Density N_t (cm $^{-3}$.eV $^{-1}$)
□ Not Aged
○ Aged 50 h
△ Aged 250 h
▽ Aged 700 h
◇ Aged 1050 h

Figure 4a

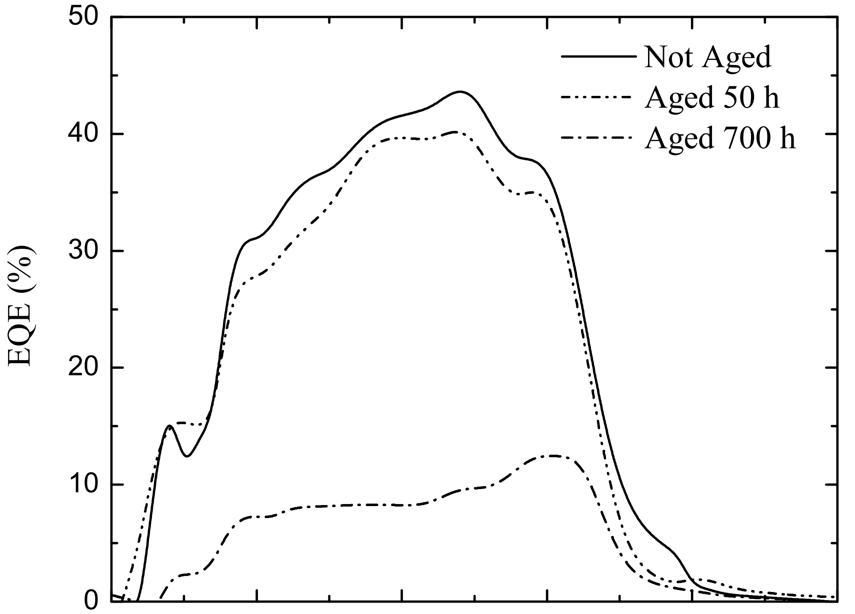
50
40
30
20
10
0
EQE (%)
300
400
500
600
700
800
Wavelength (nm)
Not Aged
Aged 50 h
Aged 700 h

Figure 4b

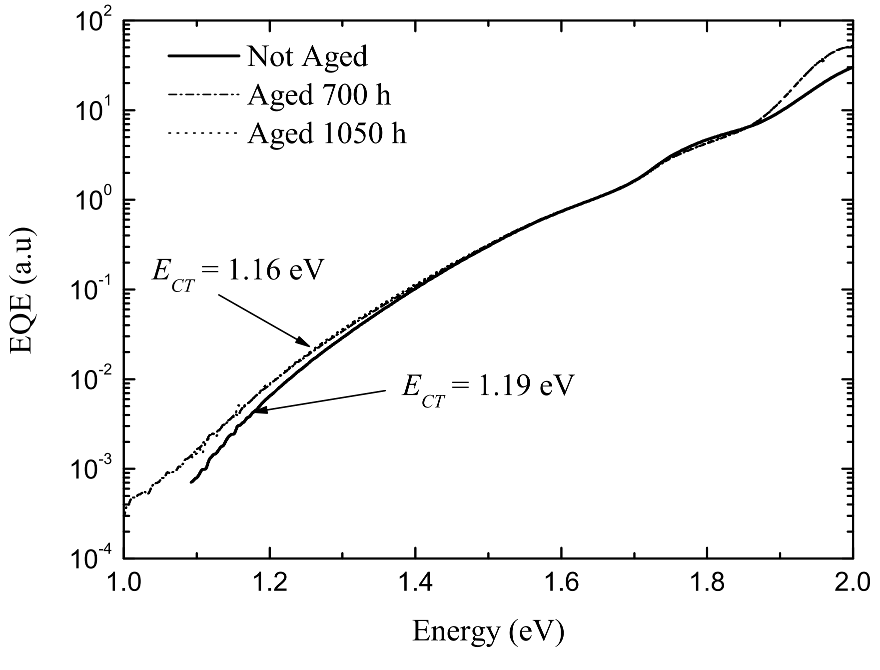

Not Aged
Aged 700 h
Aged 1050 h
$E_{CT} = 1.16$ eV
$E_{CT} = 1.19$ eV
EQE (a.u)
Energy (eV)
10^{2}
10^{1}
10^{0}
10^{-1}
10^{-2}
10^{-3}
10^{-4}
1.0
1.2
1.4
1.6
1.8
2.0

Figure 5a

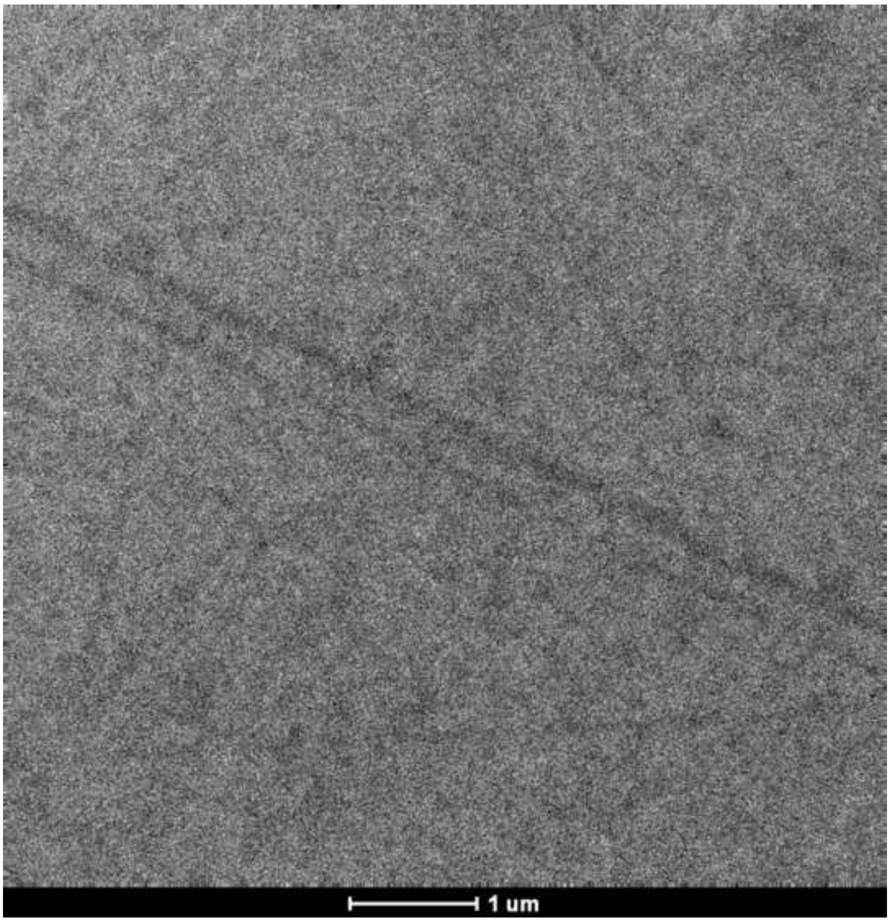

Figure 5b

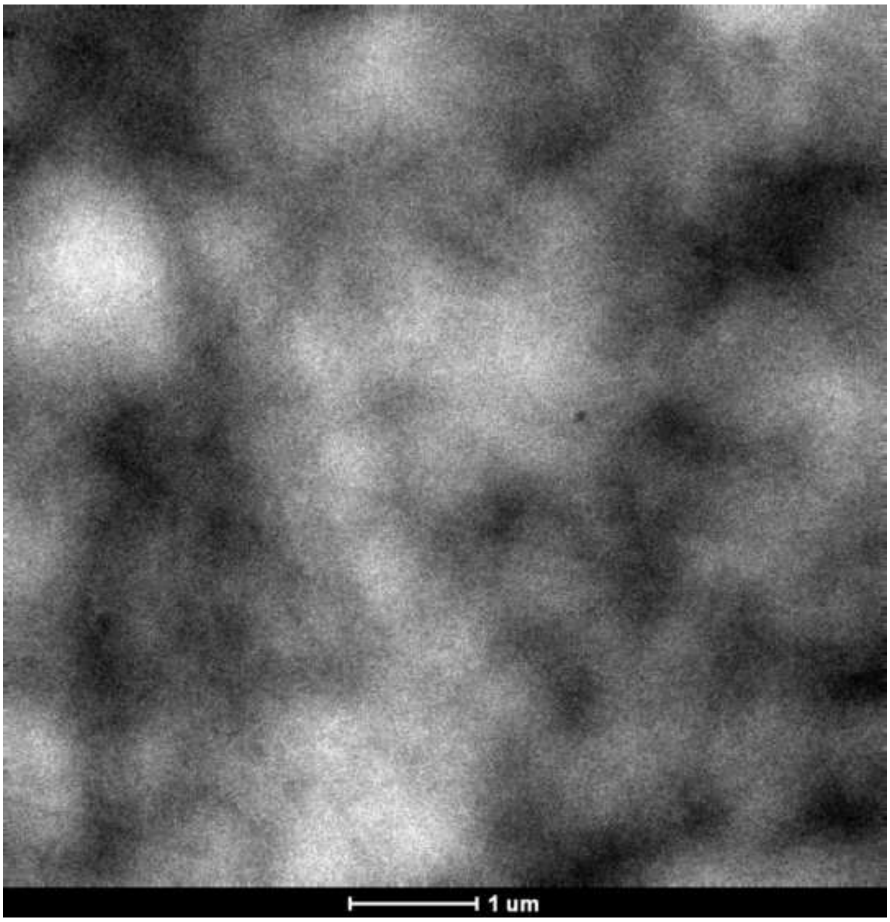

Figure 6

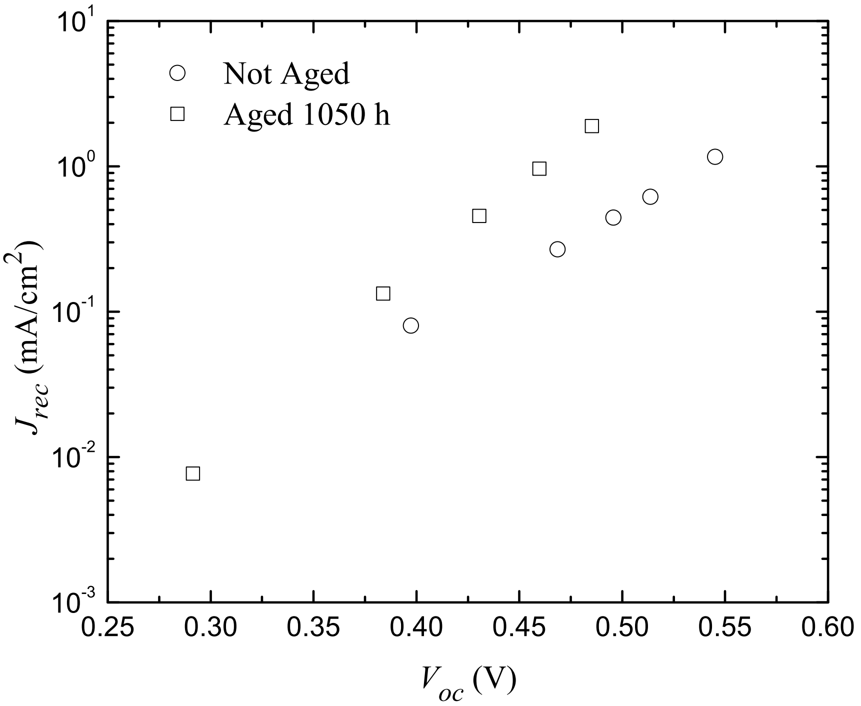
10^1
10^0
10^{-1}
10^{-2}
10^{-3}
J_{rec} (mA/cm^2)
0.25
0.30
0.35
0.40
0.45
0.50
0.55
0.60
V_{oc} (V)
○ Not Aged
□ Aged 1050 h

Figure 7

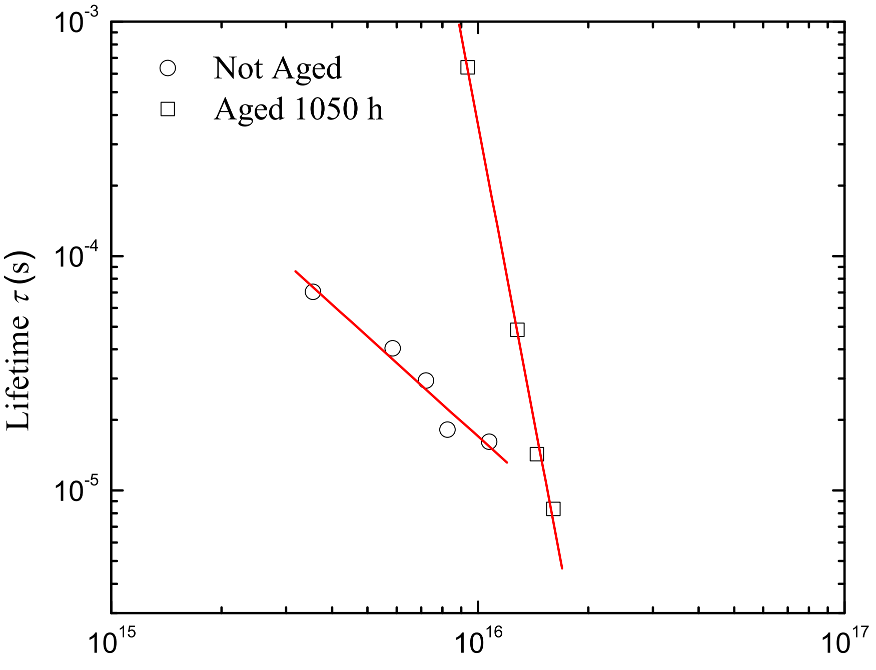
○ Not Aged
□ Aged 1050 h
Lifetime τ (s)
10^{-3}
10^{-4}
10^{-5}
10^{15}
10^{16}
10^{17}
Photogenerated carrier density n (cm^{-3})

Figure 8a

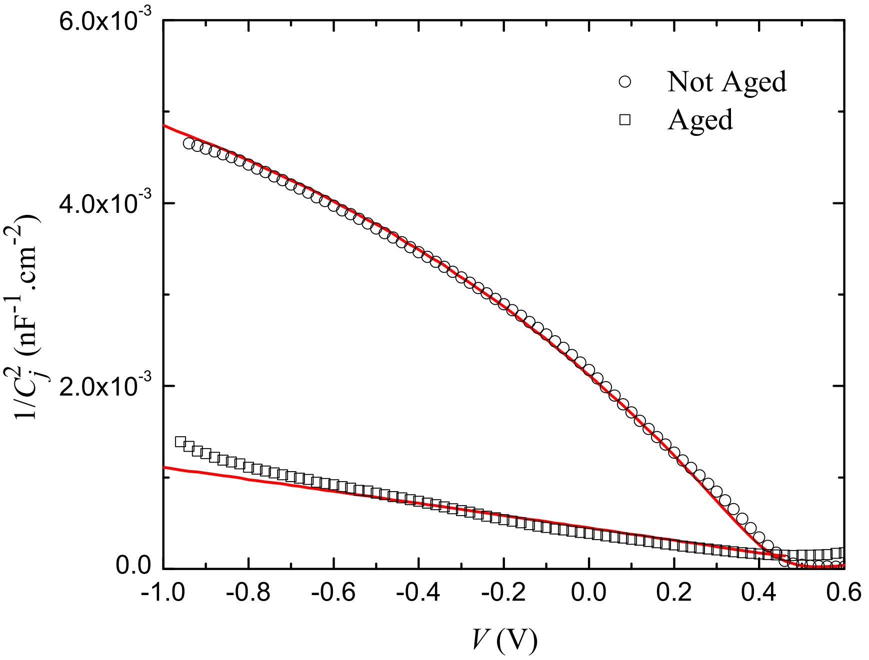
6.0x10^{-3}
4.0x10^{-3}
2.0x10^{-3}
0.0
$1/C_j^2$ (nF^{-1}.cm^{-2})
-1.0
-0.8
-0.6
-0.4
-0.2
0.0
0.2
0.4
0.6
V (V)
○ Not Aged
□ Aged

Figure 8b

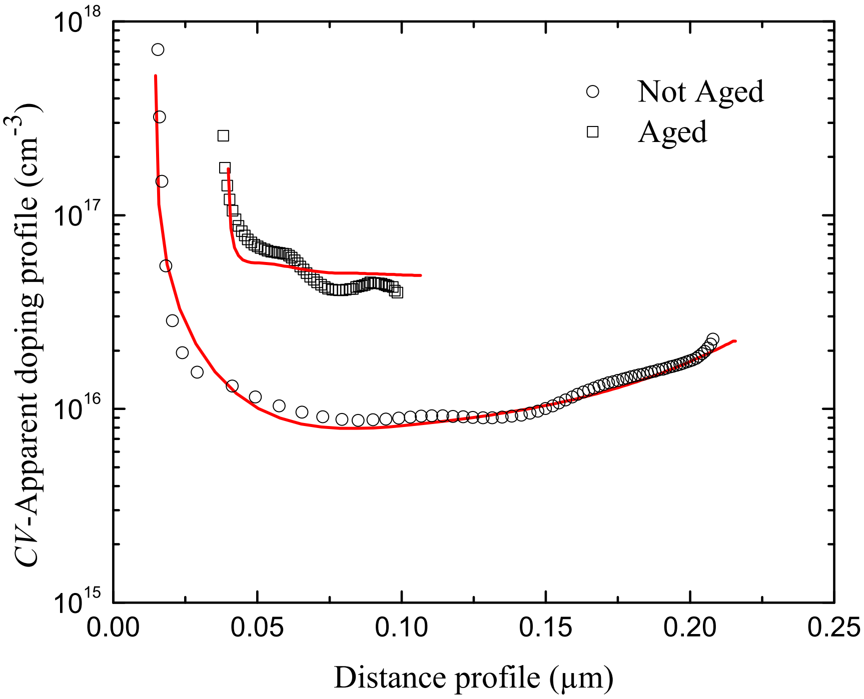
10^{18}
10^{17}
10^{16}
10^{15}
0.00
0.05
0.10
0.15
0.20
0.25
CV-Apparent doping profile (cm^{-3})
Distance profile (μm)
○ Not Aged
□ Aged

Figure 9

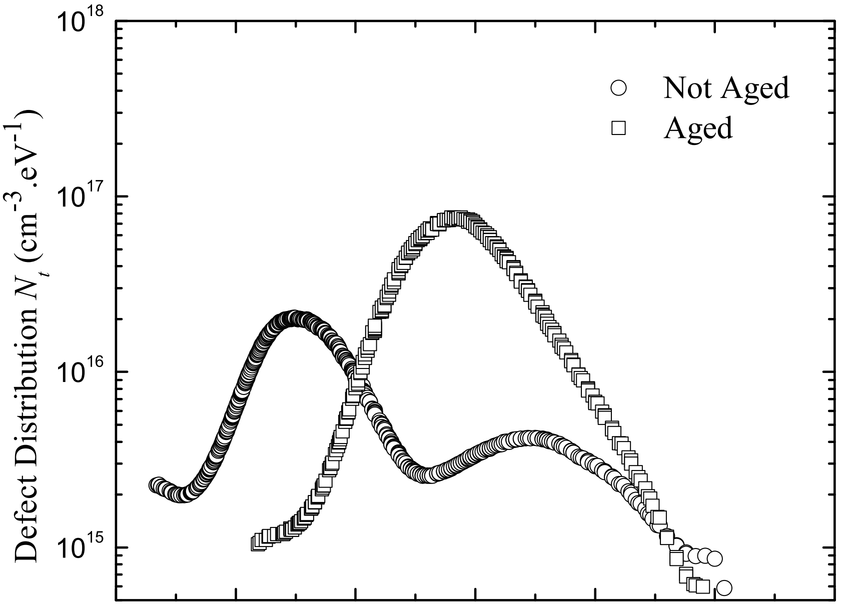
10^{18}
10^{17}
10^{16}
10^{15}
Defect Distribution N_t (cm^{-3}.eV^{-1})
○ Not Aged
□ Aged
0.00
0.05
0.10
0.15
0.20
0.25
0.30
Energy (eV)

Figure 10

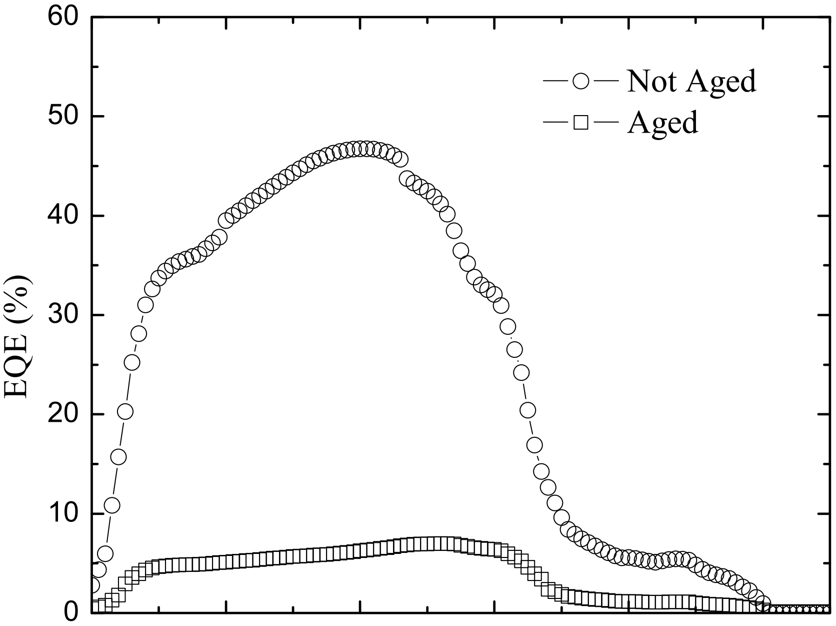

Not Aged
Aged
EQE (%)
Wavelength (nm)
0
10
20
30
40
50
60
300
400
500
600
700
800

Figure 11

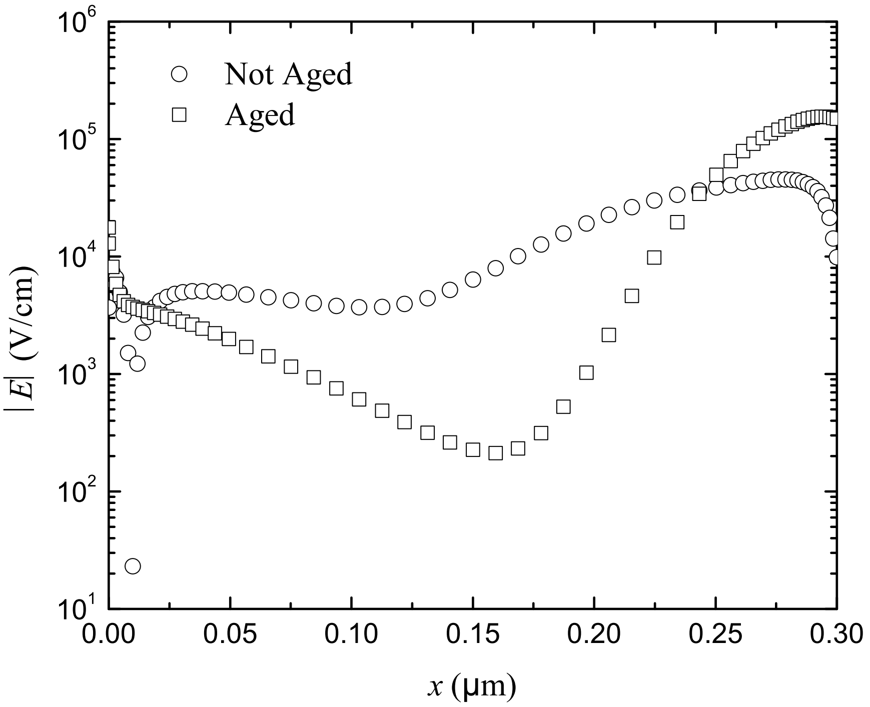
Not Aged
Aged
10^6
10^5
10^4
10^3
10^2
10^1
|E| (V/cm)
0.00
0.05
0.10
0.15
0.20
0.25
0.30
x (μm)

Figure 12

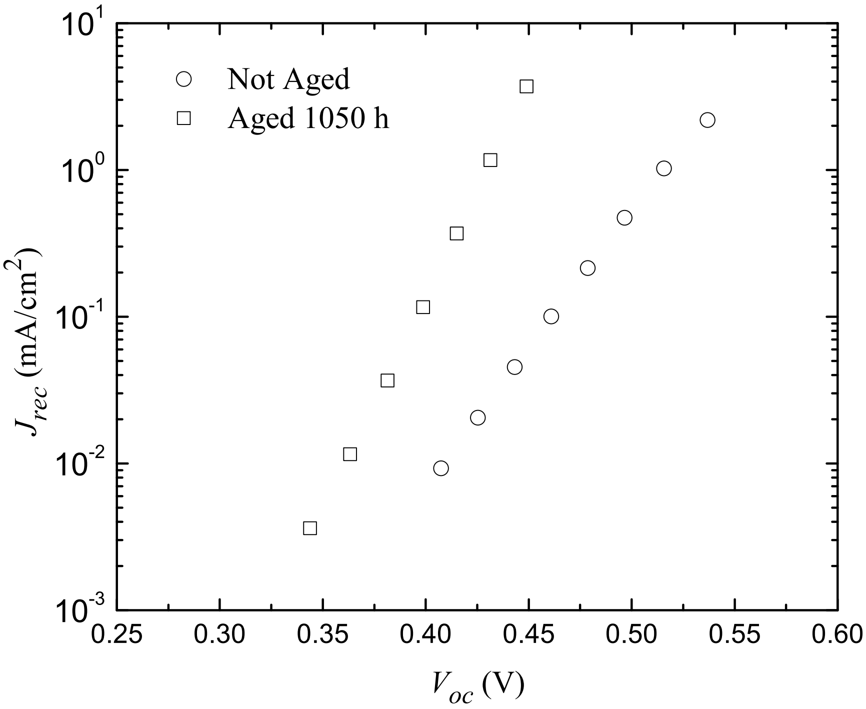

10^1
10^0
10^{-1}
10^{-2}
10^{-3}
J_{rec} (mA/cm^2)
○ Not Aged
□ Aged 1050 h
0.25
0.30
0.35
0.40
0.45
0.50
0.55
0.60
V_{oc} (V)

Figure 13

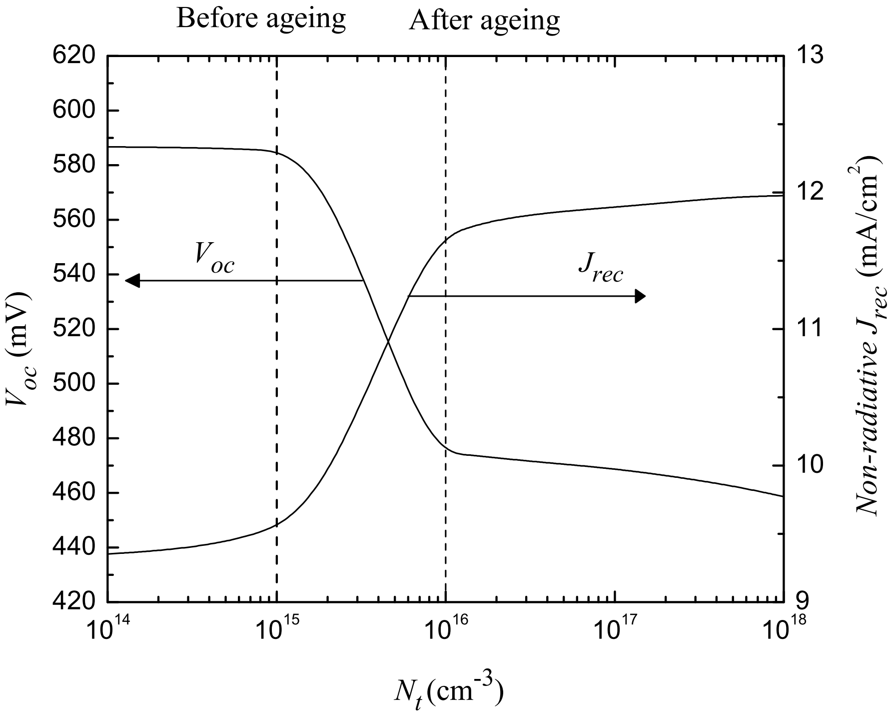
Before ageing
After ageing
620
600
580
560
540
520
500
480
460
440
420
13
12
11
10
9
V_{oc}
J_{rec}
V_{oc} (mV)
Non-radiative J_{rec} (mA/cm^2)
10^{14}
10^{15}
10^{16}
10^{17}
10^{18}
N_t (cm^{-3})

Figure 14a

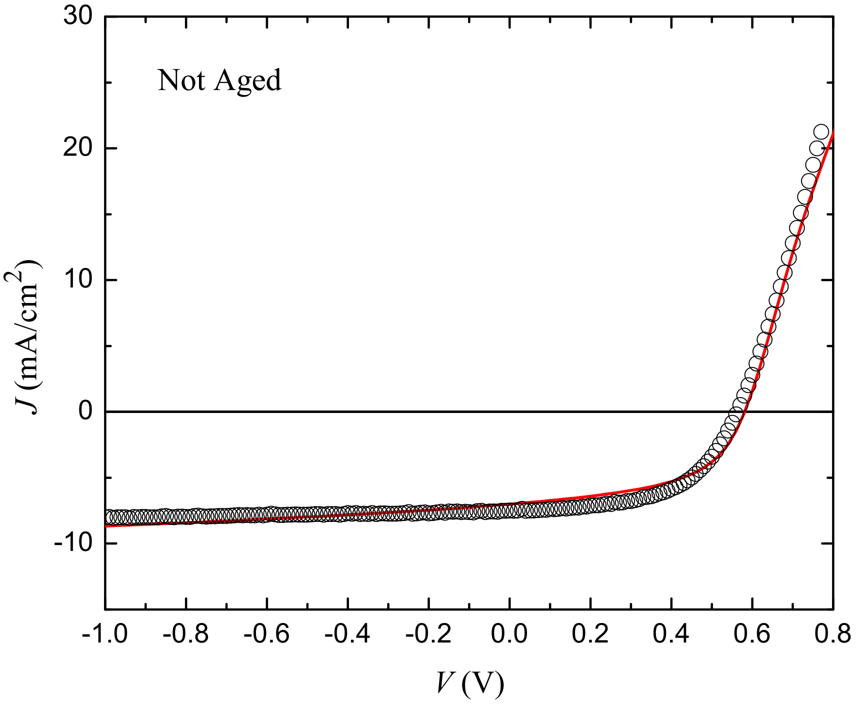

Figure 14b

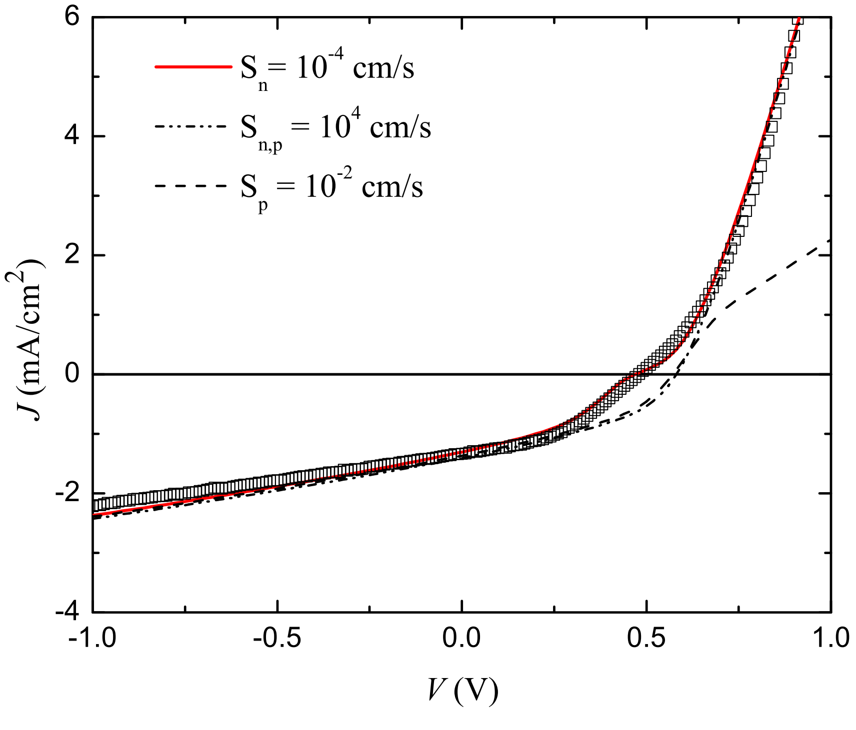

Paper D

B. Conings, L. Baeten, H.-G. Boyen, D. Spoltore, J. D'Haen, M.K. Van Bael, and J.V. Manca, *"Generalized approach to the description of recombination kinetics in bulk heterojunction solar cells-extending from fully organic to hybrid solar cells"* Applied Physics Letters 100, 203905 (2012)

Generalized approach to the description of recombination kinetics in bulk heterojunction solar cells—extending from fully organic to hybrid solar cells

Bert Conings,[1,a)] Linny Baeten,[2] Hans-Gerd Boyen,[1,3] Donato Spoltore,[1] Jan D'Haen,[1,3]
Marlies K. Van Bael,[2,3] and Jean V. Manca[1,3]
[1]*Hasselt University, Institute for Materials Research, Materials Physics, Wetenschapspark 1, 3590 Diepenbeek, Belgium*
[2]*Hasselt University, Institute for Materials Research, Inorganic and Physical Chemistry, Agoralaan building D, 3590 Diepenbeek, Belgium*
[3]*Imec vzw, Division IMOMEC, Wetenschapspark 1, 3590 Diepenbeek, Belgium*

(Received 27 March 2012; accepted 20 April 2012; published online 15 May 2012)

Lately, research efforts in photovoltaics towards hybrid solar cells based on nanostructured metal oxides and conjugated polymers have been intensifying. However, very limited effort has been spent so far to investigate their recombination kinetics in comparison with their fully organic counterpart. In this work, impedance spectroscopy under different illumination intensities is used to probe the recombination kinetics of hybrid solar cells based on ZnO nanorod arrays and poly(3-hexylthiophene). A recombination-based model developed for fully organic solar cells is effectively applied in our hybrid solar cells, demonstrating their similarity in device physics and establishing the nanorod array/polymer compound as true bulk heterojunction. © *2012 American Institute of Physics*. [http://dx.doi.org/10.1063/1.4714902]

Photovoltaics have proven to be a key contender to meet the world's need for clean and sustainable energy.[1] Silicon-based solar cells find their origin in the 1950's but are still under development, the main goals now being directed not only toward performance improvement but also very much toward cost-effectiveness, which is a challenge.[2,3] Consequently, despite their performance-wise inferiority compared to their silicon counterparts, newer types of solar cells like organic and hybrid solar cells are gaining ground primarily because of their potential for cheaper fabrication.[4,5] The most mature device type in this respect is the organic bulk heterojunction (OBHJ) solar cell, the active layer of which consists of an interpenetrating network of a light absorbing electron-donating material and an electron-accepting material, typically a conjugated polymer and a fullerene-derivative, respectively.[6,7] However, these OBHJ devices are more prone to temperature-driven phase separation, thus degradation, whereas hybrid (organic/inorganic) solar cells are intrinsically more stable due to their template-based morphology.[8,9] It is well established that for OBHJ solar cells, non-geminate recombination is the main loss mechanism that limits their performance.[10–12] For hybrid solar cells, however, recombination-related studies are rather scarce,[13] leaving the identification of the underlying loss mechanisms (as compared to their fully organic counterpart) still an open question. Consequently, in order to optimize hybrid solar cells in a systematic manner, the understanding of recombination dynamics in such devices urgently needs to be improved.

In this work, we demonstrate with impedance spectroscopy measurements under varying light intensity that for hybrid solar cells based on ZnO nanorod arrays and poly(3-hexylthiophene) (P3HT), the presiding mechanism that governs the open circuit voltage is a strongly light intensity- and charge carrier density-dependent non-geminate recombination, together with a virtual absence of non-geminate recombination at short circuit conditions. Based on these results, we demonstrate that the approach used to describe recombination kinetics in fully organic P3HT:1-(3-methoxycarbonyl)propyl-1-phenyl-[6,6]-methano fullerene (PCBM) devices can be generalized and extended to hybrid solar cells.

In order to uncover the device physics of OBHJ solar cells, the combination of P3HT and PCBM has been and still is the most frequently used model system, even though its performance has been surpassed by combinations of low-bandgap polymers and alternative PCBM-derivatives.[14,15] In contrast to the widespread assumption of a simple binary mixture of both materials within a corresponding thin film,[16,17] a thin layer of P3HT:PCBM is dominated by a rather complex film morphology comprising crystalline P3HT domains, crystalline PCBM domains, and compound domains of both amorphous P3HT and PCBM, being subject to both horizontal and vertical phase separation.[18,19] The formation of these different kinds of domains is inherent to solution processing, for which the resulting film microstructure is strongly dependent on solvent, drying time, possible additives and annealing treatments.[19–22] Naturally, microstructure affects device performance, and much effort has been undertaken to reveal correlations between domain size and photocurrent as well as charge recombination.[17,23,24] However, the intricacy of controlling domain size and structure makes the investigation of recombination dynamics equally challenging. Template-based solar cells enable more control over morphology as they are fabricated in a two-step process where the "template" acceptor part is pre-synthesized and subsequently infiltrated by the donor part.[25,26] This type of devices could thereby help designing recombination

---

[a)] Author to whom correspondence should be addressed. Electronic mail: bert.conings@uhasselt.be.

dynamics-related experiments that rely on careful control over morphology. A suitable platform for this purpose is the combination of ZnO nanorod arrays and P3HT, which was introduced in 2006 by Olson and co-workers, followed by regular improvements in performance and basic understanding.[25,27,28] We demonstrated recently that by tuning the morphology of the nanorod array together with the bulk and interfacial P3HT morphologies, the performance of these devices can be systematically manipulated and optimized, with efficiencies passing 0.8% so far.[28,29]

Figure 1(a) illustrates the device setup of such solar cells, together with their equivalent circuit as identified earlier, part of which will be further exploited in this work.[28] A corresponding SEM image is depicted in Figure 1(b), where the brightest areas delineate the ITO (bottom) and the Ag (top) electrode. For this work, a range of devices was prepared, thereby varying parameters such as nanorod length, diameter and spacing, as well as thermal treatment of the polymer, as described elsewhere and in supplemental information.[26,29,53]

A hint towards the recombination behavior of photoexcited charge carriers is provided by the dependence of the short circuit current J_{sc} as well as the open circuit voltage V_{oc} on light intensity. A representative example is given in Figure 2, covering a wide range of light intensities varying from 0.001 to 1 sun. J_{sc} follows a power law dependence on illumination intensity, $J_{sc} \sim I^{\alpha}$ with $\alpha > 0.95$, which is very similar to values reported for P3HT:PCBM cells in the literature.[24,30] This indicates a very limited presence of space-charge buildup,[31,32] and suggests the absence of a strong non-geminate recombination at short circuit conditions.[11]

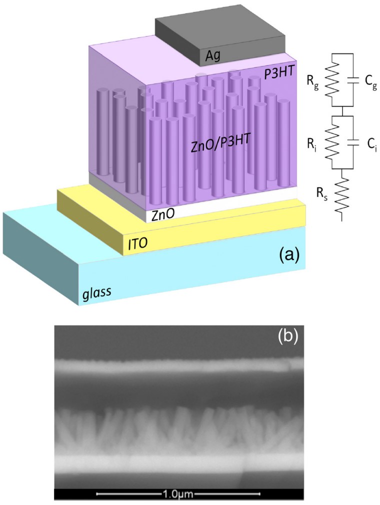

FIG. 1. (a) Hybrid ZnO nanorod array/P3HT device structure with corresponding equivalent circuit and (b) cross-section scanning electron micrograph of a typical device.

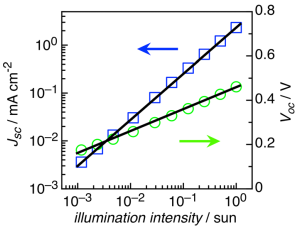

FIG. 2. Light intensity dependence of short circuit current and open circuit voltage for a typical hybrid ZnO nanorod array/P3HT device. The black lines indicate their power law and logarithmic behavior, respectively.

Simultaneously, V_{oc} depends linearly on the logarithm of the light intensity, as was also observed for fully organic solar cells.[33] The slope of the curve is unaffected by processing conditions, which implies a steady amount of trap-assisted recombination.[34,35]

Aiming to unravel the similarities/differences between hybrid and organic solar cells regarding recombination kinetics, we adopt a model recently developed for organic solar cells by the Durrant group, which is based on matching the flux of photogenerated charges with the flux of non-geminate recombination.[11] Accordingly, the total current extracted from a solar cell can be considered to arise from two contributions, namely the photocurrent (resulting from illumination) and, in opposite direction, the loss current.[11,36]

$$J(V) = J_{photo}(V) + J_{loss}(V). \tag{1}$$

The loss current J_{loss} can be estimated from the charge carrier density and lifetime under illumination by[11,37]

$$J_{loss} = ed\frac{n(V_{oc})}{\tau_n(V_{oc})} \tag{2}$$

with e representing the elementary charge, d the active layer thickness, n the average charge carrier density, and τ_n the average charge carrier lifetime.

Charge carrier densities and loss mechanisms in solar cells have been investigated before by a variety of techniques, including transient absorption spectroscopy,[38–40] transient photovoltage (TPV) and transient photocurrent (TPC),[39,41–43] time-of-flight,[44–46] and impedance spectroscopy.[35,47,48] Here, we use impedance spectroscopy to probe the charge carrier densities and lifetimes for ZnO nanorod array/P3HT solar cells. The main asset of impedance spectroscopy is that it can easily distinguish between different phenomena occurring in the same device, such as diffusion and recombination processes. During a measurement, a signal consisting of a small sinusoidal voltage $V_{ac}(\omega)$ superimposed on a bias voltage V_{dc} is applied to the device, thereby allowing to measure the current output $J_{ac}(\omega)$ with high precision using lock-in technology. The complex impedance is then given by:

$$Z(\omega) = Z'(\omega) + iZ''(\omega) = \frac{V_{dc} + V_{ac}(\omega)}{J_{ac}(\omega)}. \tag{3}$$

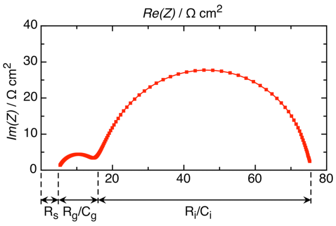

FIG. 3. Typical impedance spectrum revealing the equivalent circuit elements as indicated in Figure 1(a).

Acquiring $Z(\omega)$ for ZnO nanorod array/P3HT solar cells for a range of frequencies yields spectra that typically contain features as can be seen in Figure 3. These spectral features can be used to identify the underlying physical parameters, which allows to assign them to circuit elements as indicated in Figure 1(a).[28] Here, resistor R_s represents the series resistance created by the electrodes (offset on the real axis, thus representing a purely ohmic contribution). The parallel combination of R_g and C_g stands for the geometric (volume) contribution of the polymer (left semicircle), while the parallel elements R_i and C_i put forward the interface between ZnO and P3HT (bias-dependent right semicircle). It is the latter R_i and C_i combination that will be focused on in this work as it provides easy access to the photogenerated carrier recombination (R_i) and storage (C_i) at the donor/acceptor interface. Additionally, it defines a time constant $\tau_{\Delta n} = R_i C_i$ that represents the corresponding small-perturbation charge carrier lifetime.

Charge carrier density and lifetime are highly dependent on solar cell working conditions, and can only be properly obtained by considering a small perturbation of a steady-state.[49] This steady-state condition is created, for each light intensity, by biasing the cell with the appropriate V_{oc}, i.e., the voltage which allows to completely suppress the total current flowing through the cell. Subsequently, a small perturbation is created by superimposing a small oscillating voltage V_{ac} thus giving impedance spectroscopy the intrinsic advantage that the measurement is not affected by charging effects that are known to cause problems in TPV and TPC measurements.[35] Repeating this procedure for different light intensities thus enables to access the dependence of the charge carrier density n and small-perturbation lifetime $\tau_{\Delta n}$ on V_{oc} by using the following relations:[11]

$$n = n_0 e^{\gamma V_{oc}} \tag{4}$$

$$\tau_{\Delta n} = \tau_{\Delta n_0} e^{-\beta V_{oc}}. \tag{5}$$

Here, n is calculated by integration of the capacitance C_i at each V_{oc} value:

$$n = \frac{1}{ed}\int_0^{V_{oc}} C_i(V)\,\mathrm{d}V \tag{6}$$

with d the active layer thickness. This is an established technique also used in case of TPV, and equivalent to a direct measurement of n using charge extraction (CE).[11,39,50] Inserting now Eqs. (4) and (5) into Eq. (2) and considering that the effective lifetime depends on the small-perturbation lifetime as $\tau_n = (1 + \beta/\gamma)\tau_{\Delta n}$[11,51] results in an alternative expression of the loss current:

$$J_{loss} = \frac{edn_0 e^{V_{oc}(\beta+\gamma)}}{(1+\beta/\gamma)\tau_{\Delta n_0}}. \tag{7}$$

By taking into account that, at open circuit condition, $J_{loss} = J_{sc}$,[11,52] from Eq. (7) an expression for V_{oc} can be derived:

$$V_{oc} = \frac{1}{\beta+\gamma} ln\left[\frac{(1+\beta/\gamma)\tau_{\Delta n_0} J_{sc}}{edn_0}\right]. \tag{8}$$

Figure 4(a) shows n and $\tau_{\Delta n}$ as a function of V_{oc} for a typical solar cell. n shows an exponential behavior with respect to V_{oc}, which justifies a fit according to Eq. (4) to extract the values of n_0 and γ. A negative exponential trend is observed for $\tau_{\Delta \mathrm{n}}(V_{oc})$, allowing to obtain $\tau_{\Delta n_0}$ and β by fitting to Eq. (5). Inserting these values in Eq. (8) ultimately results in an independent prediction of V_{oc}, using exclusively the above mentioned circuit elements derived experimentally by means of impedance spectroscopy. This now enables us to compare with V_{oc} values extracted directly from corresponding J/V curves and, therefore, to critically test the applicability of the model (which was established using purely organic solar cells) to hybrid photovoltaic devices. Figure 4(b) contains the V_{oc} values extracted using the above formalism as

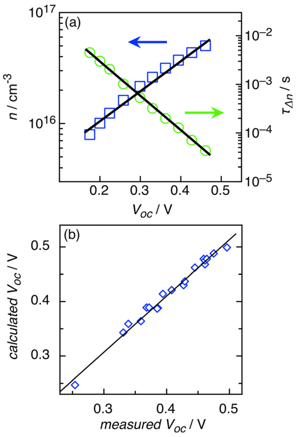

FIG. 4. Typical behavior of charge carrier density and small-perturbation carrier lifetime obtained from impedance spectroscopy measurements as a function of V_{oc}. Black lines are fits to the data. (b) Calculated values of V_{oc} by means of Eq. (8) versus measured values of V_{oc} for a representative selection of solar cells in various degrees of optimization (Refs. 26 and 29).

compared to experimentally determined V_{oc} values measured on a number of solar cells prepared in various degrees of optimization.[26,29] The correlation between measured and calculated values of V_{oc} is excellent, with an average deviation of 10 mV. This result gives strong confidence that the most essential conceptions with respect to recombination kinetics of organic photovoltaics are also valid in metal-oxide/polymer solar cells. The effective application of the model suggests that the idea of a sustained quasi-Fermi level for holes in the strongly p-doped P3HT and a light intensity dependent quasi-Fermi level for electrons, as adopted for P3HT:PCBM, is also valid for the hybrid ZnO/P3HT system and substantiates the equivalency of PCBM and ZnO in this sense.[10,50,52] In both cases, the presiding mechanism that governs the open circuit voltage is a strongly light intensity- and, thus, charge carrier density-dependent non-geminate recombination, together with a virtual absence of non-geminate recombination at short circuit conditions as evidenced by the nearly linear dependence of J_{sc} on light intensity (Figure 2).[11] Additionally, the nanorod array/polymer compound can now be morphologically considered as true bulk heterojunction since the presence of direct pathways for charge carriers instead of sinuous percolative ones does not appear to induce a divergent recombination signature.

In summary, a light intensity-dependent study reveals that hybrid solar cells based on ZnO nanorod arrays and P3HT function according to the same basic principles of photo-excitation and recombination as found for the model system P3HT:PCBM. This finding is achieved by extracting voltage-dependent charge carrier densities and lifetimes by means of impedance spectroscopy, serving as input parameters for a recombination model developed for purely organic solar cells. The predicted values for V_{oc} are accurately confirmed by experiment, thereby extending the validity range of the recombination model towards inorganic/organic hybrid solar cells and, consequently, towards a more general applicability. This result conclusively demonstrates that hybrid and organic photovoltaics can be treated equally from a device physics point of view and thus provides confidence that fundamental recombination-related insights are interchangeable between them.

[1] D. M. Bagnall and M. Boreland, Energy Policy **36**, 4390–4396 (2008).
[2] R. W. Miles, G. Zoppi, and I. Forbes, Mater. Today **10**(11), 20–27 (2007).
[3] R. E. I. Schropp, R. Carius, and G. Beaucarne, MRS Bull. **32**(3), 219–224 (2007).
[4] N. Espinosa, M. Hosel, D. Angmo, and F. C. Krebs, Energy Environ. Sci. **5**(1), 5117–5132 (2012).
[5] R. Po, M. Maggini, and N. Camaioni, J. Phys. Chem. C **114**(2), 695–706 (2009).
[6] H. Hoppe and N. S. Sariciftci, J. Mater. Res. **19**(7), 1924–1945 (2004).
[7] R. R. Lunt, T. P. Osedach, P. R. Brown, J. A. Rowehl, and V. Bulović, Adv. Mater. **23**(48), 5712–5727 (2011).
[8] M. Jørgensen, K. Norrman, and F. C. Krebs, Sol. Energy Mater. Sol. Cells **92**(7), 686–714 (2008).
[9] S. Bertho, I. Haeldermans, A. Swinnen, W. Moons, T. Martens, L. Lutsen, D. Vanderzande, J. Manca, A. Senes, and A. Bonfiglio, Sol. Energy Mater. Sol. Cells **91**, 385–389 (2007).
[10] C. G. Shuttle, B. O'Regan, A. M. Ballantyne, J. Nelson, D. D. C. Bradley, and J. R. Durrant, Phys. Rev. B **78**(11), 113201 (2008).
[11] D. Credgington, R. Hamilton, P. Atienzar, J. Nelson, and J. R. Durrant, Adv. Funct. Mater. **21**(14), 2744–2753 (2011).
[12] T. Kirchartz, B. E. Pieters, J. Kirkpatrick, U. Rau, and J. Nelson, Phys. Rev. B **83**(11), 115209 (2011).
[13] T.-W. Zeng, C.-C. Ho, Y.-C. Tu, G.-Y. Tu, L.-Y. Wang, and W.-F. Su, Langmuir **27**(24), 15255–15260 (2011).
[14] M. T. Dang, L. Hirsch, and G. Wantz, Adv. Mater. **23**(31), 3597–3602 (2011).
[15] S. H. Park, A. Roy, S. Beaupre, S. Cho, N. Coates, J. S. Moon, D. Moses, M. Leclerc, K. Lee, and A. J. Heeger, Nat. Photonics **3**(5), 297–302 (2009).
[16] K. Maturová, S. S. van Bavel, M. M. Wienk, R. A. J. Janssen, and M. Kemerink, Nano Lett. **9**(8), 3032–3037 (2009).
[17] B. Ray, P. R. Nair, and M. A. Alam, Sol. Energy Mater. Sol. Cells **95**(12), 3287–3294 (2011).
[18] M. Pfannmöller, H. Flügge, G. Benner, I. Wacker, C. Sommer, M. Hanselmann, S. Schmale, H. Schmidt, F. A. Hamprecht, T. Rabe, W. Kowalsky, and R. R. Schröder, Nano Lett. **11**(8), 3099–3107 (2011).
[19] M. Campoy-Quiles, T. Ferenczi, T. Agostinelli, P. G. Etchegoin, Y. Kim, T. D. Anthopoulos, P. N. Stavrinou, D. D. C. Bradley, and J. Nelson, Nature Mater. **7**(2), 158–164 (2008).
[20] X. Yang, J. Loos, S. C. Veenstra, W. J. H. Verheers, M. M. Wienk, J. M. Kroon, M. A. J. Michels, and R. A. J. Janssen, Nano Lett. **5**(4), 579–583 (2005).
[21] J. Peet, J. Y. Kim, N. E. Coates, W. L. Ma, D. Moses, A. J. Heeger, and G. C. Bazan, Nature Mater. **6**, 497–500 (2007).
[22] M. A. Ruderer, S. Guo, R. Meier, H.-Y. Chiang, V. Körstgens, J. Wiedersich, J. Perlich, S. V. Roth, and P. Müller-Buschbaum, Adv. Funct. Mater. **21**(17), 3382–3391 (2011).
[23] N. D. Treat, C. G. Shuttle, M. F. Toney, C. J. Hawker, and M. L. Chabinyc, J. Mater. Chem. **21**(39), 15224 (2011).
[24] R. Hamilton, C. G. Shuttle, B. O'Regan, T. C. Hammant, J. Nelson, and J. R. Durrant, J. Phys. Chem. Lett. **1**(9), 1432–1436 (2010).
[25] D. C. Olson, J. Piris, R. T. Collins, S. E. Shaheen, and D. S. Ginley, Thin Solid Films **496**(1), 26–29 (2006).
[26] L. Baeten, B. Conings, H.-G. Boyen, J. D'Haen, A. Hardy, M. D'Olieslaeger, J. V. Manca, and M. K. Van Bael, Adv. Mater. **23**(25), 2802–2805 (2011).
[27] F. Wu, W. Shen, Q. Cui, D. Bi, W. Yue, Q. Qu, and M. Wang, J. Phys. Chem. C **114**(47), 20225–20235 (2010).
[28] B. Conings, L. Baeten, H.-G. Boyen, D. Spoltore, J. D'Haen, L. Grieten, P. Wagner, M. K. Van Bael, and J. V. Manca, J. Phys. Chem. C **115**(33), 16695–16700 (2011).
[29] L. Baeten, B. Conings, J. D'Haen, C. D. Dobbelaere, A. Hardy, J. V. Manca, and M. K. Van Bael, ChemPhysChem (2012), doi:10.1002/cphc.201200102.
[30] L. J. A. Koster, M. Kemerink, M. M. Wienk, K. Maturova, and R. A. J. Janssen, Adv. Mater. **23**(14), 1670 (2011).
[31] L. J. A. Koster, V. D. Mihailetchi, H. Xie, and P. W. M. Blom, Appl. Phys. Lett. **87**, 203502 (2005).
[32] H. Azimi, A. Senes, M. C. Scharber, K. Hingerl, and C. J. Brabec, Adv. Energy Mater. **1**(6), 1162–1168 (2011).
[33] S. R. Cowan, A. Roy, and A. J. Heeger, Phys. Rev. B **82**(24), 245207 (2010).
[34] S. R. Cowan, W. L. Leong, N. Banerji, G. Dennler, and A. J. Heeger, Adv. Funct. Mater. **21**(16), 3083–3092 (2011).
[35] W. L. Leong, S. R. Cowan, and A. J. Heeger, Adv. Energy Mater. **1**(4), 517–522 (2011).
[36] J. Bisquert and G. Garcia-Belmonte, J. Phys. Chem. Lett. **2**(15), 1950–1964 (2011).
[37] C. G. Shuttle, A. Maurano, R. Hamilton, B. O'Regan, J. C. de Mello, and J. R. Durrant, Appl. Phys. Lett. **93**(18) (2008).
[38] A. F. Nogueira, I. Montanari, J. Nelson, J. R. Durrant, C. Winder, N. S. Sariciftci, and C. Brabec, J. Phys. Chem. B **107**(7), 1567–1573 (2003).
[39] C. G. Shuttle, B. O'Regan, A. M. Ballantyne, J. Nelson, D. D. C. Bradley, J. d. Mello, and J. R. Durrant, Appl. Phys. Lett. **92**, 093311 (2008).
[40] H. Ohkita and S. Ito, Polymer **52**(20), 4397–4417 (2011).
[41] A. Maurano, C. G. Shuttle, R. Hamilton, A. M. Ballantyne, J. Nelson, W. Zhang, M. Heeney, and J. R. Durrant, J. Phys. Chem. C **115**(13), 5947–5957 (2011).
[42] Z. Li, F. Gao, N. C. Greenham, and C. R. McNeill, Adv. Funct. Mater. **21**(8), 1419–1431 (2011).
[43] H. Nakanishi and B. A. Grzybowski, J. Phys. Chem. Lett. **1**(9), 1428–1431 (2010).
[44] C. Jäger, D. Haarer, B. Peng, and M. Thelakkat, Appl. Phys. Lett. **85**, 6185 (2004).
[45] A. J. Morfa, A. M. Nardes, S. E. Shaheen, N. Kopidakis, and J. van de Lagemaat, Adv. Funct. Mater. **21**(13), 2580–2586 (2011).

[46] A. J. Morfa, A. M. Nardes, S. E. Shaheen, N. Kopidakis, and J. van de Lagemaat, Adv. Funct. Mater. **21**(22), 4210–4210 (2011).

[47] G. Garcia-Belmonte, A. Munar, E. M. Barea, J. Bisquert, I. Ugarte, and R. Pacios, Org. Electron. **9**(5), 847–851 (2008).

[48] B. J. Leever, C. A. Bailey, T. J. Marks, M. C. Hersam, and M. F. Durstock, Adv. Energy Mater. **2**(1), 120–128 (2012).

[49] J. Bisquert, F. Fabregat-Santiago, I. Mora-Seró, G. Garcia-Belmonte, and S. Giménez, J. Phys. Chem. C **113**(40), 17278–17290 (2009).

[50] G. Garcia-Belmonte, P. P. Boix, J. Bisquert, M. Sessolo, and H. J. Bolink, Sol. Energy Mater. Sol. Cells **94**(2), 366–375 (2010).

[51] B. C. O'Regan, J. R. Durrant, P. M. Sommeling, and N. J. Bakker, J. Phys. Chem. C **111**(37), 14001–14010 (2007).

[52] A. Maurano, R. Hamilton, C. G. Shuttle, A. M. Ballantyne, J. Nelson, B. O'Regan, W. Zhang, I. McCulloch, H. Azimi, M. Morana, C. J. Brabec, and J. R. Durrant, Adv. Mater. **22**(44), 4987–4992 (2010).

[53] See supplementary material at http://dx.doi.org/10.1063/1.4714902 for experimental details.